Comparison of Alternative Kinematical Approaches to Finite Element Formulations with Embedded Strong Discontinuities

Barış İrhan

Report/Preprint No. 03–I–03
Institut für Mechanik (Bauwesen) · Lehrstuhl I · Prof. C. Miehe
Universität Stuttgart, 70550 Stuttgart, Pfaffenwaldring 7, Germany

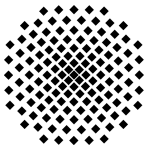

Contents

Master of Science Thesis supervised by M.Sc. Ercan Gürses and Prof. Dr.-Ing. C. Miehe
Stuttgart, May 2003

Contents

List of Figures

Acknowledgements

I would like to thank Prof. Dr.-Ing. Christian Miehe, who gave me the possibility to work on a fruitful subject during my thesis period. The financial support provided by the Institute of Applied Mechanics (Chair I) is gratefully acknowledged. Thanks also go to M.Sc. Ercan Gürses for his careful overview of the manuscript and helpful suggestions. In the first year of the program I learned quite a lot of new things during the lectures. I would like to appreciate all lecturers for their excellent contribution and afford. During the last three semesters I was supported financially by Office of International Affairs. I gratefully acknowledge the support they provided.

1. Introduction

In most of the engineering structures the loss of integrity, structural collapse, is signalled by intense deformations localized at certain region of the body due to softening behavior that the material exhibit in the post-peak regime. There are three different possible kinematic descriptions, which might be valid at the localized region. In the first description, the displacement field is assumed to be continuous in the localization band, whereas there is a jump in certain strain components (Figure 1a.). This type of discontinuities are referred to as weak discontinuities. In the second description, (Figure 1b.), the displacement field is assumed to be two times continuously differentiable along the band. This assumption results in the strain field also be continuous with steep gradients leading transition from higher strain level to the lower one in the band. This type of kinematic descriptions can be obtained by theories based on enriched continua such as nonlocal or higher-gradient continua [20; 36; 68]. In the final description, we assume that the band in which localization occurs is so small that it collapses down to a point, where approximation with a discontinuity in the displacement field makes sense (Figure 1c.). Note that in this case Dirac distribution appears in the strain expression. This final description will be referred to as strong discontinuities in the subsequent developments.

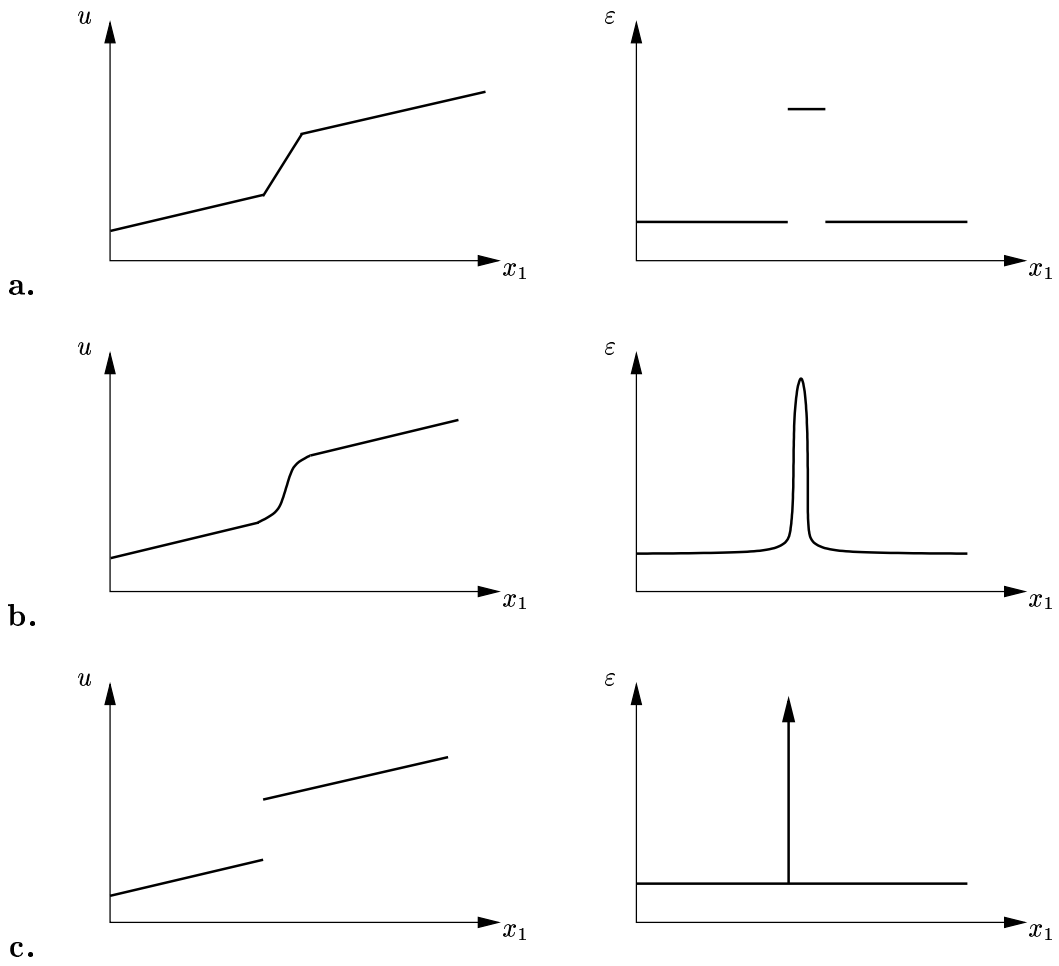

Figure 1: Possible kinematic descriptions for localized deformation.

The material behavior in the localization band, which is governed by the softening branch of constitutive equation, controls the overall global behavior. While the deformation localizes in the band, the part of the structure outside unloads elastically. In the absence of a chracteristic length [68; 36; 56] which fixes the band of localized deformation, the attempts to simulate this physical phenomena by numerics, such as standard finite element method, fails to yield mesh objective global response. To clarify the idea, we consider a one dimensional problem. Let consider the bar in Figure 2, where the dimensions and boundary conditions are also depicted. Further, assume that the material behavior is governed by a damage model with linear softening (see Figure 3).

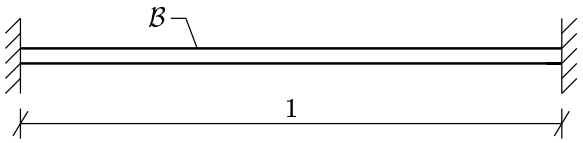

Figure 2: Description of the geometry and boundary conditions for one dimensional problem.

Next, we pose that in a band of width "k" the material strength is slightly lower than the other part of the body. Here we can think of "k" be a material parameter defining the band in which the strain localizes, i.e., the stress response is governed by the softening branch of stress-strain diagram in the post-peak regime. Note that to have a softening material is necessary but not enough to have an inhomogeneous deformation state in which the strain localizes at some part of the body.

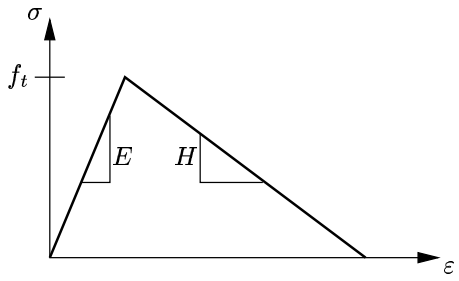

Figure 3: Stress strain diagram for a damage model with linear softening.

In addition, there has to be some inhomogeneity in the structure, for example in one dimensional case it might be non-uniformity of cross sectional area or material properties along the axis of the bar, to bifurcate from homogeneous deformation state to inhomogeneous one, and in reality no structure can be thought of perfectly homogeneous. Therefore, if the material is of softening type one expects always localization to occur.
Now, with the softening modulus "H" and width "k" of localization band at hand, we look for the solution of boundary value problem described in Figure 4. The field equations governing the response and boundary conditions are given in Box 1.

Box 1 : Field Equations and Boundary Conditions for One Dimensional Boundary Value Problem

1. Balance Equation	$\dfrac{d\sigma}{dx} = 0$
2. Kinematic Equation	$\varepsilon = \dfrac{du}{dx}$
3. Constitutive Equation	$\sigma = \begin{cases} E\varepsilon, & \text{if } \varepsilon \leq \varepsilon_c = f_t/E \\ f_t + H(\varepsilon - \varepsilon_c), & \text{if } \varepsilon > \varepsilon_c \end{cases}$
4. Traction Continuity	$\left[\sigma \cdot (+1)\right]_k = \left[\sigma \cdot (+1)\right]_{\mathcal{B}/k}$
5. Compatibility	$\delta = \delta_k + \delta_{\mathcal{B}/k}$
6. Boundary Conditions	$u = 0 \quad \text{at } x = 0$ $u = \delta \quad \text{at } x = 1$

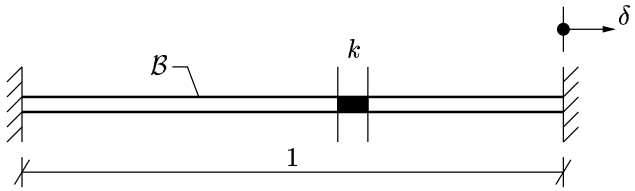

Figure 4: Description of boundary value problem – Loading and boundary conditions.

If one inserts the kinematic relation (2.) into constitutive equation (3.) and then combine the resulting expression with balance equation (1.), with the use of traction continuity along the localization band, a closed form solution relating the tip displacement to tip force is obtained (1), which is visualized in Figure 5.

$$F = \begin{cases} E\delta & \text{if} \quad \delta < \delta_c = \dfrac{\bar{f}_t}{E} \\ \dfrac{1}{\frac{1-k}{E} + \frac{k}{H}} \left[\delta + k\left(\dfrac{1}{H} - \dfrac{1}{E}\right)\bar{f}_t\right] & \text{if} \quad \delta \geq \delta_c \end{cases} \tag{1}$$

At this stage, we try to simulate the localized behavior described above by finite element method using two-noded linear elements. The only thing that we know at the beginning is that there is a band in which the strain localization occurs. However, in standard formulation, no information is available about the size and position where the band is located. Note that in this particular formulation the global response is independent of the location of the band, it only depends on the size of it (1). So what one simply can do, actually it is the only choice, is to attach the localized zone to an element, the one which is dimensioned in Figure 6, by weakining it to initiate localization.

Since the approximation by finite elements and closed form solution are of the same order

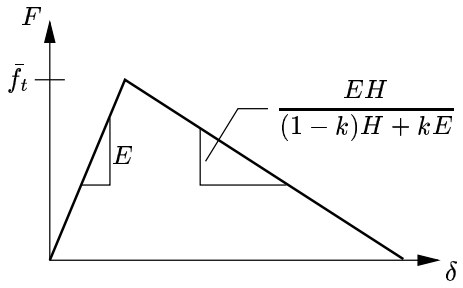

Figure 5: Load displacement diagram – Reference solution.

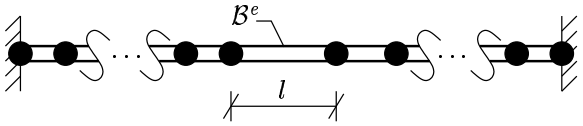

Figure 6: Discretization of the domain by standard two-noded linear elements.

for this particular problem, one can directly write a very similar expression to (1) as

$$F = \begin{cases} E\delta & \text{if} \quad \delta < \delta_c = \dfrac{\bar{f}_t}{E} \\ \dfrac{1}{\frac{1-l}{E} + \frac{l}{H}} \left[\delta + l \left(\dfrac{1}{H} - \dfrac{1}{E} \right) \bar{f}_t \right] & \text{if} \quad \delta \geq \delta_c \end{cases} \tag{2}$$

which can be obtained simply replacing "k" in (1) by "l". From (2), it directly comes out that the reference solution is recovered if and only if

$$\boxed{l = k} \tag{3}$$

that means, unless (3) is satisfied, the global response that we have in the post–peak regime is strictly speaking mesh dependent.
After having shown that the standard finite element approximation failed to capture strain localization in a mesh objective manner, we peresent the enhanced element formulation proposed by [10] to overcome sensitivity to mesh structure. The basic idea presented in that paper is the insertion of localization band directly within the element domain, which requires the width "k" of localization band to be provided from outside. Provided that the element size is greater than "k" the proposed methodology yields completely mesh independent results. The steps to be followed are as follows. We consider simply the two–noded linear element, into which the localization band is inserted (see Figure 7).

Again, equivalence of order of approximation with that of exact result yields the following expression

$$F_j = -F_i = \begin{cases} E\delta & \text{if} \quad \dfrac{d_j - d_i}{l} < \delta_c = \dfrac{\bar{f}_t}{E} \\ \dfrac{1}{\frac{l-k}{E} + \frac{k}{H}} \left[\underbrace{d_j - d_i}_{\delta_k} + k \left(\dfrac{1}{H} - \dfrac{1}{E} \right) \bar{f}_t \right] & \text{if} \quad \dfrac{d_j - d_i}{l} \geq \delta_c \end{cases} \tag{4}$$

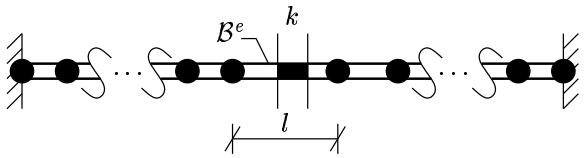

Figure 7: Discretization of the domain by standard two-noded linear elements plus one element with embedded localization zone.

which is valid in the element domain and subscripts i and j refer to nodes of the element. Now, with the above equation, the global load diplacement relationship valid at the post-paek regime can be obtained as

$$\begin{aligned}\delta &= \delta_k + \delta_{\mathcal{B}/k} \\ &= \underbrace{F\left[\frac{l-k}{E}+\frac{k}{H}\right]-k\left[\frac{1}{H}-\frac{1}{E}\right]\bar{f}_t}_{\delta_k} + \underbrace{\frac{F}{E}(1-l)}_{\delta_{\mathcal{B}/k}} \\ &= F\left[\frac{1-k}{E}+\frac{k}{H}\right]-k\left[\frac{1}{H}-\frac{1}{E}\right]\bar{f}_t.\end{aligned} \tag{5}$$

If F is extracted from above equation, it is arrived at that, together with pre-peak solution,

$$F = \begin{cases} E\delta & \text{if} \quad \delta < \delta_c = \dfrac{\bar{f}_t}{E} \\ \dfrac{1}{\frac{1-k}{E}+\frac{k}{H}}\left[\delta + k\left(\dfrac{1}{H}-\dfrac{1}{E}\right)\bar{f}_t\right] & \text{if} \quad \delta \geq \delta_c \end{cases} \tag{6}$$

which is identical to the reference solution given by (1), and as can easily be checked no information about the mesh is included, i.e., the result is completely independent of the mesh structure.

The idea of embedding a weak discontinuity into finite elements was first introduced in [65], where the authors enriched the strain field such that one weak discontinuity line can be captured. This idea was later extended by [10], as described above, such that two weak discontinuity lines can be embedded into element domain. The deficiency in their approach is the constraint that the element size must be greater than band of localization, which preclude the mesh refinement to be performed when more detailed information about the solution of the problem is necessary.

Like weak discontinuities, it is also possible to embed strong discontinuities into finite elements. This idea was first considered in [28] as an alternative for discrete modeling of cracks, which were traditionally treated by interface elements placed between element edges. In their formulation, virtual work expression including the virtual work done by cohesive tractions on virtual displacement jumps was used to develop a quadrilateral element. Later, based on same reasoning, a quadrilateral [40] and a constant strain triangle element [64] were developed. A fully consistent variational derivation of a quadrilateral element with strong discontinuities starting from a three-field Hu-Washizu functional was demonstrated in [43].

The relationship between the appearance of strong discontinuities and rate independent

softening constitutive equations were explored in detail in [6; 57; 59; 60; 61; 62; 63; 77; 76; 89], where the authors with the so-called strong discontinuity analysis, by taking traction continuity and stress boundedness requirement into account, proved that constitutive equations of softening type are compatible with the appearance of strong discontinuities in the post-peak regime, if some requirements are met, where, for instance in softening plasticity, the most remarkable one is the distributional character of the softening modulus. In their formulation, in a consistent manner, they ended up with a discrete traction seperation law governing the material response along the discontinuity surface from continuum constitutive equation. In numerical simulations, although possible, there is no need to resort to discrete traction seperation law. The whole simulation can be performed staying in the continuum framework. The only thing that must be done is to regularize the Dirac delta distribution appearing in the strain field and constitutive eqution by defining a delta sequence with the aid of a regularization parameter, which converges to a delta function when regularization parameter tends to zero.
Application of elements with embedded strong discontinuities to model shear bands and cracks can be found in [1; 2; 3; 13; 34; 35; 47; 58; 78; 91]. In [14; 73] these elements were used to model soil plasticity described by strain-softening Drucker-Prager constitutive model. In [5; 15; 41; 79] loaclization phenomena in porous materials has been studied by using elements with embedded discontinuities. Extension of the formulation to include large strain kinematics was first done in [7; 29], which was followed by [4; 42; 80]. Three dimensional modeling of shear bands and cracks were considered in [89; 93; 95]. In [61], the concept was used in the context of J2 plasticity to model localization, which initially is confined to a region and collapses down to a line during the inelastic deformations ruled out by a bandwidth evolution equation.
There exists conceptually three different element formulations, in which the strong discontinuity is embedded into element domain. They are called as, kinematically optimal symmetric (KOS) formulation, statically optimal symmetric (SOS) formulation and statically and kinematically optimal non-symmetric (SKON) formulation, respectively. In KOS formulation, displacement field is enhanced with a discontinuous contribution and use of extended principle of virtual work is made, where the standard expression is extended by including the virtual work done by cohesive tractions on virtual displacement jumps. Whereas, in SOS formulation a term is added to strain field to take the contribution coming from the jump in the displacement field into account. Actually SOS formulation falls in the scope of enhanced assumed strain element formulations based on method of incompatible modes first proposed in [75], where the variational statements are obtained by taking the variation of three-field Hu-Washizu functional and considering orthogonality of enhanced strains to independent stress field. As pointed out in [35], SOS formulation is based on natural traction continuity but it can not reflect the kinematics of a fully opened crack leading spurious stresses to develop in element domain. Whereas, in KOS formulation full strain relaxation is possible, i.e., the element is capable of simulating rigid body motions without straining. However, there is an ambiguity in traction continuity in this formulation. Because traction continuity is maintained by equating the sum of fictititous nodal equivalent forces on positive (or negative) side of the discontinuity to traction components. Traction components obtained in this manner need not be necessarily compatible with the ones obtained from the stress field in the element by contraction with the normal, unless some special conditions are met. The deficiencies that the both methods have motivates the element formulation which is variationally inconsistent but performs

well both kinematically and statically. In the so-called SKON formulation the idea is to interpolate the enhanced part of the strain field as in KOS formulation and to enforce traction continuity as in SOS formulation.
If the displacement jump is assumed to be piecewise constant in the element domain, i.e., if no interelement continuity is enforced on the displacement jump, the structure provided by the formulations summarized above allow the degrees of freedom corresponding to jumps in the displacement field to be condensed out at element level. From implementation view point it is very advantageous because only standard degrees of freedom are kept at global structural level, and the number of global equations and structure stiffness matrix do not change the size when discontinuity propagates further and new elements are cut by the discontinuity. Therefore, by making some simple modifications at element level and with the aid of a global discontinuity tracking algorithm, it is easy to integrate the idea into an existing general purpose finite element codes, such as CMP.
Although some simplifications are provided by the methodology, one has to consider some weak points of the approach. The most efficient SKON formulation yields unsymmetric tangent matrix irrespective of the material model used, which brings some overburden during the computations. In addition for the elements cut by the discontinuity the strain on both sides of discontinuity is fully coupled. It is good from implementation view point, because standard quadrature can be used to integrate element contributions. However, one expects, at least partially, uncoupling between strain on both sides of the discontinuity, for instance, when a crack opens wide. In these formulations the discontinuities are extended through the element domain. Therefore, the discontinuity tip has to lie on one of the element edges, it can not be embedded into element domain. In addition, since displacement jump is assumed to be piecewise constant in the element, zero displacement jump condition at the crack tip can not be maintained. Finally, in [34], it has been shown by examining a constant strain triangle cut by discontinuity that some convergence problems arise if the elements cut by the discontinuity has not a proper shape and size.
Recently a new methodology, extended finite element method (XFEM), has been emerged, which in a particular form offers a different possibility to treat the discontinuities embedded into element domain. In [45], it has been shown that by using the partition of unity property of standard finite element shape functions, it is possible to enhance the approximation field of interest (displacement, temperature, etc.) at some critical region of the body (at a crack tip or internal boundary) with the products of some suitable enrichment functions by global nodal shape functions. These enrichment functions have the information about the local character of the problem and are usually constructed by exact solution of the problem obtained under some simplified conditions. In this context, to simulate a cohesive crack growth, it is just enough to consider a discontinuous enrichment function along the crack faces, such as heaviside step function, in the extended interpolation, i.e., there is no need for near tip asymptotic fields to be included in the enhancement strategy, because cohesive traction seperation law valid on the crack face removes stress singularity at the crack tip (see [36; 89]). Here the extended displacement interpolation can be understood as the interpolation of discontinuity from the existing nodes of the finite elements in a global manner with the aid of enhanced degrees of freedom assigned to the nodes whose support is cut by the discontinuity. Since the enhanced base function, here the heaviside step function, is multiplied by global nodal finite element shape functions, the enhancement has a limited support defined by the shape functions which belong to the enhanced nodes.

In addition, since the displacement jump within the element domain is interpolated using standard nodal shape functions, resulting approximation is conforming, i.e., displacement jump is interelement continuous without any incompatibilities, in contrast to kinematic description given by KOS, SOS, SKON formulations, where displacement jump is assumed to be piecewise constant inside the elements yielding a non-conforming interpolation. Also note that in extended interpolation displacement jump is not constant in element domain and approximated with the order provided by base element.
Partition of unity concept was first appeared in [9] to model elastic crack growth by using near tip asymptotic fields to locally enrich the finite element approximation. Later, in [21; 52] the idea presented in [9] was further extended by incorporating a discontinuous field across the crack faces away from the crack tip. In [81], the XFEM was combined with a level set method to provide a general framework for evolving cracks, whereas in [82] this combination was used to solve problems involving inclusions and holes. In [11; 19] the extension of the method to model arbitrary branched and intersecting cracks were demonstrated. Application of the method to model fracture in Reissner-Mindlin plates was presented in [21; 23; 24]. Crack growth with frictional contact by incorporating XFEM was studied in [25]. The method was also used to model crack propagation in polycrystalline microstructures [85]. Recently a paper on the computation of stress intensity factors in functionally graded materials with XFEM was published [22]. The extension of the idea to model three dimensional cracks was first pioneered in [84], which was followed by [18; 83] for three dimensional fatique crack propagation and by [53] for the modeling of non-planar three dimensional cracks. The modeling of displacement discontinuities in strain softening solids by XFEM was considered in [89; 92; 96] for quasi-static and dynamic loading conditions. In [27; 51; 89; 94] cohesive crack growth by XFEM were demonstrated, whereas in [89; 90] delamination phenomena in composites was studied within the context of large strain kinematics. The XFEM provides also some challenges for fluid flow problems [17; 88], and phase change problems [33; 46]. The exploitation of the method in nonlocal continuum damage mechanics was presented in [70]. Recently the method was applied to solids defined by implicit surfaces [12].
From implementation view point, there arise some technical difficulties to integrate the idea suggested by XFEM into a standard finite element code. First of all, since displacement jump is interpolated in a global manner, it is not possible to condense extra degrees of freedom assigned to active nodes at element level. This implies that for an evolving discontinuity the size of the global matrices has to be continuously readjusted. Furthermore, there has to be a mechanism for the node activation working at both global and element level in addition to global tracking algorithm, which is itself enough for KOS, SOS and SKON formulations. In the strain interpolation by XFEM , it is possible to obtain partially uncoupling between the strain fields on both sides of the discontinuity. Although this uncoupling sounds well physically, it requires modification in the standard quadrature rule, which would be enough in SOS, KOS, SKON formulations, where the strain on both side of a crack is fully coupled. Kinematical description by XFEM gives also the possibility to embed discontinuity tip inside element domain and it is easy to enforce zero displacement jump condition at a crack tip. Finally, we point out that the resulting formulation is symmetric if the material tangent is also symmetric.
In this thesis we attempt to compare formulations based on elemental and nodal enrichments (see [27; 36; 37; 60; 89]). In the first chapter we will give a general framework for the thermodynamical treatment of cohesive surfaces of displacement discontinuity, and

we will derive damage type traction seperation laws. In the third chapter elemental enrichment strategy for the modeling of cohesive crack growth by elements with embedded discontinuities is discussed, whereas in the fourth chapter the phenomena is investigated by recently emerged method based on nodal enrichment strategy. We give some numerical examples in fifth chapter, and close by chapter six with some concluding remarks.

2. A Thermodynamically Consistent Framework for Cohesive Surfaces of Displacement Discontinuities

When standard virtual work expression is extended to include displacement discontinuities, such as cracks, embedded into domain of the body, a term representing the virtual work of tractions transmitted through discontinuity on displacement jumps comes automatically into picture. These tractions should somehow be expressed by a constitutive equation. In the simplest case, we may assume that crack surface is traction free, which is the usual assumption in linear elastic fracture mechanics and applys only if the process zone is so small when compared with the dimensions of the structure. In small scale structures, however, the finite size of the process zone must be considered. Normal treatment is to lump all inelastic effects in the direction normal to the discontinuity and represent them by the equivalent displacement jump. Before the growing microdefects coalesce and form a true physical crack, the process zone still carries some stresses, which are represented in the model as cohesive tractions transmitted by discontinuity. Actually cohesive traction seperation laws provide a smooth transition between continuum and discontinuum, which is physically more sound. The area under the traction seperation curve corresponds to the energy necessary to create a stress free crack of unit area, and is called as the fracture energy, which is assumed to be a material constant. The traction seperation laws are easy to implement in small deformation context. However in large deformations, the unique definition of normal to discontinuity line can not be defined because a point on the crack line in reference configuration splits into two in current configurtion, i.e., normal map is not unique. To overcome this difficulty a mean map is used to transform normal [67; 89; 90]. Discrete traction seperation laws were first inspired in the works [26; 8], which motivated the fictitious crack model of Hillerborg [32]. The idea, recently, was put into a modern framework in [16; 54; 55; 66; 67; 69; 86; 87]. In [66], a derivation of a traction seperation law for Mode-I from a micromechanical motivation based on array of collinear cracks was presented.

2.1. Thermodynamical Treatment of Cohesive Surfaces

In this section a general framework for the derivation of irreversible cohesive constitutive laws of traction seperation defined at the surface of displacement discontinuity is given. In the formulation, we assume a totally mechanical process and deformations are small. To begin with, we consider a homogeneous body $\mathcal{B} \subset \mathbb{R}^3$ loaded by external body and contact forces by actions from a distance and at a vicinity (Figure 8). In addition, we let body be crossed by a single discontinuity surface $\partial\mathcal{B}_d$ seperating parts $\mathcal{B}^+$ and $\mathcal{B}^-$. Per definition, the normal $(\boldsymbol{n})$ to $\partial\mathcal{B}_d$ points towards $\mathcal{B}^+$.

The kinetic energy $(\mathcal{K})$ and internal energy $(\mathcal{U}+\mathcal{W})$ for the body are defined as

$$\left.\begin{aligned} \mathcal{K} &= \int_{\mathcal{B}} \frac{1}{2}\boldsymbol{v}\cdot\rho\boldsymbol{v}\,dV \\ \mathcal{U} &= \int_{\mathcal{B}} \rho u\,dV \\ \mathcal{W} &= \int_{\partial\mathcal{B}_d} w\,dA \end{aligned}\right\} \tag{7}$$

where ρ, $\boldsymbol{v}$ are the density and velocity fields, whereas u, w are the internal energy

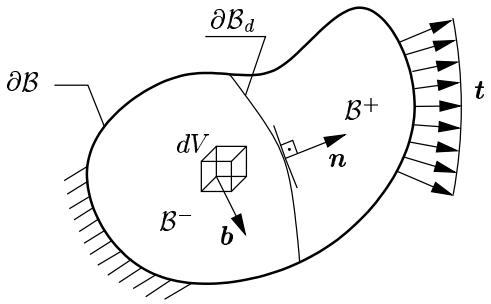

Figure 8: Body $\mathcal{B}$ crossed by a discontinuity $\partial\mathcal{B}_d$.

stored per unit mass of the body and per unit surface area of discontinuity, respectively. Moreover, the dissipation functions for bulk and discontinuity are postulated as

$$\boxed{\begin{aligned}\mathcal{D}_b &= \int_{\mathcal{B}} d_b \, dV \\ \mathcal{D}_d &= \int_{\partial\mathcal{B}_d} d_d \, dA\end{aligned}} \tag{8}$$

where d_b, d_d are the volume specific and area specific dissipated energy in the bulk and along the discontinuity surface, and they are restricted by second law of thermodynamics (entropy inequality), which states that dissipation is ever increasing function, i.e.,

$$\boxed{\begin{aligned}\dot{d}_b &\geq 0 \\ \dot{d}_d &\geq 0\end{aligned}}. \tag{9}$$

In addition, we assume the principal of local action to hold, i.e., constitutive equations evaluated at a point are functions of (in isothermal case) some deformation measure (displacement, strain, strain rate, etc.) plus internal state variables (plastic strain, viscous strain, etc.) representing the inelastic part of the deformation at the same point (see [49; 50]). With this assumption, we postulate the following forms for u, d_b, w and d_d:

$$\left.\begin{aligned}u(\boldsymbol{x}) &= u\Big(\boldsymbol{\varepsilon}(\boldsymbol{x}), \mathcal{I}_b(\boldsymbol{x})\Big) \\ d_b(\boldsymbol{x}) &= d_b\Big(\boldsymbol{\varepsilon}(\boldsymbol{x}), \mathcal{I}_b(\boldsymbol{x})\Big)\end{aligned}\right\} \text{with } \boldsymbol{x} \in \mathcal{B}$$
$$\left.\begin{aligned}w(\boldsymbol{x}) &= w\Big(\left[\!\left[\boldsymbol{u}\right]\!\right](\boldsymbol{x}), \mathcal{I}_d(\boldsymbol{x})\Big) \\ d_d(\boldsymbol{x}) &= d_d\Big(\left[\!\left[\boldsymbol{u}\right]\!\right](\boldsymbol{x}), \mathcal{I}_d(\boldsymbol{x})\Big)\end{aligned}\right\} \text{with } \boldsymbol{x} \in \partial\mathcal{B}_d \tag{10}$$

where $\boldsymbol{\varepsilon}$, $[\![\boldsymbol{u}]\!]$ are small strain tensor and jump in the displacement field, whereas $\mathcal{I}_b$, $\mathcal{I}_d$ are set of internal state variables defining inelastic behavior in the bulk and on the discontinuity surface, respectively.
The mechanical power supplied to the system is

$$\mathcal{P} = \int_{\mathcal{B}} \boldsymbol{v} \cdot \rho \boldsymbol{b} \, dV + \int_{\partial\mathcal{B}} \boldsymbol{v} \cdot \boldsymbol{t} \, dA \tag{11}$$

where $\boldsymbol{t}$ are tractions acting on the external boundary $\partial\mathcal{B}$ and $\boldsymbol{b}$ are the body forces per unit mass. When the power term (11) is extended by including the discontinuity surface $\partial\mathcal{B}_d$ embedded into body, we obtain

$$\begin{aligned}\mathcal{P} = \int\limits_{\mathcal{B}^+\cup\mathcal{B}^-} \boldsymbol{v}\cdot\rho\boldsymbol{b}\,dV + \int\limits_{\partial\mathcal{B}^+\cup\partial\mathcal{B}_d} \boldsymbol{v}\cdot\boldsymbol{t}\,dA + \int\limits_{\partial\mathcal{B}_d\cup\partial\mathcal{B}^-} \boldsymbol{v}\cdot\boldsymbol{t}\,dA - \\ \int_{\partial\mathcal{B}_d} \boldsymbol{v}^+\cdot\boldsymbol{t}^{-n}\,dA - \int_{\partial\mathcal{B}_d} \boldsymbol{v}^-\cdot\boldsymbol{t}^{n}\,dA\end{aligned} \tag{12}$$

where $\boldsymbol{v}^+$, $\boldsymbol{v}^-$ are the velocity fields at opposite sides of discontinuity surface, and $\boldsymbol{t}^n$, $\boldsymbol{t}^{-n}$ are the traction vectors belonging to the surfaces oriented by the normal $(\boldsymbol{n})$ and $(-\boldsymbol{n})$, respectively. By resorting to the Cauchy's lemma for traction continuity $(\boldsymbol{t}^n = -\boldsymbol{t}^{-n})$ (see [30; 31]), (12) can be rephrased as

$$\begin{aligned}\mathcal{P} = \int\limits_{\mathcal{B}^+\cup\mathcal{B}^-} \boldsymbol{v}\cdot\rho\boldsymbol{b}\,dV + \int\limits_{\partial\mathcal{B}^+\cup\partial\mathcal{B}_d} \boldsymbol{v}\cdot\boldsymbol{t}\,dA + \int\limits_{\partial\mathcal{B}_d\cup\partial\mathcal{B}^-} \boldsymbol{v}\cdot\boldsymbol{t}\,dA - \\ \int_{\partial\mathcal{B}_d} \underbrace{\left[\boldsymbol{v}^+ - \boldsymbol{v}^-\right]}_{[\![\boldsymbol{v}]\!]}\cdot\boldsymbol{t}^n\,dA.\end{aligned} \tag{13}$$

Note that (13) reproduces the classical form (11) when there is no jump in the velocity field $(\boldsymbol{v}^+ = \boldsymbol{v}^-)$. If it is not the case, as will be shown later, this additional term drives "internal" surface energy of the body, when postulated, defined on $\partial\mathcal{B}_d$.
First law of thermodynamics (energy equation) (14) states that the sum of temporal changes of internal and kinetic energy, which is reversible, is equal to the external mechanical power minus the rate of energy dissipated during inelastic deformations, which is irreversible.

$$\boxed{\frac{d}{dt}\left[\mathcal{K}+\mathcal{U}+\mathcal{W}\right] = \mathcal{P} - \frac{d}{dt}\left[\mathcal{D}_b+\mathcal{D}_d\right]}. \tag{14}$$

In view of (7), the left hand side of (14) is written as

$$\frac{d}{dt}\left[\mathcal{K}+\mathcal{U}+\mathcal{W}\right] = \int_{\mathcal{B}} \boldsymbol{v}\cdot\rho\dot{\boldsymbol{v}}\,dV + \int_{\mathcal{B}} \rho\dot{u}\,dV + \int_{\partial\mathcal{B}_d} \dot{w}\,dA. \tag{15}$$

In addition, the right hand side, with the aid of Cauchy $(\boldsymbol{t} = \boldsymbol{\sigma}\cdot\boldsymbol{n})$ and Gauss integral $(\int_{\partial\mathcal{B}}(\cdot)\otimes\boldsymbol{n}\,dA = \int_{\mathcal{B}}\nabla(\cdot)\,dV)$ theorems takes the form

$$\begin{aligned}\mathcal{P} = \int_{\mathcal{B}} \boldsymbol{v}\cdot\left[\boldsymbol{\sigma}\cdot\nabla + \rho\boldsymbol{b}\right]\,dV + \int_{\mathcal{B}} (\boldsymbol{v}\otimes\nabla)\cdot\boldsymbol{\sigma}\,dV + \\ \int_{\partial\mathcal{B}_d} [\![\boldsymbol{v}]\!]\cdot\boldsymbol{t}^n\,dA - \int_{\mathcal{B}} \dot{d}_b\,dV - \int_{\partial\mathcal{B}_d} \dot{d}_d\,dA\end{aligned} \tag{16}$$

where $\nabla = \partial/\partial\boldsymbol{x}$ is the gradient vector.
By inserting (16) and (15) into (14) and using the balance equation for linear momentum $(\rho\dot{\boldsymbol{v}} = \boldsymbol{\sigma}\cdot\nabla + \rho\boldsymbol{b})$ and symmetry of the stress tensor $(\text{skew}\,\boldsymbol{\sigma} = \boldsymbol{0})$, we arrive at

$$\int_{\mathcal{B}} \rho\dot{u}\,dV + \int_{\partial\mathcal{B}_d} \dot{w}\,dA = \int_{\mathcal{B}} \dot{\boldsymbol{\varepsilon}}\cdot\boldsymbol{\sigma}\,dV + \int_{\partial\mathcal{B}_d} [\![\boldsymbol{v}]\!]\cdot\boldsymbol{t}^n\,dA - \int_{\mathcal{B}} \dot{d}_b\,dV - \int_{\partial\mathcal{B}_d} \dot{d}_d\,dA \tag{17}$$

which can be rearranged as

$$\boxed{\int_{\mathcal{B}} \left(\rho\dot{u} - \dot{\boldsymbol{\varepsilon}} \cdot \boldsymbol{\sigma} + \dot{d}_b\right)\, dV + \int_{\partial\mathcal{B}_d} \left(\dot{w} - [\![\boldsymbol{v}]\!] \cdot \boldsymbol{t}^n + \dot{d}_d\right)\, dA = 0.} \tag{18}$$

Finally, we obtain the expressions

$$\boxed{\rho\dot{u} - \dot{\boldsymbol{\varepsilon}} \cdot \boldsymbol{\sigma} + \dot{d}_b = 0} \tag{19}$$

$$\boxed{\dot{w} - [\![\boldsymbol{v}]\!] \cdot \boldsymbol{t}^n + \dot{d}_d = 0} \tag{20}$$

from which constitutive equations for $\boldsymbol{\sigma}$, $\boldsymbol{t}^n$, d_b and d_d are obtained by following the so-called Coleman's exploitation method (see [49; 50]). Procedure is as follows. First, we compute the rate form of u and w using (9) and (10) as

$$\dot{u} = \frac{\partial u}{\partial \boldsymbol{\varepsilon}} \cdot \dot{\boldsymbol{\varepsilon}} + \frac{\partial u}{\partial \boldsymbol{\mathcal{I}}_b} \cdot \dot{\boldsymbol{\mathcal{I}}}_b \tag{21}$$

$$\dot{w} = \frac{\partial w}{\partial [\![\boldsymbol{u}]\!]} \cdot \dot{\boldsymbol{v}} + \frac{\partial w}{\partial \boldsymbol{\mathcal{I}}_d} \cdot \dot{\boldsymbol{\mathcal{I}}}_d. \tag{22}$$

Then, we insert (21) into (19), and (22) into (20) and obtain

$$\left[\rho\frac{\partial u}{\partial \boldsymbol{\varepsilon}} - \boldsymbol{\sigma}\right] \cdot \dot{\boldsymbol{\varepsilon}} + \left[\rho\frac{\partial u}{\partial \boldsymbol{\mathcal{I}}_b} \cdot \dot{\boldsymbol{\mathcal{I}}}_b + \dot{d}_b\right] = 0 \tag{23}$$

$$\left[\frac{\partial w}{\partial [\![\boldsymbol{u}]\!]} - \boldsymbol{t}^n\right] \cdot [\![\boldsymbol{v}]\!] + \left[\frac{\partial w}{\partial \boldsymbol{\mathcal{I}}_d} \cdot \dot{\boldsymbol{\mathcal{I}}}_d + \dot{d}_d\right] = 0. \tag{24}$$

If we postulate the bracket in the first terms of (23) and (24) vanish, the constitutive equations are obtained as follows:

$$\boxed{\begin{aligned} \boldsymbol{\sigma} &= \rho\frac{\partial u}{\partial \boldsymbol{\varepsilon}} \\ \dot{d}_b &= -\rho\frac{\partial u}{\partial \boldsymbol{\mathcal{I}}_b} \cdot \dot{\boldsymbol{\mathcal{I}}}_b \geq 0 \end{aligned}} \tag{25}$$

$$\boxed{\begin{aligned} \boldsymbol{t}^n &= \frac{\partial w}{\partial [\![\boldsymbol{u}]\!]} \\ \dot{d}_d &= -\frac{\partial w}{\partial \boldsymbol{\mathcal{I}}_d} \cdot \dot{\boldsymbol{\mathcal{I}}}_d \geq 0 \end{aligned}}. \tag{26}$$

With the above equations formulation comes to end. It was shown that cohesive traction seperation laws can be determined from a surface energy function in a consistent way, provided that it satisfies $(26)_2$, positive dissipation. Derivation of irreversible cohesive constitutive laws for traction seperation in the large strain context can be found in [67].

2.2. Isotropic Damage Models of Traction Seperation

In this section a general framework for the damage type traction seperation laws is given by assuming purely elastic unloading branch. The formal procedure is as follows [37; 48; 74]. We start with the surface energy of the form

$$w = (1 - d)w_0 \tag{27}$$

defined per unit area of cohesive discontinuity. In (27), w_0 is the elastic undamaged surface energy, which in case of pure elastic unloading is expressed as

$$w_0 = \frac{1}{2} [\![\boldsymbol{u}]\!] \cdot \boldsymbol{T} \cdot [\![\boldsymbol{u}]\!] \tag{28}$$

where $\boldsymbol{T}$ is the symmetric tangent moduli and $[\![\boldsymbol{u}]\!]$ is the vector of displacement jump, and d is the scalar damage variable, which controls the degradation of stiffness along the discontinuity.
Standard thermodynamical arguments requires local dissipation be always positive, i.e., recall

$$\dot{d}_d = \boldsymbol{t}^n \cdot [\![\boldsymbol{v}]\!] - \dot{w} \geq 0. \tag{29}$$

If (27) is written in rate form, and then inserted into (29) it is arrived at that

$$\dot{d}_d = \left[\boldsymbol{t}^n - \frac{\partial w}{\partial [\![\boldsymbol{u}]\!]} \right] \cdot [\![\boldsymbol{v}]\!] + w_0 \dot{d} \geq 0 \tag{30}$$

which leads us to the following forms for the constitutive equation and reduced form of the local dissipation:

$$\left.\begin{aligned} \boldsymbol{t}^n &= \frac{\partial w}{\partial [\![\boldsymbol{u}]\!]} = (1 - d)\boldsymbol{T} \cdot [\![\boldsymbol{u}]\!] \\ \dot{d}_{d_{red}} &= w_0 \dot{d} \geq 0 \end{aligned}\right\}. \tag{31}$$

Note that elastic surface energy w_0 is the thermodynamical force driving the evolution of damage. Since the elastic surface energy is always positive, reduced form of local dissipation puts a constraint on the form of damage variable, i.e.,

$$\boxed{\dot{d} \geq 0}. \tag{32}$$

The final ingredient which is necessary to complete the formulation is the evolution equation for damage variable. Here the standard treatment is to relate the damage evolution to history of a deformation measure. Explicitly, we pose that damage is a function of the maximum elastic surface energy "r" which has been reached in the history of deformation process, i.e.,

$$d = g(r), \quad \text{with} \boxed{\frac{dg}{dr} = H \geq 0}. \tag{33}$$

Furthermore, damage evolution is also controlled by history dependent parameter "r", and it is assumed that damage evolves if and only if currently attained elastic surface energy w_0 exceeds the threshold defined by "r". In other words, the parameter "r" defines an elastic domain in the space of displacement jumps such that

$$\phi(w_0, r) = w_0 - r \leq 0 \tag{34}$$

which bounds the traction response. The above constraint together with reduced form of local dissipation inequality defines a minimization problem (principle of maximum dissipation) with inequality constraints, which can be solved by Lagrange multiplier method. The Lagrange functional has the form

$$\mathscr{L} = -w_0\dot{d} + \dot{\mu}\phi \Rightarrow \text{stationary} \tag{35}$$

where $\dot{\mu}$ is the Lagrange multiplier. Standard manupulations then yields the following evolution equation for the damage variable:

$$\dot{d} = \dot{\mu} = H\dot{r} \tag{36}$$

with loading-unloading (Karush-Kuhn-Tucker) conditions

$$\dot{\mu} \geq 0,\ \phi \leq 0,\ \dot{\mu}\phi = 0. \tag{37}$$

After having obtained the evolution equation, there remains the computation of continuous elasto-damage tangent moduli. The procedure is as follows. We start by writing the constitutive eqution in rate form as

$$\dot{\boldsymbol{t}}^n = (1-d)\boldsymbol{T}\cdot[\![\boldsymbol{v}]\!] - \dot{d}\boldsymbol{T}\cdot[\![\boldsymbol{u}]\!]\,. \tag{38}$$

From consistency ($\dot{\phi} = 0$) condition, the Lagrange multiplier may easily be obtained as

$$\dot{\mu} = \dot{d} = H\dot{w}_0 = H\left(\boldsymbol{T}\cdot[\![\boldsymbol{u}]\!]\right)\cdot[\![\boldsymbol{v}]\!]\,. \tag{39}$$

With the insertion of (39) into (38), we are then led to

$$\left.\begin{aligned}
\dot{\boldsymbol{t}}^n &= (1-d)\boldsymbol{T}\cdot[\![\boldsymbol{v}]\!] - H\Big[\left(\boldsymbol{T}\cdot[\![\boldsymbol{u}]\!]\right)\cdot[\![\boldsymbol{v}]\!]\Big]\boldsymbol{T}\cdot[\![\boldsymbol{u}]\!] \\
&= (1-d)\boldsymbol{T}\cdot[\![\boldsymbol{v}]\!] - H\Big[\left([\![\boldsymbol{u}]\!]\cdot\boldsymbol{T}\right)\otimes\underbrace{\left(\boldsymbol{T}\cdot[\![\boldsymbol{u}]\!]\right)}_{\boldsymbol{t}^n/(1-d)}\Big]\cdot[\![\boldsymbol{v}]\!] \\
&= \underbrace{(1-d)\left[\boldsymbol{T} - \frac{H}{(1-d)^3}\boldsymbol{t}\otimes\boldsymbol{t}\right]}_{\boldsymbol{T}^{ed}}\cdot[\![\boldsymbol{v}]\!]
\end{aligned}\right\}. \tag{40}$$

The summary of the results obtained so far are given in Box 1. A particular form of the constitutive laws described in this section will be used in numerical simulations.

Box 2 : Isotropic Damage Model of Traction Seperation – Continuous Formulation

1. Surface Energy	$w = (1-d)w_0$, with $w_0 = \frac{1}{2}[\![\boldsymbol{u}]\!]\cdot\boldsymbol{T}\cdot[\![\boldsymbol{u}]\!]$
2. Traction	$\boldsymbol{t}^n = (1-d)\boldsymbol{T}\cdot[\![\boldsymbol{u}]\!]$
3. Elastic Domain	$\phi = w_0 - r \leq 0$
4. Loading/Unloading	$\dot{\mu} \geq 0,\ \phi \leq 0,\ \dot{\mu}\phi = 0$
5. Tangent Moduli	$\dot{\boldsymbol{t}}^n = \boldsymbol{T}^{ed}[\![\boldsymbol{v}]\!]$, with $\boldsymbol{T}^{ed} = (1-d)\left[\boldsymbol{T} - \frac{H}{(1-d)^3}\boldsymbol{t}^n\otimes\boldsymbol{t}^n\right]$

3. Modeling of Cohesive Crack Growth by Finite Elements with Embedded Strong Discontinuity: Formulations Based on Elemental Enrichment

In this section detailed analysis of three different element formulations, namely kinematically optimal symmetric (KOS) formulation, statically optimal symmetric (SOS) formulation, and statically and kinematically optimal non-symmetric (SKON) formulation, based on elemental enrichment strategy are given.

3.1. Kinematically Optimal Symmetric (KOS) Formulation

3.1.1. Virtual Work Expression

The domain $\mathcal{B} \subset \mathbb{R}^3$ with a smooth boundary $\partial\mathcal{B}$ is loaded by surface tractions ($\boldsymbol{t}$) and vector field of body forces ($\boldsymbol{b}$) as shown in Figure 9.

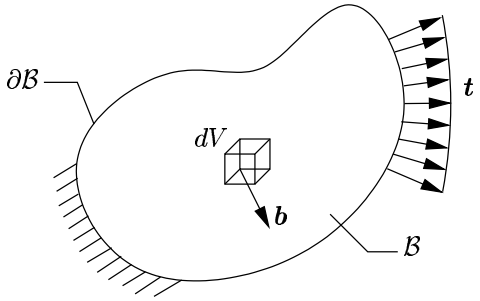

Figure 9: Body $\mathcal{B}$ loaded by mechanical actions.

In D'Alembert's principle (41) the basic idea is, first, to weight balance equation of linear momentum with kinematically admissible displacement variations and, then, to enforce the domain integral of expression obtained vanish (see [30; 31]).

$$\int_{\mathcal{B}} \delta\boldsymbol{u} \cdot [\rho\dot{\boldsymbol{v}} - \operatorname{div}\boldsymbol{\sigma} - \rho\boldsymbol{b}]\, dV = 0 \tag{41}$$

The expression (41) is also known as weak form of equation of motion. When (41) is written for quasi-static case ($\dot{\boldsymbol{v}} = \boldsymbol{0}$), it is called the principle of virtual work (42), which we refer as weak form of equilibrium equations.

$$\int_{\mathcal{B}} \delta\boldsymbol{u} \cdot [\operatorname{div}\boldsymbol{\sigma} + \rho\boldsymbol{b}]\, dV = 0 \tag{42}$$

In (41), (42) $\rho, \boldsymbol{v}, \boldsymbol{\sigma}$ are density, velocity and stress fields, respectively, and $\delta\boldsymbol{u}$ are the kinematically admissible displacement variations, which vanish wherever essential boundary conditions are defined and have continuous first partial derivatives in the interior of the body.
(42), with the use of Cauchy ($\boldsymbol{t} = \boldsymbol{\sigma} \cdot \boldsymbol{n}$) and Gauss integral ($\int_{\partial\mathcal{B}} (\cdot) \otimes \boldsymbol{n}\, dA = \int_{\mathcal{B}} \nabla(\cdot)\, dV$) theorems and symmetry of the stress tensor (skew $\boldsymbol{\sigma} = \boldsymbol{0}$), can be rewritten as

$$\int_{\mathcal{B}} \delta\boldsymbol{\varepsilon} :\ \boldsymbol{\sigma}\, dV = \int_{\partial\mathcal{B}_\sigma} \delta\boldsymbol{u} \cdot \boldsymbol{t}\, dA + \int_{\mathcal{B}} \delta\boldsymbol{u} \cdot \rho\boldsymbol{b}\, dV \tag{43}$$

where $\delta\boldsymbol{\varepsilon}$ is the variation of the strain field and $\partial\mathcal{B}_\sigma$ is the portion of outer boundary, where surface tractions are applied.
Next, we consider the same body, which is now splitted into two, namely $\mathcal{B}^+$ and $\mathcal{B}^-$, by a single material surface $\partial\mathcal{B}_d$, along which some displacement components are discontinuous, as shown in Figure 10. The normal ($\boldsymbol{n}$) to the discontinuity surface, per definition, points towards $\mathcal{B}^+$. In addition, for later use, the domain $\mathcal{B}_h \subset \mathcal{B}$ enclosing $\partial\mathcal{B}_d$ is also defined.

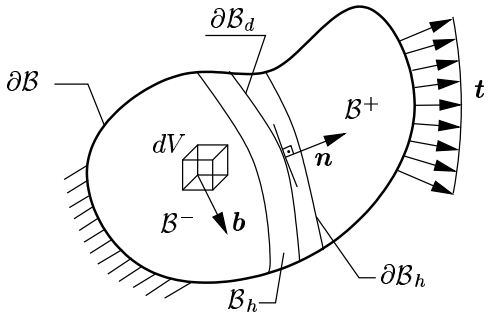

Figure 10: Body $\mathcal{B}$ with a surface of discontinuity $\partial\mathcal{B}_d$.

Then, we attempt, again, to write virtual work expression for the body. We can not obtain, this time, the expression for the whole body since first derivative of some displacement components is undefined along $\partial\mathcal{B}_d$. Instead, we write it for the parts $\mathcal{B}^+$ and $\mathcal{B}^-$, in which the derivatives are continuous (44).

$$\left.\begin{aligned}\int_{\mathcal{B}^+} \delta\boldsymbol{\varepsilon} :\ \boldsymbol{\sigma}\, dV &= \int_{\partial\mathcal{B}^+_\sigma} \delta\boldsymbol{u}\cdot\boldsymbol{t}\, dA + \int_{\mathcal{B}^+} \delta\boldsymbol{u}\cdot\rho\boldsymbol{b}\, dV + \int_{\partial\mathcal{B}_d} \delta\boldsymbol{u}^+\cdot\boldsymbol{t}^{-n}\, dA \\ \int_{\mathcal{B}^-} \delta\boldsymbol{\varepsilon} :\ \boldsymbol{\sigma}\, dV &= \int_{\partial\mathcal{B}^-_\sigma} \delta\boldsymbol{u}\cdot\boldsymbol{t}\, dA + \int_{\mathcal{B}^-} \delta\boldsymbol{u}\cdot\rho\boldsymbol{b}\, dV + \int_{\partial\mathcal{B}_d} \delta\boldsymbol{u}^-\cdot\boldsymbol{t}^{n}\, dA\end{aligned}\right\} \tag{44}$$

In (44), $\delta\boldsymbol{u}^+$, $\delta\boldsymbol{u}^-$ are the displacement variations at opposite sides of discontinuity surface, and $\boldsymbol{t}^n$, $\boldsymbol{t}^{-n}$ are the traction vectors belonging to the surfaces oriented by normals ($\boldsymbol{n}$) and ($-\boldsymbol{n}$), respectively. If $(44)_1$ is added to $(44)_2$, and use of Cauchy's lemma for traction continuity ($\boldsymbol{t}^n = -\boldsymbol{t}^{-n}$) is made, we reach

$$\int_{\mathcal{B}/\partial\mathcal{B}_d} \delta\boldsymbol{\varepsilon} :\ \boldsymbol{\sigma}\, dV = \int_{\partial\mathcal{B}_\sigma} \delta\boldsymbol{u}\cdot\boldsymbol{t}\, dA + \int_{\mathcal{B}/\partial\mathcal{B}_d} \delta\boldsymbol{u}\cdot\rho\boldsymbol{b}\, dV - \int_{\partial\mathcal{B}_d} [\delta\boldsymbol{u}^+ - \delta\boldsymbol{u}^-]\cdot\boldsymbol{t}^n\, dA. \tag{45}$$

Note that (45) reduces down to classical expression when there is no jump in displacement variations ($\delta\boldsymbol{u}^+ = \delta\boldsymbol{u}^-$). We complete the formulation by rearranging (45) as

$$\boxed{\int_{\mathcal{B}/\partial\mathcal{B}_d} \delta\boldsymbol{\varepsilon} :\ \boldsymbol{\sigma}\, dV + \int_{\partial\mathcal{B}_d} [\![\delta\boldsymbol{u}]\!]\cdot\boldsymbol{t}^n\, dA = \int_{\partial\mathcal{B}_\sigma} \delta\boldsymbol{u}\cdot\boldsymbol{t}\, dA + \int_{\mathcal{B}/\partial\mathcal{B}_d} \delta\boldsymbol{u}\cdot\rho\boldsymbol{b}\, dV} \tag{46}$$

where $[\![\delta\boldsymbol{u}]\!]$ stands for the jump in displacement variations along $\partial\mathcal{B}_d$. To conclude, we point out that the principle outlined has nothing to do with conservation of mechanical energy (although as it looks like) and even apply when the mechanical energy is not conserved (see, for example, [44]).

3.1.2. Kinematics

Let consider the body seperated into two parts, $\mathcal{B}^+$ and $\mathcal{B}^-$, by a single surface of material discontinuity (Figure 10). The point of departure in kinematically optimal symmetric (KOS) formulation is to decompose displacement field into continuous and discontinuous parts as

$$\boxed{\boldsymbol{u} = \underbrace{\hat{\boldsymbol{u}}}_{\text{continuous}} + \underbrace{\tilde{\boldsymbol{u}}}_{\text{discontinuous}}} \,. \tag{47}$$

Then we presuppose the following form for discontinuous part:

$$\tilde{\boldsymbol{u}} = (H_{\partial\mathcal{B}_d} - \varphi_h)\bar{\boldsymbol{u}} \tag{48}$$

where $H_{\partial\mathcal{B}_d}$ is the heaviside step function placed on $\partial\mathcal{B}_d$ and takes the values

$$H_{\partial\mathcal{B}_d} = \begin{cases} 1, & \forall\, \boldsymbol{x} \in \mathcal{B}^+ \\ 0, & \text{otherwise} \end{cases} , \tag{49}$$

whereas φ_h is a continuous function of the form

$$\varphi_h = \begin{cases} 1, & \forall\, \boldsymbol{x} \in \mathcal{B}^+/\mathcal{B}_h \\ 0, & \forall\, \boldsymbol{x} \in \mathcal{B}^-/\mathcal{B}_h \end{cases} , \tag{50}$$

and, $\bar{\boldsymbol{u}}$ is a constant function of space coordinates, which gives the amount of jump in the displacement field.
The kinematic description by (48) gives a local character to the discontinuous part of the displacement field, which in turn removes difficulty on imposition of essential boundary conditions (provided $\partial\mathcal{B}_h \cap \partial\mathcal{B}_u = \emptyset$) . For a detailed discussion of this topic (see [57; 76]). In addition, it is worth to point out that the selection of the subdomain $\mathcal{B}_h$, as far as it encloses $\partial\mathcal{B}_d$, and φ_h, unless (50) is violated, is completely arbitrary.
Finally, with the insertion of (48), jump in the displacement field and the strain are obtained as

$$\boxed{[\![\boldsymbol{u}]\!] = \boldsymbol{u}^+ - \boldsymbol{u}^- = \bar{\boldsymbol{u}}} \,, \tag{51}$$

$$\boxed{\boldsymbol{\varepsilon} = (\boldsymbol{u} \otimes \nabla)^s = \underbrace{(\hat{\boldsymbol{u}} \otimes \nabla)^s - ([\![\boldsymbol{u}]\!] \otimes \nabla\varphi_h)^s}_{\boldsymbol{\varepsilon}_{\mathcal{B}/\partial\mathcal{B}_d}} + \underbrace{\delta_{\partial\mathcal{B}_d}([\![\boldsymbol{u}]\!] \otimes \boldsymbol{n})^s}_{\boldsymbol{\varepsilon}_{\partial\mathcal{B}_d}}} \tag{52}$$

where $\nabla = \partial/\partial\boldsymbol{x}$ is the gradient vector, $(\cdot)^s$ indicates the symmetric part of $(\cdot)$, and $\delta_{\partial\mathcal{B}_d}$ is the Dirac distribution placed at the discontinuity, which makes the strain field unbounded along $\partial\mathcal{B}_d$. However, this has no consequence for our formulation, because the kinematic quantity used on singular surface is described by the jump in the displacement field (51), which is work conjugate to the traction transmitted (see (46)). A different approach has been developed in [57; 58; 63; 77; 76], where the authors showed that materials exhibiting softening behavior are compatible with appearance of strong discontinuities (jump in the displacement field) in the post-peak regime, and with the so-called strong discontinuity analysis they proved that continuum constitutive equations are compatible with unbounded strains, if some special requirements are met, where, for instance in softening plasticity, the most remarkable one is the distributional character of the softening modulus.

3.1.3. Finite Element Formulation

In this section implementation aspects and solution procedure are investigated. Before a detailed description is given, some definitions are made regarding the input fields mostly used in all conventional finite element codes. Let consider the discretization of the domain of interest by standard displacement finite elements given in Figure 11 such that the discontinuity aligns arbitrarily with the mesh. Related to this mesh, following fields are defined:

- n_{elem}: It is the total number of finite elements in the given mesh.
- n_{nodes}: It is the total number of nodes in the given mesh.
- n_{dim}: It is the space dimension, e.g., $n_{dim} = 2$ for plane problems.
- n_{max}: It is the maximum number of element, which could be connected to a node.
- $\alpha_{\bar{J}}$: It is the number of element connected to global node $\bar{J}$.
- nen: It is, for a mesh made up of same element type, the number of nodes per element.
- con: It is an array of dimension $(n_{elem} \times nen)$, and stores the information about element connectivity. Element $con(I, J)$ returns the global node number $\bar{J}$ corresponding to J th local node of I th element.
- dof: It is an array of dimension $(n_{nodes} \times n_{dim})$, and stores the information about global degrees of freedom assigned to nodes of finite element mesh. Element $dof(I, J)$ returns the global degree of freedom number in J th direction assigned to global node I.
- $nsup$: It is an array of dimension $(n_{nodes} \times n_{max})$, and stores the information about the elements connected to nodes of finite element mesh. Element $nsup(I, J)$ returns the element number $\bar{J}$ of the J th element connected to global node I. In standard formulation there is no need for this input field. However, it is used in the following formulation, and have been found very efficient in node activation mechanism, which will be discussed in the following chapter.

After having introduced the input fields, the approximation to position of a point $\boldsymbol{x} \in \mathcal{B}$ takes the form in standard vector notation ([71; 72]).

$$^{h}\boldsymbol{x} = \sum_{I=1}^{n_{nodes}} N_I^g(\boldsymbol{x})\, \boldsymbol{x}_I \tag{53}$$

where $^{h}\boldsymbol{x} = [^{h}x_1 \ldots ^{h}x_{n_{dim}}]^T$ is the position vector, $N_I^g(\boldsymbol{x})$ is the continuous global shape function belonging to the node I, which takes the value 1 at that node and vanish at all other nodes of the mesh, and $\boldsymbol{x}_I$ is the position vector of I th node. With this notation, the position vector within an element domain $\mathcal{B}^e$ $(e = 1, \ldots, n_{elem})$ is interpolated from the nodes of element as

$$^{h}\boldsymbol{x}^e = \sum_{I=1}^{nen} N_I^e(\boldsymbol{x}(\boldsymbol{\xi}))\, \boldsymbol{x}_I^e \tag{54}$$

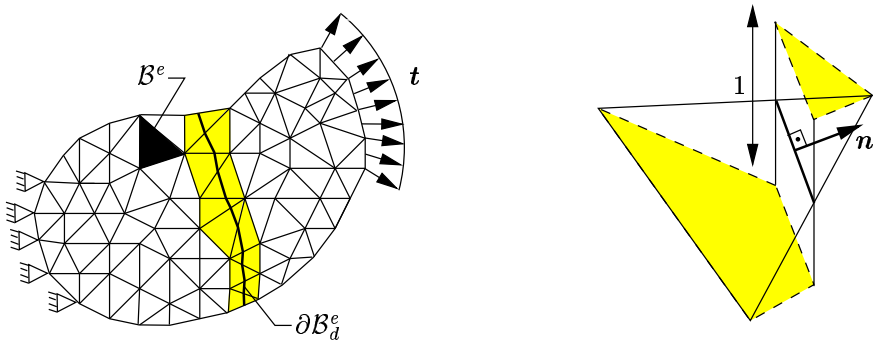

a. b.

Figure 11: a.) Discretization of the domain by finite elements. Colored elements are enhanced with internal degrees of freedom representing the displacement jump inside the element. b.) Discontinuous mode added to elements crossed by discontinuity.

where ${}^h\boldsymbol{x}^e = [{}^h x_1^e \dots {}^h x_{n_{dim}}^e]^T$ is the position vector of a point inside element domain, $N_I^e(\boldsymbol{x}(\boldsymbol{\xi}))$ is I th nodal shape function of element, which is reparametrized in terms of isoparametric coordinates $\boldsymbol{\xi}$, and possesses the same properties as global shape function defined in (53), i.e., it is continuous inside element domain, takes value 1 at node I and vanishes at all other nodes of element, and $\boldsymbol{x}_I^e$ is the position vector of I th node of the element. From this point on, the bracket terms corresponding to global and element shape functions are omitted to have clear appearance. When the displacement jump is assumed to be piecewise constant within each element domain, i.e., if no interelement continuity be enforced on displacement jump, the approximation made to the displacement field (47), in view of (48), over the whole domain takes the form in vector notation

$$\boxed{{}^h\boldsymbol{u} = \underbrace{\sum_{I=1}^{n_{nodes}} N_I^g \boldsymbol{d}_I}_{\text{continuous}} + \underbrace{\sum_{e=1}^{n_{elem}} \chi^e [H_{\partial\mathcal{B}_d^e} - \sum_{K\in\mathcal{B}^{e+}} N_K^e]\boldsymbol{g}^e}_{\text{discontinuous}}} \tag{55}$$

where ${}^h\boldsymbol{u} = [u_1^h \dots u_{n_{dim}}^h]^T$ is the displacement vector, $\boldsymbol{d}_I = [d_{I_1} \dots d_{I_{n_{dim}}}]^T$ is the vector of standard nodal degrees of freedom, $\boldsymbol{g}^e = [g_1^e \dots g_{n_{dim}}^e]^T$ is the vector of internal degrees of freedom representing the displacement jump within the element, and χ^e, $H_{\partial\mathcal{B}_d^e}$ are collocation and heaviside step functions of the form

$$\chi^e = \begin{cases} 1, & \forall\, \boldsymbol{x} \in \mathcal{B}^e \\ 0, & \text{otherwise} \end{cases}, \tag{56}$$

$$H_{\partial\mathcal{B}_d^e} = \begin{cases} 1, & \forall\, \boldsymbol{x} \in \mathcal{B}^{e+} \\ 0, & \forall\, \boldsymbol{x} \in \mathcal{B}^{e-} \end{cases}. \tag{57}$$

Here note that the function φ_h given in (50) is constructed by

$$\varphi_h^e = \sum_{K\in\mathcal{B}^{e+}} N_K^e \tag{58}$$

in an element domain $\mathcal{B}^e$, which exactly satisfies conditions given therein.
(55), when written in an element domain, then takes the form

$$\boxed{{}^h\boldsymbol{u}^e = \underbrace{\sum_{I=1}^{nen} N_I^e \boldsymbol{d}_I^e}_{\text{continuous}} + \underbrace{[H_{\partial\mathcal{B}_d^e} - \sum_{K\in\mathcal{B}^e{}^+} N_K^e]\boldsymbol{g}^e}_{\text{discontinuous}}} \tag{59}$$

and, in view of (51), (52) and (59), jump in the displacement field and the strain are obtained as

$$\boxed{[\![\boldsymbol{u}]\!]^e = \boldsymbol{g}^e} \tag{60}$$

$$\boldsymbol{\varepsilon}^e = \underbrace{\sum_{I=1}^{nen} \boldsymbol{B}_I^e \boldsymbol{d}_I^e - \Big[\sum_{K\in\mathcal{B}^e{}^+} \boldsymbol{B}_K^e\Big]\boldsymbol{g}^e}_{\boldsymbol{\varepsilon}_{\mathcal{B}^e/\partial\mathcal{B}_d^e}} + \underbrace{\delta_{\partial\mathcal{B}_d^e}\boldsymbol{n}^e\boldsymbol{g}^e}_{\boldsymbol{\varepsilon}_{\partial\mathcal{B}_d^e}} \tag{61}$$

where $\boldsymbol{\varepsilon}^e$, $\boldsymbol{n}^e$ and $\boldsymbol{B}_I^e$ are the vector form of the strain tensor, the matrix form of normal to the discontinuity and nodal discrete strain operator, respectively, and they are defined, for $n_{dim} = 3$, as

$$\boldsymbol{\varepsilon}^e = [\varepsilon_{11}^e\ \varepsilon_{22}^e\ \varepsilon_{33}^e\ 2\varepsilon_{12}^e\ 2\varepsilon_{23}^e\ 2\varepsilon_{31}^e]^T, \tag{62}$$

$$\boldsymbol{n}^e = \begin{bmatrix} n_1^e & 0 & 0 & n_2^e & 0 & n_3^e \\ 0 & n_2^e & 0 & n_1^e & n_3^e & 0 \\ 0 & 0 & n_3^e & 0 & n_2^e & n_1^e \end{bmatrix}^T, \tag{63}$$

$$\boldsymbol{B}_I^e = \begin{bmatrix} \partial N_I^e/\partial x_1 & 0 & 0 & \partial N_I^e/\partial x_2 & 0 & \partial N_I^e/\partial x_3 \\ 0 & \partial N_I^e/\partial x_2 & 0 & \partial N_I^e/\partial x_1 & \partial N_I^e/\partial x_3 & 0 \\ 0 & 0 & \partial N_I^e/\partial x_3 & 0 & \partial N_I^e/\partial x_2 & \partial N_I^e/\partial x_1 \end{bmatrix}^T. \tag{64}$$

and $\delta_{\partial\mathcal{B}_d^e}$ is the Dirac delta function placed on the discontinuity line inside the element domain.
With the definition of discrete enhanced strain operator

$$\boldsymbol{G}^e = -\sum_{K\in\mathcal{B}^e{}^+} \boldsymbol{B}_K^e, \tag{65}$$

final form for the strain in the element domain is obtained as

$$\boxed{\boldsymbol{\varepsilon}^e = \underbrace{\sum_{I=1}^{nen} \boldsymbol{B}_I^e \boldsymbol{d}_I^e + \boldsymbol{G}^e\boldsymbol{g}^e}_{\boldsymbol{\varepsilon}_{\mathcal{B}^e/\partial\mathcal{B}_d^e}} + \underbrace{\delta_{\partial\mathcal{B}_d^e}\boldsymbol{n}^e\boldsymbol{g}^e}_{\boldsymbol{\varepsilon}_{\partial\mathcal{B}_d^e}}}. \tag{66}$$

After having obtained the expressions for the strain and jump in the displacement field, we consider the virtual work expression (66) for the body, and write it, in vector notation, as

$$\sum_{e=1}^{n_{elem}} \left[\int_{\mathcal{B}^e} \delta\boldsymbol{\varepsilon}^{e^T}\boldsymbol{\sigma}^e\, dV + \int_{\partial\mathcal{B}_d^e} \delta\boldsymbol{g}^{e^T}\boldsymbol{t}^{n^e}\, dA\right] = \sum_{\bar{i}=1}^{n_{nodes}} \delta\boldsymbol{d}_{\bar{i}}^T \boldsymbol{f}_{ext_{\bar{i}}} \tag{67}$$

where $\boldsymbol{\sigma}^e$, $\boldsymbol{t}^{n^e}$ are the vector form of stress tensor and traction transmitted through discontinuity, respectively, which, for $n_{dim} = 3$, are given by

$$\boldsymbol{\sigma}^e = [\sigma^e_{11}\ \sigma^e_{22}\ \sigma^e_{33}\ \sigma^e_{12}\ \sigma^e_{23}\ \sigma^e_{31}]^T, \tag{68}$$

$$\boldsymbol{t}^{n^e} = [t^{n^e}_1\ t^{n^e}_2\ t^{n^e}_3]^T, \tag{69}$$

and

$$\boldsymbol{f}_{ext_{\bar{i}}} = \sum_{e=1}^{\alpha_{\bar{i}}} \boldsymbol{f}^{\bar{e}}_{ext_{\bar{i}}} \tag{70}$$

with

$$\boldsymbol{f}^{\bar{e}}_{ext_{\bar{i}}} = \int_{\partial\mathcal{B}^{\bar{e}}\cap\partial\mathcal{B}_\sigma} N^{\bar{e}}_i \boldsymbol{t}^{\bar{e}}\, dA + \int_{\mathcal{B}^{\bar{e}}} N^{\bar{e}}_i \rho^{\bar{e}} \boldsymbol{b}^{\bar{e}}\, dV \tag{71}$$

where $\rho^{\bar{e}}$, $\boldsymbol{b}^{\bar{e}}$ are the the density field and the vector field of body force per unit mass defined in the element domain, respectively, and $\boldsymbol{t}^{\bar{e}}$ represents the surface tractions applied on $\partial\mathcal{B}^{\bar{e}} \cap \partial\mathcal{B}_\sigma$. Note that first integral in (71) is meaningful only for the elements which have an edge located at the outer boundary, and $\bar{e} = nsup(\bar{i}, e)$ and $i = con^{-1}(\bar{e}, \bar{i})$. Insertion of variation of (66) into (67) then leads us to

$$\begin{aligned}\sum_{e=1}^{n_{elem}} \Bigg[\sum_{i=1}^{nen} \Big(\delta \boldsymbol{d}^{e^T}_{\bar{i}} \int_{\mathcal{B}^e} \boldsymbol{B}^{e^T}_i \boldsymbol{\sigma}^e\, dV \Big) + \\ \delta \boldsymbol{g}^{e^T} \Big(\int_{\mathcal{B}^e} \boldsymbol{G}^{e^T} \boldsymbol{\sigma}^e\, dV + \int_{\partial\mathcal{B}^e_d} \boldsymbol{t}^{n^e}\, dA \Big) \Bigg] = \sum_{\bar{i}=1}^{n_{nodes}} \delta \boldsymbol{d}^T_{\bar{i}} \boldsymbol{f}_{ext_{\bar{i}}}\end{aligned} \tag{72}$$

which with the definitions

$$\boldsymbol{f}^e_{int_{\bar{i}}} = \int_{\mathcal{B}^e} \boldsymbol{B}^{e^T}_i \boldsymbol{\sigma}^e\, dV \tag{73}$$

and

$$\boldsymbol{h}^e = \int_{\mathcal{B}^e} \boldsymbol{G}^{e^T} \boldsymbol{\sigma}^e\, dV + \int_{\partial\mathcal{B}^e_d} \boldsymbol{t}^{n^e}\, dA \tag{74}$$

takes the form

$$\sum_{e=1}^{n_{elem}} \Bigg[\sum_{i=1}^{nen} \delta \boldsymbol{d}^{e^T}_{\bar{i}} \boldsymbol{f}^e_{int_{\bar{i}}} + \delta \boldsymbol{g}^{e^T} \boldsymbol{h}^e \Bigg] = \sum_{\bar{i}=1}^{n_{nodes}} \delta \boldsymbol{d}^T_{\bar{i}} \boldsymbol{f}_{ext_{\bar{i}}}. \tag{75}$$

Note that, in (75) $\bar{i} = con(e, i)$. Further, it is important to note that (73) is the contribution of element e to the discrete equilibrium equation written at global node $\bar{i}$.
To really make a physical interpretation, we put (75) into a different format as

$$\sum_{\bar{i}=1}^{n_{nodes}} \Bigg[\delta \boldsymbol{d}^T_{\bar{i}} \Big(\sum_{e=1}^{\alpha_{\bar{i}}} \boldsymbol{f}^{\bar{e}}_{int_{\bar{i}}} \Big) \Bigg] + \sum_{e=1}^{n_{elem}} \delta \boldsymbol{g}^{e^T} \boldsymbol{h}^e = \sum_{\bar{i}=1}^{n_{nodes}} \delta \boldsymbol{d}^T_{\bar{i}} \boldsymbol{f}_{ext_{\bar{i}}} \tag{76}$$

where $\bar{e} = nsup(\bar{i}, e)$. By defining

$$\boldsymbol{f}_{int_{\bar{i}}} = \sum_{e=1}^{\alpha_{\bar{i}}} \boldsymbol{f}^{\bar{e}}_{int_{\bar{i}}} \tag{77}$$

the most compact form is arrived at as

$$\boxed{\sum_{\bar{i}=1}^{n_{nodes}} \Big[\delta \boldsymbol{d}^T_{\bar{i}} \Big(\boldsymbol{f}_{int_{\bar{i}}} - \boldsymbol{f}_{ext_{\bar{i}}} \Big) \Big] + \sum_{e=1}^{n_{elem}} \delta \boldsymbol{g}^{e^T} \boldsymbol{h}^e = 0}\ . \tag{78}$$

By considering the independent variations of nodal displacements ($\delta \boldsymbol{d}_{\bar{i}}^{e^T}$) and displacement jumps ($\delta \boldsymbol{g}^{e^T}$) within the elements, (78) yields following set of equations:

$$\boxed{\begin{aligned} \boldsymbol{f}_{\bar{i}} = \boldsymbol{f}_{int_{\bar{i}}} - \boldsymbol{f}_{ext_{\bar{i}}} &= \boldsymbol{0} \quad (\bar{i} = 1, \ldots, n_{nodes}) \\ \boldsymbol{h}^e &= \boldsymbol{0} \quad (e = 1, \ldots, n_{elem}) \end{aligned}}. \tag{79}$$

We refer to $(79)_1$ as the discrete nodal equilibrium equations, and to $(79)_2$ as the internal equilibrium equations. Note that the number of equations provided in (79) is equal to total number of unknowns. However, in order to account for increasing number of total internal degrees of freedom ($\boldsymbol{g}^e$) in case of evolving discontinuity, the size of the system matrices have to be continuously readjusted, which brings some technical difficulties in implementation. To overcome these problems we use the structure provided by internal equilibrium equations to condense internal degrees of freedom at element level. By doing so the size of the global matrices do not change as the discontinuity propagates, if the same mesh is used throughout the analysis (no mesh adaptivity etc.).
Next, we discuss the condensation procedure. Consider the "k" th iteration step in a <u>one</u> full global Newton iteration, at which we seek to improve solution and advance it from $\boldsymbol{d}_{\bar{i}}^{<k>}$ to $\boldsymbol{d}_{\bar{i}}^{<k+1>}$ ($\bar{i} = 1, \ldots, n_{nodes}$) and from $\boldsymbol{g}^{e^{<k>}}$ to $\boldsymbol{g}^{e^{<k+1>}}$ ($e = 1, \ldots, n_{elem}$). We explain the condensation procedure by considering one of the nodal discrete equilibrium equations, say

$$\boxed{\boldsymbol{f}_{\bar{i}} = \boldsymbol{0} \quad (\bar{i} \leq n_{nodes})}. \tag{80}$$

Linearization of (80) around the current iteration step reads as

$$\mathrm{Lin}[\boldsymbol{f}_{\bar{i}}] = \boldsymbol{f}_{\bar{i}}^{<k>} + \Delta \boldsymbol{f}_{\bar{i}}^{<k>} \tag{81}$$

where

$$\boldsymbol{f}_{\bar{i}}^{<k>} = \sum_{e=1}^{\alpha_{\bar{i}}} \boldsymbol{f}_{int_{\bar{i}}}^{\bar{e}^{<k>}} - \boldsymbol{f}_{ext_{\bar{i}}}^{<k>} \tag{82}$$

and

$$\Delta \boldsymbol{f}_{\bar{i}}^{<k>} = \sum_{e=1}^{\alpha_{\bar{i}}} \Delta \boldsymbol{f}_{int_{\bar{i}}}^{\bar{e}^{<k>}} \tag{83}$$

with $\bar{e} = nsup(\bar{i}, e)$. (83) can be expressed, in view of definition (73), as

$$\Delta \boldsymbol{f}_{\bar{i}}^{<k>} = \sum_{e=1}^{\alpha_{\bar{i}}} \left[\int_{\mathcal{B}^{\bar{e}}} \boldsymbol{B}_{\bar{i}}^{\bar{e}^T} \Delta \boldsymbol{\sigma}^{\bar{e}^{<k>}} \, dV \right] \tag{84}$$

where

$$\Delta \boldsymbol{\sigma}^{\bar{e}^{<k>}} = \underbrace{\left. \frac{\partial \boldsymbol{\sigma}^{\bar{e}}}{\partial \boldsymbol{\varepsilon}^{\bar{e}}} \right|^{<k>}}_{\boldsymbol{C}^{\bar{e}^{<k>}}} \Delta \boldsymbol{\varepsilon}^{\bar{e}^{<k>}} \tag{85}$$

with

$$\Delta \boldsymbol{\varepsilon}^{\bar{e}^{<k>}} = \sum_{j=1}^{nen} \boldsymbol{B}_{\bar{j}}^{\bar{e}} \Delta \boldsymbol{d}_{\bar{j}}^{<k>} + \boldsymbol{G}^{\bar{e}} \Delta \boldsymbol{g}^{\bar{e}^{<k>}}. \tag{86}$$

Note that $\boldsymbol{C}^{\bar{e}<k>}$ in (85) is the algorithmic tangent moduli, which represents the sensitivity of stresses to the total strains within the element domain. Combination of (85) and (86) and then insertion of the result into (84) yields

$$\begin{aligned}\Delta \boldsymbol{f}_{\bar{i}}^{<k>} = \sum_{e=1}^{\alpha_{\bar{i}}} \sum_{j=1}^{nen} \left[\int_{\mathcal{B}^{\bar{e}}} \boldsymbol{B}_{\bar{i}}^{\bar{e}T} \boldsymbol{C}^{\bar{e}<k>} \boldsymbol{B}_{\bar{j}}^{\bar{e}} \, dV \right] \Delta \boldsymbol{d}_{\bar{j}}^{<k>} + \\ \sum_{e=1}^{\alpha_{\bar{i}}} \left[\int_{\mathcal{B}^{\bar{e}}} \boldsymbol{B}_{\bar{i}}^{\bar{e}T} \boldsymbol{C}^{\bar{e}<k>} \boldsymbol{G}^{\bar{e}} \, dV \right] \Delta \boldsymbol{g}^{\bar{e}<k>}\end{aligned} \tag{87}$$

which by the definitions

$$\boldsymbol{K}_{\bar{i}\bar{j}}^{\bar{e}<k>} = \int_{\mathcal{B}^{\bar{e}}} \boldsymbol{B}_{\bar{i}}^{\bar{e}T} \boldsymbol{C}^{\bar{e}<k>} \boldsymbol{B}_{\bar{j}}^{\bar{e}} \, dV \tag{88}$$

and

$$\boldsymbol{H}_{\bar{i}}^{\bar{e}<k>} = \int_{\mathcal{B}^{\bar{e}}} \boldsymbol{B}_{\bar{i}}^{\bar{e}T} \boldsymbol{C}^{\bar{e}<k>} \boldsymbol{G}^{\bar{e}} \, dV \tag{89}$$

takes the form

$$\boxed{\Delta \boldsymbol{f}_{\bar{i}}^{<k>} = \sum_{e=1}^{\alpha_{\bar{i}}} \sum_{j=1}^{nen} \boldsymbol{K}_{\bar{i}\bar{j}}^{\bar{e}<k>} \Delta \boldsymbol{d}_{\bar{j}}^{<k>} + \sum_{e=1}^{\alpha_{\bar{i}}} \boldsymbol{H}_{\bar{i}}^{\bar{e}<k>} \Delta \boldsymbol{g}^{\bar{e}<k>}} \, . \tag{90}$$

Insertion of (90) into (81) then yields

$$\mathrm{Lin}[\boldsymbol{f}_{\bar{i}}] = \sum_{e=1}^{\alpha_{\bar{i}}} \boldsymbol{f}_{int_{\bar{i}}}^{\bar{e}<k>} - \boldsymbol{f}_{ext_{\bar{i}}}^{<k>} + \sum_{e=1}^{\alpha_{\bar{i}}} \sum_{j=1}^{nen} \boldsymbol{K}_{\bar{i}\bar{j}}^{\bar{e}<k>} \Delta \boldsymbol{d}_{\bar{j}}^{<k>} + \sum_{e=1}^{\alpha_{\bar{i}}} \boldsymbol{H}_{\bar{i}}^{\bar{e}<k>} \Delta \boldsymbol{g}^{\bar{e}<k>} \tag{91}$$

At this stage we consider the internal equilibrium equation corresponding to element $\bar{e}$, which reads as

$$\boxed{\boldsymbol{h}^{\bar{e}} = \boldsymbol{0} \quad (\bar{e} \leq n_{elem})} \, . \tag{92}$$

If this equation is linearized around the current iteration step, it is arrived at that

$$\mathrm{Lin}[\boldsymbol{h}^{\bar{e}}] = \boldsymbol{h}^{\bar{e}<k>} + \Delta \boldsymbol{h}^{\bar{e}<k>} = \boldsymbol{0} \tag{93}$$

where $\boldsymbol{h}^{\bar{e}<k>}$ is given by (74) and

$$\Delta \boldsymbol{h}^{\bar{e}<k>} = \int_{\mathcal{B}^{\bar{e}}} \boldsymbol{G}^{\bar{e}T} \Delta \boldsymbol{\sigma}^{\bar{e}<k>} + \int_{\partial \mathcal{B}_d^{\bar{e}}} \Delta \boldsymbol{t}^{n^{\bar{e}}<k>} \, dA \tag{94}$$

Expression for the second integrand is given by

$$\Delta \boldsymbol{t}^{\bar{n}e<k>} = \underbrace{\left. \frac{\partial \boldsymbol{t}^{n^{\bar{e}}}}{\partial \boldsymbol{g}^{\bar{e}}} \right|^{<k>}}_{\boldsymbol{T}^{\bar{e}<k>}} \Delta \boldsymbol{g}^{\bar{e}<k>} \, . \tag{95}$$

where $\boldsymbol{T}^{\bar{e}<k>}$ is the algorithmic tangent moduli for the sensitivity of tractions transmitted through discontinuity with respect to jumps in the total displacement within the element

domain. Finally, with the insertion of (85), (95) into (94) we reach

$$\Delta \boldsymbol{h}^{\bar{e}<k>} = \sum_{j=1}^{nen} \Bigg[\underbrace{\int_{\mathcal{B}^{\bar{e}}} \boldsymbol{G}^{\bar{e}T} \boldsymbol{C}^{\bar{e}<k>} \boldsymbol{B}_{\bar{j}}^{\bar{e}} \, dV}_{\boldsymbol{H}_{\bar{j}}^{\bar{e}<k>T}} \Bigg] \Delta \boldsymbol{d}_{\bar{j}}^{<k>} + \Bigg[\int_{\mathcal{B}^{\bar{e}}} \boldsymbol{G}^{\bar{e}T} \boldsymbol{C}^{\bar{e}<k>} \boldsymbol{G}^{\bar{e}} \, dV + \int_{\partial \mathcal{B}_d^{\bar{e}}} \boldsymbol{T}^{\bar{e}<k>} \, dA \Bigg] \Delta \boldsymbol{g}^{\bar{e}<k>} \tag{96}$$

which with the definition

$$\boldsymbol{\Gamma}^{\bar{e}<k>} = \int_{\mathcal{B}^{\bar{e}}} \boldsymbol{G}^{\bar{e}T} \boldsymbol{C}^{\bar{e}<k>} \boldsymbol{G}^{\bar{e}} \, dV + \int_{\partial \mathcal{B}_d^{\bar{e}}} \boldsymbol{T}^{\bar{e}<k>} \, dA \tag{97}$$

takes the final form

$$\boxed{\Delta \boldsymbol{h}^{\bar{e}<k>} = \sum_{j=1}^{nen} \boldsymbol{H}_{\bar{j}}^{\bar{e}<k>T} \Delta \boldsymbol{d}_{\bar{j}}^{<k>} + \boldsymbol{\Gamma}^{\bar{e}<k>} \Delta \boldsymbol{g}^{\bar{e}<k>}} \, . \tag{98}$$

By substituting (98) into (93), we are led to

$$\mathrm{Lin}[\boldsymbol{h}^{\bar{e}}] = \boldsymbol{h}^{\bar{e}<k>} + \sum_{j=1}^{nen} \boldsymbol{H}_{\bar{j}}^{\bar{e}<k>T} \Delta \boldsymbol{d}_{\bar{j}}^{<k>} + \boldsymbol{\Gamma}^{\bar{e}<k>} \Delta \boldsymbol{g}^{\bar{e}<k>} = \boldsymbol{0} \tag{99}$$

from which incremental displacement jumps $\Delta \boldsymbol{g}^{\bar{e}<k>}$ can be extracted as

$$\boxed{\Delta \boldsymbol{g}^{\bar{e}<k>} = -\boldsymbol{\Gamma}^{\bar{e}<k>-1} \Bigg[\boldsymbol{h}^{\bar{e}<k>} + \sum_{j=1}^{nen} \boldsymbol{H}_{\bar{j}}^{\bar{e}<k>T} \Delta \boldsymbol{d}_{\bar{j}}^{<k>} \Bigg]} \, . \tag{100}$$

Here note that since internal degrees of freedom $\boldsymbol{g}^{\bar{e}<k-1>}$ are eliminated at the element level by the procedure outlined above at the "k-1" th iteration in one full global Newton iteration, it is not possible to update them outside the element subrouitine. Therefore, when the element subroutine is entered, the first thing to be done is to update internal degrees of freedom, which for the "k" th iteration reads as

$$\boldsymbol{g}^{\bar{e}<k>} = \boldsymbol{g}^{\bar{e}<k-1>} + \Delta \boldsymbol{g}^{\bar{e}<k-1>} \tag{101}$$

where increments of internal degrees of freedom are given by

$$\Delta \boldsymbol{g}^{\bar{e}<k-1>} = -\boldsymbol{\Gamma}^{\bar{e}<k-1>-1} \Bigg[\boldsymbol{h}^{\bar{e}<k-1>} + \sum_{j=1}^{nen} \boldsymbol{H}_{\bar{j}}^{\bar{e}<k-1>T} \Delta \boldsymbol{d}_{\bar{j}}^{<k-1>} \Bigg] \tag{102}$$

similar to (100). The equation (102) implies that when explicit (forward Euler) integration scheme is used to update internal degrees of freedom the terms $\boldsymbol{g}^{\bar{e}<k-1>}$, $\boldsymbol{\Gamma}^{\bar{e}<k-1>}$, $\boldsymbol{H}^{\bar{e}<k-1>}$, $\boldsymbol{h}^{\bar{e}<k-1>}$ and $\Delta \boldsymbol{d}_{\bar{j}}^{<k-1>}$ belonging to "k-1" th iteration step must be stored as element history. However, if implicit (backward Euler) scheme is used to make this update

storage of $\boldsymbol{g}^{\bar{e}<k-1>}$, $\boldsymbol{h}^{\bar{e}<k-1>}$ and $\Delta\boldsymbol{d}_{\bar{j}}^{<k-1>}$ as element history is enough. Note that in this implicit update increments of internal degrees of freedom are given by

$$\Delta\boldsymbol{g}^{\bar{e}<k-1>} = -\boldsymbol{\Gamma}^{\bar{e}<k>^{-1}}\left[\boldsymbol{h}^{\bar{e}<k-1>} + \sum_{j=1}^{nen}\boldsymbol{H}_{\bar{j}}^{\bar{e}<k>^T}\Delta\boldsymbol{d}_{\bar{j}}^{<k-1>}\right] \tag{103}$$

and $\boldsymbol{\Gamma}^{\bar{e}<k>}$, $\boldsymbol{H}^{\bar{e}<k>}$ are computable at "k" th iteration step, and in a flexible finite element code increments $\Delta\boldsymbol{d}_{\bar{j}}^{<k-1>}$ of nodal degrees of freedom can be provided from outside reducing the number of fields to be stored as element history.
Finally, with the insertion of (100) into (91) it is obtained that

$$\begin{aligned}\mathrm{Lin}[\boldsymbol{f}_{\bar{i}}] = \sum_{e=1}^{\alpha_{\bar{i}}}\left[\boldsymbol{f}_{int_{\bar{i}}}^{\bar{e}<k>} - \boldsymbol{H}_{\bar{i}}^{\bar{e}<k>}\boldsymbol{\Gamma}^{\bar{e}<k>^{-1}}\boldsymbol{h}^{\bar{e}<k>}\right] - \boldsymbol{f}_{ext_{\bar{i}}}^{<k>} + \\ \sum_{e=1}^{\alpha_{\bar{i}}}\sum_{j=1}^{nen}\left[\boldsymbol{K}_{\bar{i}\bar{j}}^{\bar{e}<k>} - \boldsymbol{H}_{\bar{i}}^{\bar{e}<k>}\boldsymbol{\Gamma}^{\bar{e}<k>^{-1}}\boldsymbol{H}_{\bar{j}}^{\bar{e}<k>^T}\right]\Delta\boldsymbol{d}_{\bar{j}}^{<k>}\end{aligned} \tag{104}$$

which is put into the most compact form by defining

$$\tilde{\boldsymbol{f}}_{\bar{i}}^{<k>} = \tilde{\boldsymbol{f}}_{int_{\bar{i}}}^{<k>} - \boldsymbol{f}_{ext_{\bar{i}}}^{<k>} \tag{105}$$

where

$$\tilde{\boldsymbol{f}}_{int_{\bar{i}}}^{<k>} = \sum_{e=1}^{\alpha_{\bar{i}}}\tilde{\boldsymbol{f}}_{int_{\bar{i}}}^{\bar{e}<k>} \tag{106}$$

with

$$\tilde{\boldsymbol{f}}_{int_{\bar{i}}}^{\bar{e}<k>} = \boldsymbol{f}_{int_{\bar{i}}}^{\bar{e}<k>} - \boldsymbol{H}_{\bar{i}}^{\bar{e}<k>}\boldsymbol{\Gamma}^{\bar{e}<k>^{-1}}\boldsymbol{h}^{\bar{e}<k>}, \tag{107}$$

and

$$\tilde{\boldsymbol{K}}_{\bar{i}\bar{j}}^{\bar{e}<k>} = \boldsymbol{K}_{\bar{i}\bar{j}}^{\bar{e}<k>} - \boldsymbol{H}_{\bar{i}}^{\bar{e}<k>}\boldsymbol{\Gamma}^{\bar{e}<k>^{-1}}\boldsymbol{H}_{\bar{j}}^{\bar{e}<k>^T} \tag{108}$$

as

$$\boxed{\mathrm{Lin}[\boldsymbol{f}_{\bar{i}}] = \tilde{\boldsymbol{f}}_{\bar{i}}^{<k>} + \sum_{e=1}^{\alpha_{\bar{i}}}\sum_{j=1}^{nen}\tilde{\boldsymbol{K}}_{\bar{i}\bar{j}}^{\bar{e}<k>}\Delta\boldsymbol{d}_{\bar{j}}^{<k>}}. \tag{109}$$

Here it is very important to note that (107) is the modified contribution of element $\bar{e}$ to the nodal equilibrium equation written at node $\bar{n}$, whereas (108) is the sensitivity of (107) to the displacement vector defined at the node $\bar{j} = con(\bar{e}, j)$. To make long story short, we summarize the assembly process described above in Box 3.

Box 3 : Assembly of Internal Force Vector and Tangent Matrix

initialize global matrices

FOR $\bar{i} = 1, \ldots, n_{nodes} \times n_{dim}$

$\mathbf{FG}(\bar{i}) = 0.0$

FOR $\bar{j} = 1, \ldots, n_{nodes} \times n_{dim}$

$\mathbf{KG}(\bar{i}, \bar{j}) = 0.0$

END

END

loop over nodes

FOR $\bar{i} = 1, \ldots, n_{nodes}$

1. get global degrees of freedom

FOR $I = 1, \ldots, n_{dim}$

$d_1(I) = dof(\bar{i}, I)$

END

2. loop over node support

a. get the element number $\bar{e} = nsup(\bar{i}, e)$

b. get the local node number $i = con^{-1}(\bar{e}, \bar{i})$

c. compute $\boldsymbol{f}_{int_{\bar{i}}}^{\bar{e}<k>} = \int_{\mathcal{B}^{\bar{e}}} \boldsymbol{B}_i^{\bar{e}T} \boldsymbol{\sigma}^{\bar{e}<k>} \, dV$

d. compute $\boldsymbol{H}_{\bar{i}}^{\bar{e}<k>} = \int_{\mathcal{B}^{\bar{e}}} \boldsymbol{B}_i^{\bar{e}T} \boldsymbol{C}^{\bar{e}<k>} \boldsymbol{G}^{\bar{e}} \, dV$

e. compute $\boldsymbol{\Gamma}^{\bar{e}<k>} = \int_{\mathcal{B}^{\bar{e}}} \boldsymbol{G}^{\bar{e}T} \boldsymbol{C}^{\bar{e}<k>} \boldsymbol{G}^{\bar{e}} \, dV + \int_{\partial \mathcal{B}_d^{\bar{e}}} \boldsymbol{T}^{\bar{e}<k>} \, dA$

f. compute modified internal forces $\tilde{\boldsymbol{f}}_{int_{\bar{i}}}^{\bar{e}<k>} = \boldsymbol{f}_{int_{\bar{i}}}^{\bar{e}<k>} - \boldsymbol{H}_{\bar{i}}^{\bar{e}<k>} \boldsymbol{\Gamma}^{\bar{e}<k>{}^{-1}} \boldsymbol{h}^{\bar{e}<k>}$

g. assemble modified internal forces

FOR $I = 1, \ldots, n_{dim}$

$\mathbf{FG}\Big(d_1(I)\Big) = \mathbf{FG}\Big(d_1(I)\Big) + \tilde{\boldsymbol{f}}_{int_{\bar{i}}}^{\bar{e}<k>}(I)$

END

h. loop over nodes of element $\bar{e}$

FOR $j = 1, \ldots, nen$

get global node number $\bar{j} = con(\bar{e}, j)$

get global degrees of freedom

FOR $I = 1, \ldots, n_{dim}$

$d_2(I) = dof(\bar{j}, I)$

END

compute $\boldsymbol{H}_{\bar{j}}^{\bar{e}<k>} = \int_{\mathcal{B}^{\bar{e}}} \boldsymbol{B}_j^{\bar{e}T} \boldsymbol{C}^{\bar{e}<k>} \boldsymbol{G}^{\bar{e}} \, dV$

compute $\boldsymbol{K}_{\bar{i}\bar{j}}^{\bar{e}<k>} = \int_{\mathcal{B}^{\bar{e}}} \boldsymbol{B}_i^{\bar{e}T} \boldsymbol{C}^{\bar{e}<k>} \boldsymbol{B}_j^{\bar{e}} \, dV$

compute modified tangent $\tilde{\boldsymbol{K}}_{\bar{i}\bar{j}}^{\bar{e}<k>} = \boldsymbol{K}_{\bar{i}\bar{j}}^{\bar{e}<k>} - \boldsymbol{H}_{\bar{i}}^{\bar{e}<k>} \boldsymbol{\Gamma}^{\bar{e}<k>{}^{-1}} \boldsymbol{H}_{\bar{j}}^{\bar{e}<k>{}^{T}}$

assemble modified tangent matrix

FOR $I = 1, \ldots, n_{dim}$

FOR $J = 1, \ldots, n_{dim}$

$\mathbf{KG}\Big(d_1(I), d_2(J)\Big) = \mathbf{KG}\Big(d_1(I), d_2(J)\Big) + \tilde{\boldsymbol{K}}_{\bar{i}\bar{j}}^{\bar{e}<k>}(I, J)$

END

END

END

END

3.2. Statically Optimal Symmetric (SOS) Formulation

3.2.1. Variational Framework

In what follows, we develop in a systematic manner the statically optimal symmetric formulation for the simulation of strong discontinuities starting from a three field mixed variational formulation with the so-called method of incompatible modes [75].
We formally start with the strain field of the form

$$\boxed{\boldsymbol{\varepsilon} = \underbrace{\hat{\boldsymbol{\varepsilon}}}_{\text{regular}} + \underbrace{\tilde{\boldsymbol{\varepsilon}}}_{\text{enhanced}}} \tag{110}$$

where $\hat{\boldsymbol{\varepsilon}}$ is the compatible part in the sense that it can directly be computed from displacement field using kinematic relations, and $\tilde{\boldsymbol{\varepsilon}}$ is the incompatible mode added, which we refer as the enhanced part of the strain field. Then, we resort to the following three standard variational equations

$$\left.\begin{aligned} \int_{\mathcal{B}} \delta\hat{\boldsymbol{\varepsilon}} : \boldsymbol{\sigma}\, dV - \int_{\partial\mathcal{B}_\sigma} \delta\boldsymbol{u} \cdot \boldsymbol{t}\, dA = 0 \\ \int_{\mathcal{B}} \delta\boldsymbol{\sigma} : [\hat{\boldsymbol{\varepsilon}} - \boldsymbol{\varepsilon}]\, dV = 0 \\ \int_{\mathcal{B}} \delta\boldsymbol{\varepsilon} : [-\boldsymbol{\sigma} + \boldsymbol{\sigma}(\boldsymbol{\varepsilon})]\, dV = 0 \end{aligned}\right\} \tag{111}$$

which can be consistently derived by taking the variation of so-called Hu-Washizu functional (see [71; 72])

$$\Pi_{HW}(\boldsymbol{u}, \boldsymbol{\varepsilon}, \boldsymbol{\sigma}) = \int_{\mathcal{B}} w(\boldsymbol{\varepsilon})\, dV - \int_{\mathcal{B}} \boldsymbol{\sigma} :\ (\hat{\boldsymbol{\varepsilon}} - \boldsymbol{\varepsilon})\, dV + \Pi_{ext.}(\boldsymbol{u}) \tag{112}$$

where w, $\boldsymbol{u}$ are the strain energy density and displacement field, respectively, whereas $\boldsymbol{\sigma}$, $\boldsymbol{\varepsilon}$ are the independent stress and strain fields. The equations (111) are valid for all admissible variations $(\delta\boldsymbol{u}, \delta\boldsymbol{\varepsilon}, \delta\boldsymbol{\sigma})$ of the actual displacements $(\boldsymbol{u})$, strains $(\boldsymbol{\varepsilon})$ and stresses $(\boldsymbol{\sigma})$, and $\boldsymbol{\sigma}(\boldsymbol{\varepsilon}), \boldsymbol{t}$ denote stresses computed from constitutive equations and prescribed surface tractions on portion $\partial\mathcal{B}_\sigma$ of outer boundary, respectively.
The next step is to put these variational statements into a more suitable format so that we could make a smooth transition to the modeling of strong discontinuities. We, for this purpose, start with taking the variation of the enhanced strain field given by (110), which leads us to

$$\delta\boldsymbol{\varepsilon} = \delta\hat{\boldsymbol{\varepsilon}} + \delta\tilde{\boldsymbol{\varepsilon}}. \tag{113}$$

When (113) is inserted into $(111)_3$ and resulting expression is combined with $(111)_1$, and (110) is substituted into $(111)_2$, we end up with the modified three field variational equations of the form

$$\left.\begin{aligned} \int_{\mathcal{B}} \delta\hat{\boldsymbol{\varepsilon}} : \boldsymbol{\sigma}(\boldsymbol{\varepsilon})\, dV - \int_{\partial\mathcal{B}_\sigma} \delta\boldsymbol{u} \cdot \boldsymbol{t}\, dA = 0 \\ \int_{\mathcal{B}} \delta\boldsymbol{\sigma} : \tilde{\boldsymbol{\varepsilon}}\, dV = 0 \\ \int_{\mathcal{B}} \delta\tilde{\boldsymbol{\varepsilon}} : [-\boldsymbol{\sigma} + \boldsymbol{\sigma}(\boldsymbol{\varepsilon})]\, dV = 0 \end{aligned}\right\}. \tag{114}$$

Now a critical assumption is made, which in turn completely removes the independent stress field from the formulation. We formally state that independent stresses ($\boldsymbol{\sigma}$) are orthogonal to the enhanced part of the strains ($\tilde{\boldsymbol{\varepsilon}}$) in the sense that

$$\boxed{\int_{\mathcal{B}} \boldsymbol{\sigma} : \tilde{\boldsymbol{\varepsilon}}\, dV = 0}. \tag{115}$$

If the variation of (115) is taken and $(114)_2$ is considered, it is arrived at that

$$\int_{\mathcal{B}} \boldsymbol{\sigma} : \delta\tilde{\boldsymbol{\varepsilon}}\, dV = 0. \tag{116}$$

Finally, insertion of the above equation into $(114)_3$ results in the following reduced form of the variational equations, namely,

$$\boxed{\begin{aligned} &\int_{\mathcal{B}} \delta\hat{\boldsymbol{\varepsilon}} : \boldsymbol{\sigma}(\boldsymbol{\varepsilon})\, dV - \int_{\partial\mathcal{B}_\sigma} \delta\boldsymbol{u} \cdot \boldsymbol{t}\, dA = 0 \\ &\int_{\mathcal{B}} \delta\tilde{\boldsymbol{\varepsilon}} : \boldsymbol{\sigma}(\boldsymbol{\varepsilon})\, dV = 0 \end{aligned}} \tag{117}$$

in terms of displacements ($\boldsymbol{u}$) and enhanced part of the strains ($\tilde{\boldsymbol{\varepsilon}}$). Here we note that due to orthogonality assumption made there is no need for interelement continuity be enforced on $\tilde{\boldsymbol{\varepsilon}}$ when constructing finite element approximations [75], which in turn permits condensation of internal degrees of freedom corresponding to enhanced strain field at element level.

3.2.2. Finite Element Formulation

The equations given in (117) play the central role in the development of SOS formulation for the modeling of strong discontinuities. Here $(117)_1$ resembles the weak form of equilibrium equations, whereas $(117)_2$ is devoted for the enforcement of the traction continuity through the discontinuity surface, which strictly speaking provides set of equations necessary to solve for additional internal parameters (jumps in the displacement field).
We start with discretizing the analysis domain $\mathcal{B} \subset \mathbb{R}^3$ by standard displacement finite elements such that discontinuity surface aligns arbitrarily with the mesh (Figure 12).

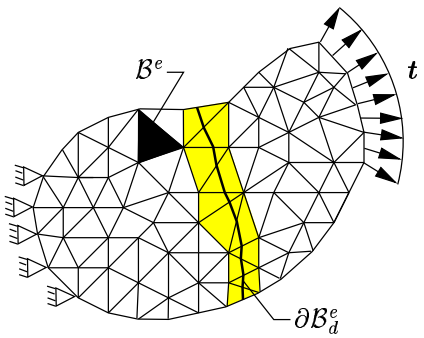

Figure 12: Discretization of the domain by finite elements. Colored elements are enhanced with internal degrees of freedom representing the displacement jump inside the element.

Then the displacement and strain interpolations inside an element domain takes the form

$$\left.\begin{aligned} {}^{h}\boldsymbol{u}^{e} &= \sum_{I=1}^{nen} N_I^e \boldsymbol{d}_I^e \\ \boldsymbol{\varepsilon}^{e} &= \sum_{I=1}^{nen} \boldsymbol{B}_I^e \boldsymbol{d}_I^e + \tilde{\boldsymbol{\varepsilon}}^{e} \end{aligned}\right\} \tag{118}$$

where ${}^{h}\boldsymbol{u}^{e} = [{}^{h}u_1^e \dots {}^{h}u_{n_{dim}}^e]^T$ is the displacement vector, N_I^e is the I th nodal shape function of the element e, $\boldsymbol{B}_I^e$ and $\boldsymbol{d}_I^e = [d_{I_1}^e \dots d_{I_{n_{dim}}}^e]^T$ are the nodal discrete strain operator and the vector of standard nodal degrees of freedom, and $\boldsymbol{\varepsilon}^e$, $\tilde{\boldsymbol{\varepsilon}}^e$ are the vector of total and enhanced strain fields, which are, for $n_{dim} = 3$, defined as

$$\left.\begin{aligned} \boldsymbol{\varepsilon}^{e} &= [\varepsilon_{11}^e\ \varepsilon_{22}^e\ \varepsilon_{33}^e\ 2\varepsilon_{12}^e\ 2\varepsilon_{23}^e\ 2\varepsilon_{31}^e]^T \\ \tilde{\boldsymbol{\varepsilon}}^{e} &= [\tilde{\varepsilon}_{11}^e\ \tilde{\varepsilon}_{22}^e\ \tilde{\varepsilon}_{33}^e\ 2\tilde{\varepsilon}_{12}^e\ 2\tilde{\varepsilon}_{23}^e\ 2\tilde{\varepsilon}_{31}^e]^T \end{aligned}\right\}. \tag{119}$$

In addition to the orthogonality condition, there are some other restrictions on the construction of enhanced part of the strain field [75]. First of all, it has to exclude any term belonging to the regular part of the strain field, if one really wishes to make enhancement. With this requirement the stability of the solution is guaranteed. Moreover, to improve convergence behavior it is forced to satisfy zero mean condition in an element domain, i.e.,

$$\boxed{\int_{\mathcal{B}^e} \tilde{\boldsymbol{\varepsilon}}^{e}\, dV = 0}. \tag{120}$$

To achieve traction continuity through discontinuity surface in an averaged sense, we propose the following form for $\tilde{\boldsymbol{\varepsilon}}$ [58]:

$$\tilde{\boldsymbol{\varepsilon}}^{e} = \left[\delta_{\partial\mathcal{B}_d^e} - \frac{A^e}{V^e}\right] \boldsymbol{n}^e \boldsymbol{g}^e \tag{121}$$

which exactly satisfies the zero mean condition (120). In (121) V^e, A^e are the volume of the element and area of the discontinuity surface inside the element, respectively, whereas $\boldsymbol{g}^e$ corresponds to jump in the displacement field and is assumed to be piecewise constant within the element domain, $\delta_{\partial\mathcal{B}_d^e}$ is Dirac distribution placed on discontinuity and $\boldsymbol{n}^e$ is the matrix form of the normal to discontinuity, which is given by (63) for $n_{dim} = 3$.
Insertion of variation of (121) into $(117)_2$ then leads to (in vector notation)

$$\delta\boldsymbol{g}^{eT} \left[\int_{\mathcal{B}^e} (\delta_{\partial\mathcal{B}_d^e} - \frac{A^e}{V^e}) \boldsymbol{n}^{eT} \boldsymbol{\sigma}^e\, dV\right] = 0 \tag{122}$$

which implies that

$$\int_{\mathcal{B}^e} \delta_{\partial\mathcal{B}_d^e} \boldsymbol{n}^{eT} \boldsymbol{\sigma}^e\, dV - \frac{A^e}{V^e} \int_{\mathcal{B}^e} \boldsymbol{n}^{eT} \boldsymbol{\sigma}^e\, dV = \boldsymbol{0}. \tag{123}$$

Finally, by using integral property of Dirac distribution, we are led to

$$\underbrace{\frac{1}{A^e} \int_{\partial\mathcal{B}_d^e} \boldsymbol{t}^{n^e}\, dA}_{\text{area average of traction on } \partial\mathcal{B}_d^e} = \underbrace{\frac{1}{V^e} \int_{\mathcal{B}^e} \boldsymbol{n}^{eT} \boldsymbol{\sigma}^e\, dV}_{\text{volume average of traction in } \mathcal{B}^e} \tag{124}$$

from which it directly comes out that the traction continuity is satisfied in an averaged sense through discontinuity, that is why the method is called statically optimal.
So with the above definition, the strain field in the element domain takes the form

$$\boxed{\boldsymbol{\varepsilon}^e = \underbrace{\sum_{I=1}^{nen} \boldsymbol{B}_I^e \boldsymbol{d}_I^e + \bar{\boldsymbol{G}}^e \boldsymbol{g}^e}_{\boldsymbol{\varepsilon}_{\mathcal{B}/\partial\mathcal{B}_d^e}} + \underbrace{\delta_{\partial\mathcal{B}_d^e} \boldsymbol{n}^e \boldsymbol{g}^e}_{\boldsymbol{\varepsilon}_{\partial\mathcal{B}_d^e}}} \tag{125}$$

with

$$\boxed{\bar{\boldsymbol{G}}^e = -\frac{A^e}{V^e}\boldsymbol{n}^e}. \tag{126}$$

From this point on, the formulation is identical with KOS formulation. Actually, the only difference between KOS and SOS formulations comes from the definition of enhanced strain interpolation matrix, which is given by (65) for KOS formulation and by (126) for SOS formulation.

3.3. Statically and Kinematically Optimal Non-Symmetric (SKON) Formulation

In this section we will, first, show that KOS formulation yields complete elements in the sense that they are capable of representing rigid body motions without straining, whereas those by SOS formulation can not simulate, unless special conditions are satisfied, this phenomena, which is the main source of locking especially at later stages of failure process, where we expect full stress relaxation (no straining in the bulk material). Next item is to emphasize that when KOS formulation is used, unless some particular requirements are met, the stress field in the bulk is not compatible with the tractions transmited through discontinuity surface. Here we note that SOS formulation is based on the natural traction continuity condition. Finally, with these observations we will develop statically and kinematically optimal non-symmetric (SKON) formulation, which is complete and at the same time free of locking. In the following formulation, three-noded linear triagle is used as base element, and further we assume that small deformation kinematics still apply.

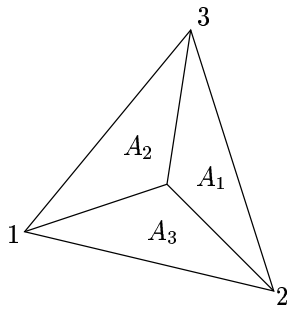

Figure 13: A three-noded linear triangle together with description of area coordinates.

We begin with the derivation of compatible strain field and consider the element given in Figure 13 in which the coordinate and displacement interpolations are of the form (in

tensor notation)

$$\left.\begin{aligned} {}^{h}\boldsymbol{x} &= \sum_{I=1}^{3} N_I(\bar{\boldsymbol{A}})\, \boldsymbol{x}_I \\ {}^{h}\boldsymbol{u} &= \sum_{I=1}^{3} N_I(\bar{\boldsymbol{A}})\, \boldsymbol{u}_I \end{aligned}\right\} \tag{127}$$

where

$$N_I(\bar{\boldsymbol{A}}) = \frac{A_I}{A} = \bar{A}_I \tag{128}$$

are the shape functions (area coordinates) with

$$\left.\begin{aligned} &\sum_{I=1}^{3} N_I(\bar{\boldsymbol{A}}) = 1 \\ &A = \sum_{I=1}^{3} A_I \end{aligned}\right\} \tag{129}$$

and, $({}^{h}\boldsymbol{x}_e,\ {}^{h}\boldsymbol{u}_e)$ are position and displacement vectors of any point inside element, whereas $(\boldsymbol{x}_I,\ \boldsymbol{u}_I)$ are those corresponding to the nodes of the element. From this point on the bracket term belonging to shape functions $N_I(\bar{\boldsymbol{A}})\,(I = 1, \ldots, 3)$ will be dropped for clarity.

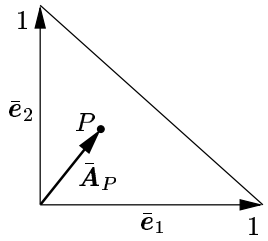

Figure 14: Point P defined in isoparametric space.

We, then, drop the dependence on $\bar{A}_3$ by taking the partition of unity property $(129)_1$ of the shape functions into account and make a redefinition for the shape functions as

$$\boxed{\begin{aligned} N_1 &= \bar{A}_1 = \frac{A_1}{A} \\ N_2 &= \bar{A}_2 = \frac{A_2}{A} \\ N_3 &= 1 - \bar{A}_1 - \bar{A}_2 \end{aligned}} \tag{130}$$

Next, we consider the differential of $\boldsymbol{x}(\bar{\boldsymbol{A}})$ (131) at a point $\bar{\boldsymbol{A}}_p$ defined in isoparametric space (Figure 14).

$$d\boldsymbol{x} = \left({}^{h}\boldsymbol{x} \otimes \bar{\nabla}\right) \cdot d\bar{\boldsymbol{A}} \tag{131}$$

In (131),

$${}^{h}\boldsymbol{x} \otimes \bar{\nabla} := \boldsymbol{J} \tag{132}$$

is the Jacobian matrix and $\bar{\nabla} = \partial/\partial\bar{\boldsymbol{A}}$ is the gradient vector in isoparametric space.
If $(127)_1$ is inserted into (131), one obtains

$$\boldsymbol{J} = \left(\sum_{I=1}^{3} N_I\, \boldsymbol{x}_I\right) \otimes \bar{\nabla} = \sum_{I=1}^{3} \boldsymbol{x}_I \otimes \bar{\nabla} N_I \tag{133}$$

which in view of (130) takes the explicit form

$$\begin{aligned} \boldsymbol{J} &= \boldsymbol{x}_1 \otimes \bar{\boldsymbol{e}}_1 + \boldsymbol{x}_2 \otimes \bar{\boldsymbol{e}}_2 + \boldsymbol{x}_3 \otimes (-\bar{\boldsymbol{e}}_1 - \bar{\boldsymbol{e}}_2) \\ \boldsymbol{J} &= \boldsymbol{x}_{13} \otimes \bar{\boldsymbol{e}}_1 - \boldsymbol{x}_{32} \otimes \bar{\boldsymbol{e}}_2 \end{aligned} \tag{134}$$

with

$$\begin{aligned} \boldsymbol{x}_{13} &:= \boldsymbol{x}_1 - \boldsymbol{x}_3 \\ \boldsymbol{x}_{32} &:= \boldsymbol{x}_3 - \boldsymbol{x}_2. \end{aligned} \tag{135}$$

For further developments we write $(134)_2$ as

$$\boldsymbol{J} = \begin{bmatrix} x_1^{13} & -x_1^{32} \\ x_2^{13} & -x_2^{32} \end{bmatrix} \boldsymbol{e}_i \otimes \bar{\boldsymbol{e}}_j \tag{136}$$

where $\boldsymbol{e}_i$ are the basis vectors in physical coordinate space, and, for example, x_1^{13} denotes x_1 component of $\boldsymbol{x}_{13}$.
When constructing a finite element, derivative of shape functions with respect to space coordinates are required. Therfore there is a need for gradient vector $\nabla = \partial/\partial\boldsymbol{x}$ in physical space, which can be constructed by

$$\boxed{\nabla = \bar{\nabla} \cdot \boldsymbol{J}^{-1}}. \tag{137}$$

The expression for $\boldsymbol{J}^{-1}$ is easily obtained from (136) as

$$\boldsymbol{J}^{-1} = \frac{1}{2A} \begin{bmatrix} -x_2^{32} & x_1^{32} \\ -x_2^{13} & x_1^{13} \end{bmatrix} \bar{\boldsymbol{e}}_i \otimes \boldsymbol{e}_j \tag{138}$$

which can be recast into a form (139) similar to $(134)_2$.

$$\boldsymbol{J}^{-1} = \frac{1}{2A} \left[\bar{\boldsymbol{e}}_1 \otimes \bar{\boldsymbol{x}}_{32} + \bar{\boldsymbol{e}}_2 \otimes \bar{\boldsymbol{x}}_{13}\right] \tag{139}$$

In (139),

$$\begin{aligned} \bar{\boldsymbol{x}}_{32} &:= -x_2^{32}\boldsymbol{e}_1 + x_1^{32}\boldsymbol{e}_2 \\ \bar{\boldsymbol{x}}_{13} &:= -x_2^{13}\boldsymbol{e}_1 + x_1^{13}\boldsymbol{e}_2 \end{aligned} \tag{140}$$

and note that

$$\boxed{\bar{\boldsymbol{x}}_{32} \cdot \boldsymbol{x}_{32} = \bar{\boldsymbol{x}}_{13} \cdot \boldsymbol{x}_{13} = 0}. \tag{141}$$

Finally, insertion of (139) into (137) yields

$$\boxed{\nabla = \frac{1}{2A}\left[\left(\frac{\partial}{\partial \bar{A}_1}\right)\bar{\boldsymbol{x}}_{32} + \left(\frac{\partial}{\partial \bar{A}_2}\right)\bar{\boldsymbol{x}}_{13}\right]}. \tag{142}$$

which can be put into a more compact form as

$$\nabla = \frac{1}{4A}\sum_{i=1}^{2} e_{ijk}\Big(\frac{\partial}{\partial \bar{A}_i}\bar{\boldsymbol{x}}_{jk}\Big) \tag{143}$$

where e_{ijk} is the permutation symbol.
Now, with this notation at hand, we will show that a three-noded linear triangular element is complete in the sense that it can represent constant strain state, and is able to simulate rigid body motions without any straining. Note that these requirements are crucial to monotonically, with increasing number of elements, converge to the solution. For this purpose we consider the element given in Figure 15, which is exposed to general deformation state described by nodal displacements.

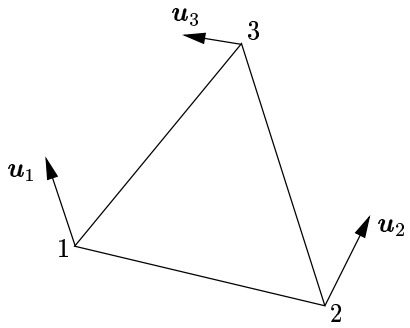

Figure 15: A three-noded linear triangle subjected to general state of deformation.

For this general case, the compatible part of the strain field appears to be of the form

$$\begin{aligned}\hat{\boldsymbol{\varepsilon}} = \Big({}^{h}\boldsymbol{u} \otimes \nabla\Big)^{s} &= \Big[\Big(\sum_{I=1}^{3} N_I \boldsymbol{u}_I\Big) \otimes \nabla\Big]^{s} \\ &= \left(\boldsymbol{u}_1 \otimes \nabla N_1 + \boldsymbol{u}_2 \otimes \nabla N_2 + \boldsymbol{u}_3 \otimes \nabla N_3\right)^{s}\end{aligned} \tag{144}$$

which, in view of (142), can be rewritten as

$$\hat{\boldsymbol{\varepsilon}} = \frac{1}{2A}\left(\boldsymbol{u}_1 \otimes \bar{\boldsymbol{x}}_{32} + \boldsymbol{u}_2 \otimes \bar{\boldsymbol{x}}_{13} + \boldsymbol{u}_3 \otimes \bar{\boldsymbol{x}}_{21}\right)^{s} \tag{145}$$

where we define

$$\bar{\boldsymbol{x}}_{21} := -x_2^{21}\boldsymbol{e}_1 + x_1^{21}\boldsymbol{e}_2 \tag{146}$$

with

$$\boxed{\bar{\boldsymbol{x}}_{21} \cdot \boldsymbol{x}_{21} = 0} \tag{147}$$

similar to (141). From (145), it directly comes out that the compatible strain field in three-noded linear trinagle is constant, which is one of the requirements for completeness. A body is said to experience rigid motion if the distance between any two points within the domain remains constant. Next, in view of this definition, we figure out the necessary conditions to be imposed on nodal displacements of a three-noded linear trinagle to have

a rigid body motion. For easy interpretation, we work with nodes of the element, i.e., we can write

$$\begin{aligned} \|\boldsymbol{x}_{21}\|^2 &= \boldsymbol{x}_{21}\cdot\boldsymbol{x}_{21} = (\boldsymbol{u}_{21}+\boldsymbol{x}_{21})\cdot(\boldsymbol{u}_{21}+\boldsymbol{x}_{21}) \\ \|\boldsymbol{x}_{32}\|^2 &= \boldsymbol{x}_{32}\cdot\boldsymbol{x}_{32} = (\boldsymbol{u}_{32}+\boldsymbol{x}_{32})\cdot(\boldsymbol{u}_{32}+\boldsymbol{x}_{32}) \\ \|\boldsymbol{x}_{13}\|^2 &= \boldsymbol{x}_{13}\cdot\boldsymbol{x}_{13} = (\boldsymbol{u}_{13}+\boldsymbol{x}_{13})\cdot(\boldsymbol{u}_{13}+\boldsymbol{x}_{13}) \end{aligned} \tag{148}$$

where

$$\left.\begin{aligned} \boldsymbol{u}_{21} &:= \boldsymbol{u}_2 - \boldsymbol{u}_1 \\ \boldsymbol{u}_{32} &:= \boldsymbol{u}_3 - \boldsymbol{u}_2 \\ \boldsymbol{u}_{13} &:= \boldsymbol{u}_1 - \boldsymbol{u}_3 \end{aligned}\right\} \tag{149}$$

and, for example, $\|\boldsymbol{x}_{13}\|$ stands for length of the edge 13.
The equations (148), in small deformation context, imply

$$\boxed{\boldsymbol{u}_{21}\cdot\boldsymbol{x}_{21} = \boldsymbol{u}_{32}\cdot\boldsymbol{x}_{32} = \boldsymbol{u}_{13}\cdot\boldsymbol{x}_{13} = 0} \tag{150}$$

which, in view of (141) and (147), leads us to

$$\boxed{\begin{aligned} \bar{\boldsymbol{x}}_{21} &= \alpha_{21}\boldsymbol{u}_{21} \\ \bar{\boldsymbol{x}}_{32} &= \alpha_{32}\boldsymbol{u}_{32} \\ \bar{\boldsymbol{x}}_{13} &= \alpha_{13}\boldsymbol{u}_{13} \end{aligned}} \tag{151}$$

where $\alpha_{ij} \subset \mathbb{R}^1$ $(i,j = 1,\ldots,3)$.
In addition, standard vector summation requires that

$$\boldsymbol{x}_{21} + \boldsymbol{x}_{32} + \boldsymbol{x}_{13} = \boldsymbol{0} \tag{152}$$

which implies, in view of (141) and (147), that

$$\boxed{\bar{\boldsymbol{x}}_{21} + \bar{\boldsymbol{x}}_{32} + \bar{\boldsymbol{x}}_{13} = \boldsymbol{0}}\,. \tag{153}$$

If the equations in (151) are added up, and (153) is considered, we are led to the conclusion that

$$\boxed{\alpha_{21} = \alpha_{32} = \alpha_{13} = \alpha}\,. \tag{154}$$

Combination of the above expression with (151), and then insertion of the result into (145) yields

$$\hat{\boldsymbol{\varepsilon}} = \frac{\alpha}{2A}\left(\boldsymbol{u}_2\otimes\boldsymbol{u}_1 - \boldsymbol{u}_1\otimes\boldsymbol{u}_2 + \boldsymbol{u}_3\otimes\boldsymbol{u}_2 - \boldsymbol{u}_2\otimes\boldsymbol{u}_3 + \boldsymbol{u}_1\otimes\boldsymbol{u}_3 - \boldsymbol{u}_3\otimes\boldsymbol{u}_1\right)^s. \tag{155}$$

Since the expression in brackets is skew-symmetric, (155) implies that

$$\boxed{\hat{\boldsymbol{\varepsilon}} = \boldsymbol{0}}\,, \tag{156}$$

i.e., element is capable of simulating any possible rigid motions without straining, the second condition to be satisfied for completeness.

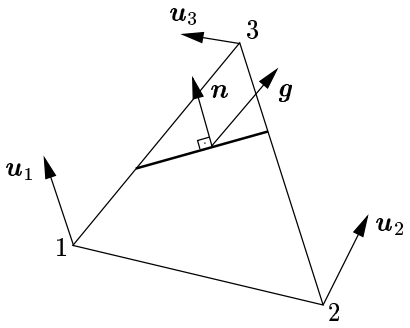

Figure 16: A three-noded linear triangle cut by a line of discontinuity.

After having proved that the base element, three-noded linear triangle, is complete, we focus our attention on the elements enhanced with the kinematics defined by KOS and SOS formulations.
Let consider the element in Figure 16, which is cut by line of discontinuity. We recall that the enhanced part of the strain field in KOS formulation, for this particular case, is given by, in tensor notation,

$$\left.\begin{aligned} \tilde{\boldsymbol{\varepsilon}} = & \; -\Big(\boldsymbol{g} \otimes \nabla N_3\Big)^s \\ = & \; -\frac{1}{2A}\Big(\boldsymbol{g} \otimes \bar{\boldsymbol{x}}_{21}\Big)^s \end{aligned}\right\}. \tag{157}$$

If the above expression is combined with compatible strain field, the enhanced strain interpolation is obtained as

$$\boldsymbol{\varepsilon} = \frac{1}{2A}\Big(\boldsymbol{u}_1 \otimes \bar{\boldsymbol{x}}_{32} + \boldsymbol{u}_2 \otimes \bar{\boldsymbol{x}}_{13} + \underbrace{(\boldsymbol{u}_3 - \boldsymbol{g})}_{\hat{\boldsymbol{u}}_3} \otimes \bar{\boldsymbol{x}}_{21}\Big)^s \tag{158}$$

which is kinematically equivalent to the case given in Figure 17,

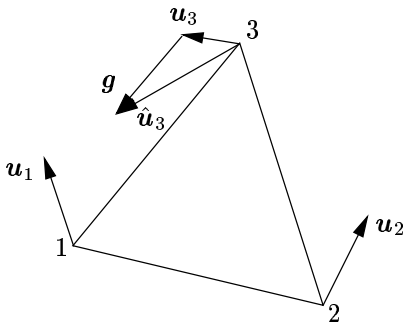

Figure 17: A three-noded linear triangle which kinematically replaces the one which is cut (see Figure 16).

and it was shown that under such circumstances the element is free of strain under rigid body motion. With this observation, we prove that the element by KOS formulation is complete. Next, we consider the strain interpolation given by SOS formulation, in which the enhanced part reads

$$\tilde{\boldsymbol{\varepsilon}} = -\frac{l}{A}\Big(\boldsymbol{g} \otimes \boldsymbol{n}\Big)^s. \tag{159}$$

If (159) is combined with compatible strain field (145), it is arrived at that

$$\boldsymbol{\varepsilon} = \frac{1}{2A}\Big(\boldsymbol{u}_1 \otimes \bar{\boldsymbol{x}}_{32} + \boldsymbol{u}_2 \otimes \bar{\boldsymbol{x}}_{13} + \boldsymbol{u}_3 \otimes \bar{\boldsymbol{x}}_{21}\Big)^s - \frac{l}{A}\Big(\boldsymbol{g} \otimes \boldsymbol{n}\Big)^s. \tag{160}$$

By comparison with (158), we immediately see that the strain field vanish under rigid body motions if and only if the following relations hold:

$$\boxed{\begin{aligned} \bar{\boldsymbol{x}}_{21} &= 2l\boldsymbol{n} \quad \text{, or} \\ \bar{\boldsymbol{x}}_{32} &= 2l\boldsymbol{n} \quad \text{, or} \\ \bar{\boldsymbol{x}}_{13} &= 2l\boldsymbol{n} \end{aligned}} \tag{161}$$

which are visualized in Figure 18.

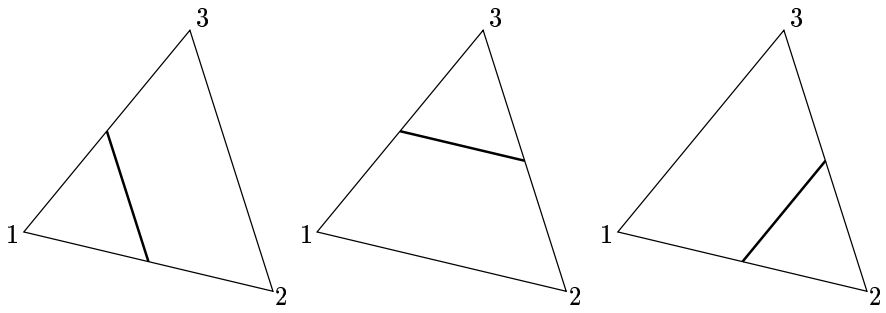

Figure 18: The special conditions to be satisfied by crack geometry inside the element domain to avoid locking in SOS formulation.

Although the KOS formulation has superior kinematic properties, the stress field in the bulk and traction transmitted through discontinuity are not compatible, i.e., there is an ambiguity in traction continuity. This is just because of the fact that in KOS formulation this condition is enforced by equating the traction components to the summation of fictitious nodal equivalent forces on positive (or negative) side of the discontinuity (see (74), $(79)_2$), i.e.,

$$\int_{\mathcal{B}} \nabla N_3 \cdot \boldsymbol{\sigma}\, dV = \int_{\partial \mathcal{B}_d} \boldsymbol{t}^n\, dA \tag{162}$$

which, in view of (142), yields

$$\boldsymbol{t}^n = \frac{1}{2l}\bar{\boldsymbol{x}}_{21} \cdot \boldsymbol{\sigma}. \tag{163}$$

As can be seen from (163), traction is not equal to the one obtained by the stress field contracted with the normal, unless

$$\boxed{\begin{aligned} \bar{\boldsymbol{x}}_{21} &= 2l\boldsymbol{n} \quad \text{, or} \\ \bar{\boldsymbol{x}}_{32} &= 2l\boldsymbol{n} \quad \text{, or} \\ \bar{\boldsymbol{x}}_{13} &= 2l\boldsymbol{n} \end{aligned}}. \tag{164}$$

It is interesting to note that the conditions necessary to eliminate locking in SOS formulation (161) are the same as those which are necessary to satisfy traction continuity along discontinuity line in KOS formulation (164) as already pointed out in [35].
As can be realized from Box 4, by using enhanced strain interpolation matrix given by KOS formulation (164) for the computation of strain and that by SOS formulation (125) for the imposition of traction continuity, an efficient element formulation can be developed. In the finite element context, this formulation is similar to Petrov-Galerkin method, in which strain and strain variations are interpolated using different kinematic operators, which are $\boldsymbol{G}$ given by (65) for the interpolation of enhanced part of the strain and $\bar{\boldsymbol{G}}$ given by (126) for the interpolation of enhanced strain variations in the present formulation. Although, this methodology provides a better description for both kinematic and static aspects, it yields unsymmetric tangent matrix, which brings some computational overburden when the solution of equations is considered. Finally, note that in this non-symmetric formulation the structure of the element subroutine remains identical with the previous formulations based on elemental enrichment.

Box 4 : Comparison of Symmetric Formulations

	Kinematically	**Traction Continuity**
KOS	Complete	Satisfied if $\bar{\boldsymbol{x}}_{21} = 2l\boldsymbol{n}$, or $\bar{\boldsymbol{x}}_{32} = 2l\boldsymbol{n}$, or $\bar{\boldsymbol{x}}_{13} = 2l\boldsymbol{n}$
SOS	Complete if $\bar{\boldsymbol{x}}_{21} = 2l\boldsymbol{n}$, or $\bar{\boldsymbol{x}}_{32} = 2l\boldsymbol{n}$, or $\bar{\boldsymbol{x}}_{13} = 2l\boldsymbol{n}$	Satisfied

4. Modeling of Cohesive Crack Growth by Finite Elements with Embedded Strong Discontinuity: Formulation Based on Nodal Enrichment

4.1. Kinematics

Let consider the body $\mathcal{B} \subset \mathbb{R}^3$ in Figure 19, which is split into parts $\mathcal{B}^+$ and $\mathcal{B}^-$ by the smooth surface of discontinuity, along which some of the displacement components are discontinuous. Further, we assume that deformations are small and the body is loaded by constant surface tractions and body force field.

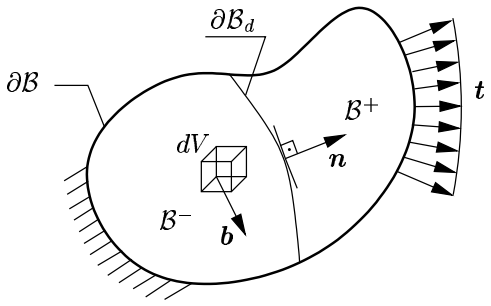

Figure 19: Body $\mathcal{B}$ crossed by a discontinuity $\partial\mathcal{B}_d$.

With the above description, we formally start with a decomposition of displacement field into continuous and discontinuous parts as

$$\boxed{\boldsymbol{u} = \underbrace{\hat{\boldsymbol{u}}}_{\text{continuous}} + \underbrace{\tilde{\boldsymbol{u}}}_{\text{discontinuous}}} \,. \tag{165}$$

Next, the following form for the discontinuous part is proposed:

$$\tilde{\boldsymbol{u}} = H_{\partial\mathcal{B}_d}\bar{\boldsymbol{u}} \tag{166}$$

where $H_{\partial\mathcal{B}_d}$ is the heaviside step function placed on $\partial\mathcal{B}_d$ and defined as

$$H_{\partial\mathcal{B}_d} = \begin{cases} 1, & \forall\, \boldsymbol{x} \in \mathcal{B}^+ \\ 0, & \text{otherwise} \end{cases} , \tag{167}$$

and $\bar{\boldsymbol{u}}$ is an arbitrary function of space coordinates, which gives the amount of jump in the displacement field. Note that the form for discontinuous part given in (166) is different from the one given in (48), where the discontinuous part has a limited support, which we do not have at the moment.
Finally, in small deformation context jump in the displacement field and the strain are obtained as

$$\boxed{[\![\boldsymbol{u}]\!] = \boldsymbol{u}^+ - \boldsymbol{u}^- = \bar{\boldsymbol{u}}\Big|_{\partial\mathcal{B}_d}} \tag{168}$$

$$\boxed{\boldsymbol{\varepsilon} = (\boldsymbol{u} \otimes \nabla)^s = \underbrace{(\hat{\boldsymbol{u}} \otimes \nabla)^s + H_{\partial\mathcal{B}_d}([\![\boldsymbol{u}]\!] \otimes \nabla)^s}_{\boldsymbol{\varepsilon}_{\mathcal{B}/\partial\mathcal{B}_d}} + \underbrace{\delta_{\partial\mathcal{B}_d}([\![\boldsymbol{u}]\!] \otimes \boldsymbol{n})^s}_{\boldsymbol{\varepsilon}_{\partial\mathcal{B}_d}}} \tag{169}$$

where $\nabla = \partial/\partial\boldsymbol{x}$ is the gradient vector, $(\cdot)^s$ indicates the symmetric part of $(\cdot)$, and $\delta_{\partial\mathcal{B}_d}$ is the Dirac distribution placed at the discontinuity.

4.2. Variational Equations

If the expressions for the jump in the displacement field and strain given by (166), (167), and their variations are inserted into the extended principal of virtual work expression (46), we are led to

$$\int_{\mathcal{B}/\partial\mathcal{B}_d} \left[(\delta\hat{\boldsymbol{u}} \otimes \nabla)^s + H_{\partial\mathcal{B}_d} (\delta\bar{\boldsymbol{u}} \otimes \nabla)^s \right] : \boldsymbol{\sigma}\, dV + \int_{\partial\mathcal{B}_d} \delta\bar{\boldsymbol{u}} \cdot \boldsymbol{t}^n\, dA = \int_{\partial\mathcal{B}_\sigma} \delta\hat{\boldsymbol{u}} \cdot \boldsymbol{t}\, dA \tag{170}$$

where the jump in the displacement field at the outer boundary $\partial\mathcal{B}_\sigma$, portion on which the surface tractions are prescribed, is set to zero for convenience, i.e., $(\delta\tilde{\boldsymbol{u}} = \boldsymbol{0}, \forall \boldsymbol{x} \in \partial\mathcal{B}_\sigma)$. By setting the independent variations of $\delta\bar{\boldsymbol{u}}$ and $\delta\tilde{\boldsymbol{u}}$ equal to zero, one obtains two variational equations of the form

$$\left.\begin{aligned} \int_{\mathcal{B}/\partial\mathcal{B}_d} (\delta\hat{\boldsymbol{u}} \otimes \nabla)^s : \boldsymbol{\sigma}\, dV &= \int_{\partial\mathcal{B}_\sigma} \delta\hat{\boldsymbol{u}} \cdot \boldsymbol{t}\, dA \\ \int_{\mathcal{B}^+/\partial\mathcal{B}_d} (\delta\bar{\boldsymbol{u}} \otimes \nabla)^s : \boldsymbol{\sigma}\, dV &= \int_{\partial\mathcal{B}_d} \delta\bar{\boldsymbol{u}} \cdot \boldsymbol{t}^{-n}\, dA \end{aligned}\right\} \tag{171}$$

which set the starting point for the finite element formulation. Here note that first variational equation in (171) corresponds to standard weak form of equilibrium equations written for the body $\mathcal{B}$, whereas the second one corresponds to the weak form written for body $\mathcal{B}^+$, which lie in "front" of the discontinuity (Figure 20), and they are coupled through the stress field.

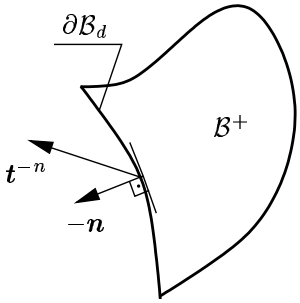

Figure 20: Body $\mathcal{B}^+$ loaded by tractions transmitted through surface of discontinuity $\partial\mathcal{B}_d$.

4.3. Finite Element Formulation

After having obtained the variational equations, we present the finite element formulation and solution procedure in detail. Starting point, as usual, is the discretization of the domain by standard displacement finite elements, such that discontinuity aligns arbitrarily with the mesh (see Figure 21).

Next we discuss the displacement interpolation over the body. It has already been shown in [45] that with the partition of unity property of standard finite element shape functions, the approximation field of interest (e.g., displacement) can be enhanced at some critical region of the body (e.g., at the crack tip) with the products of some suitable enrichment functions by global nodal shape functions. These enrichment functions have the information about the local character of the problem (e.g., near tip asymptotic fields in elastic crack growth) and are usually constructed by exact solution of the problem obtained under some simplified conditions. With this enhancement the most general form of the displacement approximation within the body takes the form in vector notation

$$\boldsymbol{u} = \sum_{I=1}^{n_{nodes}} N_I^g \left(\boldsymbol{d}_I + \chi_I \sum_{J=1}^{m} \varphi_J \bar{\boldsymbol{d}}_J^I \right) \tag{172}$$

where N_I^g, d_I are the standard global shape function and displacement degrees of freedom belonging to the node I, respectively, whereas the collocation function χ_I is redefined as

$$\chi_I = \begin{cases} 1, & \text{if node } I \text{ is enhanced} \\ 0, & \text{otherwise} \end{cases} \tag{173}$$

and φ_J, $\bar{\boldsymbol{d}}_J^I$ $(J = 1, \ldots, m)$ are the basis functions for enhancement and corresponding nodal degrees of freedom for a given particular problem.

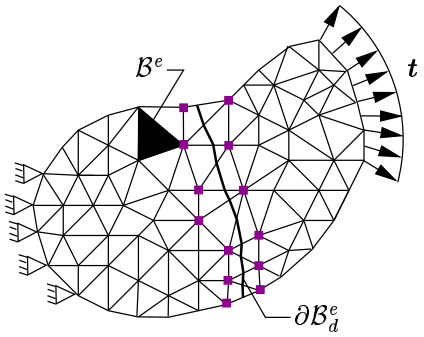

Figure 21: Discretization of the domain by finite elements. Squared nodes are enhanced with extra global degrees of freedom in order to interpolate discontinuity.

Note that superscript I in (172) implies that extra degrees of freedom can be assigned to currently used finite element mesh, i.e., there is no need for topology change while enriching the approximation at some part of the body. Therefore the methodology can also be called as nodal enrichment. In addition, since the enhanced basis functions, which are global, are multiplied by global finite element shape functions, the enrichment has a limited support defined by the shape functions belonging to the enhanced nodes (see Figure 21).
Using the "extended" interpolation by (172), we can easily construct an approximation to displacement field (174), which is discontinuous along a given surface by setting the number of enhanced basis to 1 and replacing the enhancement term by heaviside step

function.

$$\left.\begin{aligned} {}^h\boldsymbol{u} &= \sum_{I=1}^{n_{nodes}} N_I^g \left(\boldsymbol{d}_I + \chi_I H_{\partial\mathcal{B}_d} \bar{\boldsymbol{d}}_I\right) \\ {}^h\boldsymbol{u} &= \underbrace{\sum_{I=1}^{n_{nodes}} N_I^g \boldsymbol{d}_I}_{\text{continuous}} + \underbrace{H_{\partial\mathcal{B}_d} \sum_{I=1}^{n_{nodes}} \chi_I N_I^g \bar{\boldsymbol{d}}_I}_{\text{discontinuous}} \end{aligned}\right\}. \tag{174}$$

The displacement interpolation inside an element domain $\mathcal{B}^e$, in view of (174), then takes the form in standard vector notation

$${}^h\boldsymbol{u}^e = \underbrace{\sum_{I=1}^{nen} N_I^e \boldsymbol{d}_I^e}_{\text{continuous}} + \underbrace{H_{\partial\mathcal{B}_d^e} \sum_{I=1}^{nen} \chi_{\bar{I}} N_I^e \bar{\boldsymbol{d}}_I^e}_{\text{discontinuous}} \tag{175}$$

where N_I^e is the I th nodal shape function of the element (in local numbering), $\boldsymbol{d}_I^e$, $\bar{\boldsymbol{d}}_I^e$ are the standard and enhanced degrees of freedom corresponding to node I, and $H_{\partial\mathcal{B}_d^e}$, $\chi_{\bar{I}}$ are the heaviside step function defined in element domain and collocation function for global node $\bar{I} = con(e, I)$, respectively. From (175), the jump in the displacement field and the strain inside the element are obtained as

$$\boxed{[\![\boldsymbol{u}]\!]^e = \sum_{I=1}^{nen} \chi_{\bar{I}} N_I^e \bar{\boldsymbol{d}}_I^e \Big|_{\partial\mathcal{B}_d^e}} \tag{176}$$

$$\boxed{\boldsymbol{\varepsilon}^e = \underbrace{\sum_{I=1}^{nen} \boldsymbol{B}_I^e \boldsymbol{d}_I^e + H_{\partial\mathcal{B}_d^e} \sum_{I=1}^{nen} \chi_{\bar{I}} \boldsymbol{B}_I^e \bar{\boldsymbol{d}}_I^e}_{\boldsymbol{\varepsilon}^e_{\mathcal{B}/\partial\mathcal{B}_d}} + \underbrace{\delta_{\partial\mathcal{B}_d^e} ([\![\boldsymbol{u}]\!]^e \otimes \boldsymbol{n}^e)^s}_{\boldsymbol{\varepsilon}^e_{\partial\mathcal{B}_d}}}. \tag{177}$$

where $\delta_{\partial\mathcal{B}_d^e}$, $\boldsymbol{n}^e$ are the Dirac distribution placed at discontinuity surface and matrix form of the normal, which is given by (63) for $n_{dim} = 3$, to the discontinuity surface within the element domain, respectively, and $\boldsymbol{B}_I^e$ is the nodal discrete strain operator, which is given by (64) for $n_{dim} = 3$.

Note that for heaviside step function to make sense, we enrich only the nodes whose support are cut by discontinuity (Figure 21). Further, it has to be pointed out that the interpolation given by (176) enforces interelement continuity on the displacement jump and approximates it within the element domain with the order of base element, i.e., elements are conforming, which is not the case in KOS, SOS, SKON formulations based on elemental enrichment, where the displacement jump inside the elements is assumed to be piecewise constant.

After having obtained the expressions for the strain and jump in the displacement field, we consider the variational equations given by (171), and rewrite them in vector notation as

$$\left.\begin{aligned} \sum_{e=1}^{n_{elem}} \left[\sum_{i=1}^{nen} \left(\delta \boldsymbol{d}_i^T \int_{\mathcal{B}^e} \boldsymbol{B}_i^{eT} \boldsymbol{\sigma}^e \, dV\right)\right] &= \sum_{\bar{i}=1}^{n_{nodes}} \delta \boldsymbol{d}_{\bar{i}}^T \boldsymbol{f}_{ext_{\bar{i}}} \\ \sum_{e=1}^{n_{elem}} \left[\sum_{i=1}^{nen} \left(\delta \bar{\boldsymbol{d}}_{\bar{i}}^T \chi_{\bar{i}} \Big(\int_{\mathcal{B}^{e+}} \boldsymbol{B}_i^{eT} \boldsymbol{\sigma}^e \, dV + \int_{\partial\mathcal{B}_d^e} N_i^e \boldsymbol{t}^{n^e} \, dA\Big)\right)\right] &= 0 \end{aligned}\right\} \tag{178}$$

where $\boldsymbol{\sigma}^e$, $\boldsymbol{t}^{n^e}$ are the vector form of stress tensor and traction transmitted through discontinuity, respectively, which, for $n_{dim} = 3$, are given by (68), (69), and $\boldsymbol{f}_{ext_{\bar{i}}}$ is as given by (70). By defining

$$\boldsymbol{f}^e_{int_{\bar{i}}} = \int_{\mathcal{B}^e} \boldsymbol{B}^{e^T}_{\bar{i}} \boldsymbol{\sigma}^e \, dV \tag{179}$$

and

$$\boldsymbol{h}^e_{\bar{i}} = \chi_{\bar{i}} \left[\int_{\mathcal{B}^{e+}} \boldsymbol{B}^{e^T}_{\bar{i}} \boldsymbol{\sigma}^e \, dV + \int_{\partial \mathcal{B}^e_d} N^e_{\bar{i}} \boldsymbol{t}^{n^e} \, dA \right] \tag{180}$$

a more compact form is reached as

$$\left. \begin{aligned} \sum_{e=1}^{n_{elem}} \left[\sum_{i=1}^{nen} \delta \boldsymbol{d}^T_{\bar{i}} \boldsymbol{f}^e_{int_{\bar{i}}} \right] = \sum_{\bar{i}=1}^{n_{nodes}} \delta \boldsymbol{d}^T_{\bar{i}} \boldsymbol{f}_{ext_{\bar{i}}} \\ \sum_{e=1}^{n_{elem}} \left[\sum_{i=1}^{nen} \delta \bar{\boldsymbol{d}}^T_{\bar{i}} \boldsymbol{h}^e_{\bar{i}} \right] = 0 \end{aligned} \right\}. \tag{181}$$

To be able to make a physical interpretation, we write (181) in a completely equivalent form as

$$\left. \begin{aligned} \sum_{\bar{i}=1}^{n_{nodes}} \delta \boldsymbol{d}^T_{\bar{i}} \left[\boldsymbol{f}_{int_{\bar{i}}} - \boldsymbol{f}_{ext_{\bar{i}}} \right] = 0 \\ \sum_{\bar{i}=1}^{n_{nodes}} \delta \bar{\boldsymbol{d}}^T_{\bar{i}} \boldsymbol{h}_{\bar{i}} = 0 \end{aligned} \right\}. \tag{182}$$

where we define

$$\boldsymbol{f}_{int_{\bar{i}}} = \sum_{e=1}^{\alpha_{\bar{i}}} \boldsymbol{f}^{\bar{e}}_{int_{\bar{i}}} \tag{183}$$

and

$$\boldsymbol{h}_{\bar{i}} = \sum_{e=1}^{\alpha_{\bar{i}}} \boldsymbol{h}^{\bar{e}}_{\bar{i}}. \tag{184}$$

By considering independent variations of $(\delta \boldsymbol{d}_{\bar{i}})$ and $(\delta \bar{\boldsymbol{d}}_{\bar{i}})$, (182) yields the following set of equations:

$$\boxed{\begin{aligned} \boldsymbol{f}_{\bar{i}} = \boldsymbol{f}_{int_{\bar{i}}} - \boldsymbol{f}_{ext_{\bar{i}}} &= \boldsymbol{0} \quad (\bar{i} = 1, \ldots, n_{nodes}) \\ \boldsymbol{h}_{\bar{i}} &= \boldsymbol{0} \quad (\bar{i} = 1, \ldots, n_{nodes}) \end{aligned}}. \tag{185}$$

The first set of equations $(185)_1$ is referred to as discrete nodal equilibrium equations written in the directions of regular degrees of freedom, whereas the set given by $(185)_2$ corresponds to the discrete nodal equilibrium equations written in the directions of enhanced degrees of freedom. Note that $\boldsymbol{h}_{\bar{i}} (\bar{i} = 1, \ldots, n_{nodes})$ are nodal equilibrium equations and they are constructed by standard assembly operation. Remember that the internal equilibrium equations constructed in KOS, SOS and SKON formulations based on elemental enrichment are local in the sense that there is no interelement continuity requirement posed on the displacement jump within the element and due to this locality it is possible to condense internal degrees of freedom at element level.

As a final step, we consider the linearization of nodal equilibrium equations given by (185) at "k" th iteration step in <u>one</u> full global Newton iteration, at which we seek to improve

the solution and advance it from $\boldsymbol{d}_{\bar{i}}^{<k>}$ to $\boldsymbol{d}_{\bar{i}}^{<k+1>}$ $(\bar{i} = 1, \ldots, n_{nodes})$ and from $\bar{\boldsymbol{d}}_{\bar{i}}^{<k>}$ to $\bar{\boldsymbol{d}}_{\bar{i}}^{<k+1>}$ $(\bar{i} = 1, \ldots, n_{nodes})$. We explain the linearization procedure by considering one of the equations given in (185), say

$$\boxed{\begin{aligned} \boldsymbol{f}_{\bar{i}} &= \boldsymbol{0} \quad (\bar{i} \leq n_{nodes}) \\ \boldsymbol{h}_{\bar{i}} &= \boldsymbol{0} \quad (\bar{i} \leq n_{nodes}) \end{aligned}} \tag{186}$$

Linearization of the equations given by (186) around current iteration step reads as

$$\begin{aligned} \mathrm{Lin}[\boldsymbol{f}_{\bar{i}}] &= \boldsymbol{f}_{\bar{i}}^{<k>} + \Delta \boldsymbol{f}_{\bar{i}}^{<k>} \\ \mathrm{Lin}[\boldsymbol{h}_{\bar{i}}] &= \boldsymbol{h}_{\bar{i}}^{<k>} + \Delta \boldsymbol{h}_{\bar{i}}^{<k>} \end{aligned} \tag{187}$$

where

$$\begin{aligned} \boldsymbol{f}_{\bar{i}}^{<k>} &= \sum_{e=1}^{\alpha_{\bar{i}}} \boldsymbol{f}_{int_{\bar{i}}}^{\bar{e}<k>} - \boldsymbol{f}_{ext_{\bar{i}}}^{<k>} \\ \boldsymbol{h}_{\bar{i}}^{<k>} &= \sum_{e=1}^{\alpha_{\bar{i}}} \boldsymbol{h}_{int_{\bar{i}}}^{\bar{e}<k>} \end{aligned} \tag{188}$$

and

$$\begin{aligned} \Delta \boldsymbol{f}_{\bar{i}}^{<k>} &= \sum_{e=1}^{\alpha_{\bar{i}}} \Delta \boldsymbol{f}_{int_{\bar{i}}}^{\bar{e}<k>} \\ \Delta \boldsymbol{h}_{\bar{i}}^{<k>} &= \sum_{e=1}^{\alpha_{\bar{i}}} \Delta \boldsymbol{h}_{int_{\bar{i}}}^{\bar{e}<k>} \end{aligned} \tag{189}$$

by assuming that the surface tractions and body force field is not function of the displacement field.
$(189)_1$ can be expressed as

$$\Delta \boldsymbol{f}_{\bar{i}}^{<k>} = \sum_{e=1}^{\alpha_{\bar{i}}} \left[\int_{\mathcal{B}^{\bar{e}}} \boldsymbol{B}_i^{\bar{e}T} \Delta \boldsymbol{\sigma}^{\bar{e}<k>} \, dV \right] \tag{190}$$

where

$$\Delta \boldsymbol{\sigma}^{\bar{e}<k>} = \underbrace{\left. \frac{\partial \boldsymbol{\sigma}^{\bar{e}}}{\partial \boldsymbol{\varepsilon}^{\bar{e}}} \right|^{<k>}}_{\boldsymbol{C}^{\bar{e}<k>}} \Delta \boldsymbol{\varepsilon}^{\bar{e}<k>} \tag{191}$$

with

$$\Delta \boldsymbol{\varepsilon}^{\bar{e}<k>} = \sum_{j=1}^{nen} \boldsymbol{B}_j^{\bar{e}} \Delta \boldsymbol{d}_{\bar{j}}^{<k>} + H_{\partial \mathcal{B}_d^{\bar{e}}} \sum_{j=1}^{nen} \chi_{\bar{j}} \boldsymbol{B}_j^{\bar{e}} \Delta \bar{\boldsymbol{d}}_{\bar{j}}^{<k>}. \tag{192}$$

Note that $\boldsymbol{C}^{\bar{e}<k>}$ in (191) is the algorithmic tangent moduli, which represents the sensitivity of stresses to the total strains within the element domain.
By substituting (192) into (191), and then inserting the result into (190) by changing the domain of the integral, in which the heaviside step function appears in the integrand, from $\mathcal{B}^e$ to $\mathcal{B}^{e^+}$ leads us to

$$\begin{aligned} \Delta \boldsymbol{f}_{\bar{i}}^{<k>} = \sum_{e=1}^{\alpha_{\bar{i}}} \sum_{j=1}^{nen} \Bigg[& \int_{\mathcal{B}^e} \boldsymbol{B}_i^{\bar{e}T} \boldsymbol{C}^{\bar{e}<k>} \boldsymbol{B}_j^{\bar{e}} \, dV \Delta \boldsymbol{d}_{\bar{j}}^{<k>} + \\ & \chi_{\bar{j}} \int_{\mathcal{B}^{\bar{e}+}} \boldsymbol{B}_i^{\bar{e}T} \boldsymbol{C}^{\bar{e}<k>} \boldsymbol{B}_j^{\bar{e}} \, dV \Delta \bar{\boldsymbol{d}}_{\bar{j}}^{<k>} \Bigg] \end{aligned} \tag{193}$$

which by the definitions

$$\boldsymbol{K}_{\bar{i}\bar{j}}^{\bar{e}<k>} = \int_{\mathcal{B}^{\bar{e}}} \boldsymbol{B}_{\bar{i}}^{\bar{e}T} \boldsymbol{C}^{\bar{e}<k>} \boldsymbol{B}_{\bar{j}}^{\bar{e}} \, dV \tag{194}$$

and

$$\boldsymbol{H}_{\bar{i}\bar{j}}^{\bar{e}<k>} = \int_{\mathcal{B}^{\bar{e}+}} \boldsymbol{B}_{\bar{i}}^{\bar{e}T} \boldsymbol{C}^{\bar{e}<k>} \boldsymbol{B}_{\bar{j}}^{\bar{e}} \, dV \tag{195}$$

takes the compact form

$$\Delta \boldsymbol{f}_{\bar{i}}^{<k>} = \sum_{e=1}^{\alpha_{\bar{i}}} \sum_{j=1}^{nen} \left[\boldsymbol{K}_{\bar{i}\bar{j}}^{\bar{e}<k>} \Delta \boldsymbol{d}_{\bar{j}}^{<k>} + \chi_{\bar{j}} \boldsymbol{H}_{\bar{i}\bar{j}}^{\bar{e}<k>} \Delta \bar{\boldsymbol{d}}_{\bar{j}}^{<k>} \right] \tag{196}$$

Next, we focus on the second incremental term $(189)_2$, which can be rewritten as

$$\Delta \boldsymbol{h}_{\bar{i}}^{<k>} = \sum_{e=1}^{\alpha_{\bar{i}}} \chi_{\bar{i}} \left[\int_{\mathcal{B}^{\bar{e}+}} \boldsymbol{B}_{\bar{i}}^{\bar{e}T} \Delta \boldsymbol{\sigma}^{\bar{e}<k>} \, dV + \int_{\partial \mathcal{B}_d^{\bar{e}}} N_{\bar{i}}^{\bar{e}} \Delta \boldsymbol{t}^{n^{\bar{e}}<k>} \, dA \right] \tag{197}$$

where

$$\Delta \boldsymbol{t}^{n^{e}<k>} = \underbrace{\left. \frac{\partial \boldsymbol{t}^{n^{\bar{e}}}}{\partial \bar{\boldsymbol{u}}^{\bar{e}}} \right|^{<k>}}_{\boldsymbol{T}^{\bar{e}<k>}} \Delta \bar{\boldsymbol{u}}^{\bar{e}<k>} \tag{198}$$

with

$$\Delta \bar{\boldsymbol{u}}^{\bar{e}<k>} = \sum_{j=1}^{nen} \chi_{\bar{j}} N_{\bar{j}}^{\bar{e}} \Delta \bar{\boldsymbol{d}}_{\bar{j}}^{<k>}. \tag{199}$$

Note that in (198) $\boldsymbol{T}^{\bar{e}<k>}$ is the algorithmic tangent moduli for the sensitivity of tractions transmitted through discontinuity with respect to jumps in the total displacement within the element domain.
Insertion of (199) into (198), and then combination of the result with (197), considering the expression obtained for (191), leads us to

$$\begin{aligned} \Delta \boldsymbol{h}_{\bar{i}}^{<k>} = \chi_{\bar{i}} \sum_{e=1}^{\alpha_{\bar{i}}} \sum_{j=1}^{nen} \Bigg[& \underbrace{\int_{\mathcal{B}^{\bar{e}+}} \boldsymbol{B}_{\bar{i}}^{\bar{e}T} \boldsymbol{C}^{\bar{e}<k>} \boldsymbol{B}_{\bar{j}}^{\bar{e}} \, dV}_{\boldsymbol{H}_{\bar{i}\bar{j}}^{\bar{e}<k>}} \Delta \boldsymbol{d}_{\bar{j}}^{<k>} + \\ & \chi_{\bar{j}} \Big(\underbrace{\int_{\mathcal{B}^{\bar{e}+}} \boldsymbol{B}_{\bar{i}}^{\bar{e}T} \boldsymbol{C}^{\bar{e}<k>} \boldsymbol{B}_{\bar{j}}^{\bar{e}} \, dV}_{\boldsymbol{H}_{\bar{i}\bar{j}}^{\bar{e}<k>}} + \int_{\partial \mathcal{B}_d^{\bar{e}}} N_{\bar{i}}^{\bar{e}} \boldsymbol{T}^{\bar{e}<k>} N_{\bar{j}}^{\bar{e}} \, dA \Big) \Delta \bar{\boldsymbol{d}}_{\bar{j}}^{<k>} \Bigg] \end{aligned} \tag{200}$$

which by the definition

$$\boldsymbol{\Gamma}_{\bar{i}\bar{j}}^{\bar{e}<k>} = \boldsymbol{H}_{\bar{i}\bar{j}}^{\bar{e}<k>} + \int_{\partial \mathcal{B}_d^{\bar{e}}} N_{\bar{i}}^{\bar{e}} \boldsymbol{T}^{\bar{e}<k>} N_{\bar{j}}^{\bar{e}} \, dA \tag{201}$$

takes the most compact form

$$\Delta \boldsymbol{h}_{\bar{i}}^{<k>} = \chi_{\bar{i}} \sum_{e=1}^{\alpha_{\bar{i}}} \sum_{j=1}^{nen} \chi_{\bar{j}} \left[\boldsymbol{H}_{\bar{i}\bar{j}}^{\bar{e}<k>} \Delta \boldsymbol{d}_{\bar{j}}^{<k>} + \boldsymbol{\Gamma}_{\bar{i}\bar{j}}^{\bar{e}<k>} \Delta \bar{\boldsymbol{d}}_{\bar{j}}^{<k>} \right] \tag{202}$$

Finally, by inserting (202) and (196) into (187), we obtain

$$\left.\begin{aligned} \text{Lin}[\boldsymbol{f}_{\bar{i}}] &= \boldsymbol{f}_{\bar{i}}^{<k>} + \sum_{e=1}^{\alpha_{\bar{i}}} \sum_{j=1}^{nen} \left[\boldsymbol{K}_{\bar{i}\bar{j}}^{\bar{e}<k>} \Delta \boldsymbol{d}_{\bar{j}}^{<k>} + \chi_{\bar{j}} \boldsymbol{H}_{\bar{i}\bar{j}}^{\bar{e}<k>} \Delta \bar{\boldsymbol{d}}_{\bar{j}}^{<k>} \right] \\ \text{Lin}[\boldsymbol{h}_{\bar{i}}] &= \boldsymbol{h}_{\bar{i}}^{<k>} + \chi_{\bar{i}} \sum_{e=1}^{\alpha_{\bar{i}}} \sum_{j=1}^{nen} \left[\chi_{\bar{j}} \boldsymbol{H}_{\bar{i}\bar{j}}^{\bar{e}<k>} \Delta \boldsymbol{d}_{\bar{j}}^{<k>} + \chi_{\bar{j}} \boldsymbol{\Gamma}_{\bar{i}\bar{j}}^{\bar{e}<k>} \Delta \bar{\boldsymbol{d}}_{\bar{j}}^{<k>} \right] \end{aligned}\right\}. \tag{203}$$

The summary of the assembly process is given in Box 5.

4.4. Final Remarks

- Integration Scheme
  When constructing nodal fictitious equivalent forces and tangent matrix for a given element, the standard procedure is to compute corresponding integrals by a numerical integration, such as Gauss-Quadrature. In this method the domain integral of a quantity is approximated by

$$\int_{\mathcal{B}_e} f \, dV = \sum_{I=1}^{nGp} w_I f_I \tag{204}$$

  where nGp is the total number of Gauss points, w_I is the weight corresponding to I th Gauss point and f_I is the value of the function at I th Gauss point. When integrating polynomial functions, which is usually the case, the numerical procedure described yields exact result if the order of quadrature is greater than or equal to the order of poynomial function integrated.
  After this brief discussion, we focus our attention on to the elements constructed by the kinematics defined by partition of unity. To really make it clear, we consider again a three-noded linear triangle, which is subjected to a general displacement profile (Figure 22).

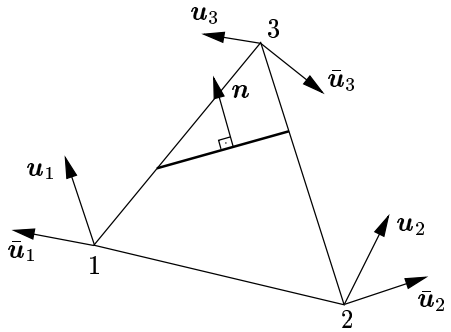

Figure 22: A three-noded linear triangle cut by a line of discontinuity.

For this general case, the strain expression in the bulk material, in view of (145) and (177), turns out to be in tensor notation

$$\boldsymbol{\varepsilon} = \frac{1}{2A} \left[(\boldsymbol{u}_1 + H\bar{\boldsymbol{u}}_1) \otimes \bar{\boldsymbol{x}}_{32} + (\boldsymbol{u}_2 + H\bar{\boldsymbol{d}}_2) \otimes \bar{\boldsymbol{x}}_{13} + (\boldsymbol{u}_3 + H\bar{\boldsymbol{d}}_3) \otimes \bar{\boldsymbol{x}}_{21} \right]^s. \tag{205}$$

Box 5 : Assembly of Internal Force Vector and Tangent Matrix

initialize global matrices

FOR $\bar{i} = 1, \ldots, n_{nodes} \times n_{dim}$

$\mathbf{FG}(\bar{i}) = 0.0$

FOR $\bar{j} = 1, \ldots, n_{nodes} \times n_{dim}$

$\mathbf{KG}(\bar{i}, \bar{j}) = 0.0$

END

END

loop over nodes

FOR $\bar{i} = 1, \ldots, n_{nodes}$

1. get global regular and enhanced degrees of freedom

FOR $I = 1, \ldots, n_{dim}$

$d_1(I) = dof(\bar{i}, I)$

$\bar{d}_1(I) = dof(\bar{i}, I + n_{dim})$

END

2. loop over node support

a. get the element number $\bar{e} = nsup(\bar{i}, e)$

b. get the local node number $i = con^{-1}(\bar{e}, \bar{i})$

c. compute $\boldsymbol{f}_{int_{\bar{i}}}^{\bar{e}<k>} = \int_{\mathcal{B}^{\bar{e}}} \boldsymbol{B}_i^{\bar{e}T} \boldsymbol{\sigma}^{\bar{e}<k>} \, dV$

d. compute $\boldsymbol{h}_{\bar{i}}^{\bar{e}<k>} = \chi_{\bar{i}} \left[\int_{\mathcal{B}^{\bar{e}}} \boldsymbol{B}_i^{\bar{e}T} \boldsymbol{\sigma}^{\bar{e}<k>} \, dV + \int_{\partial \mathcal{B}_d^{\bar{e}}} N_i^{\bar{e}} \boldsymbol{t}^{n^{\bar{e}}<k>} \, dA \right]$

e. assemble internal forces

FOR $I = 1, \ldots, n_{dim}$

$\mathbf{FG}\Big(d_1(I)\Big) = \mathbf{FG}\Big(d_1(I)\Big) + \boldsymbol{f}_{int_{\bar{i}}}^{\bar{e}<k>}(I)$

$\mathbf{FG}\Big(\bar{d}_1(I)\Big) = \mathbf{FG}\Big(\bar{d}_1(I)\Big) + \boldsymbol{h}_{\bar{i}}^{\bar{e}<k>}(I)$

END

f. loop over nodes of element $\bar{e}$

FOR $j = 1, \ldots, nen$

get global node number $\bar{j} = con(\bar{e}, j)$

get global and enhanced degrees of freedom

FOR $I = 1, \ldots, n_{dim}$

$d_2(I) = dof(\bar{j}, I)$

$\bar{d}_2(I) = dof(\bar{j}, I + n_{dim})$

END

compute $\boldsymbol{K}_{\bar{i}\bar{j}}^{\bar{e}<k>} = \int_{\mathcal{B}^{\bar{e}}} \boldsymbol{B}_i^{\bar{e}T} \boldsymbol{C}^{\bar{e}<k>} \boldsymbol{B}_j^{\bar{e}} \, dV$

compute $\boldsymbol{H}_{\bar{i}\bar{j}}^{\bar{e}<k>} = \int_{\mathcal{B}^{\bar{e}+}} \boldsymbol{B}_i^{\bar{e}T} \boldsymbol{C}^{\bar{e}<k>} \boldsymbol{B}_m^{\bar{e}} \, dV$

compute $\boldsymbol{\Gamma}_{\bar{i}\bar{j}}^{\bar{e}<k>} = \boldsymbol{H}_{\bar{i}\bar{j}}^{\bar{e}<k>} + \int_{\partial \mathcal{B}_d^{\bar{e}}} N_i^{\bar{e}} \boldsymbol{T}^{\bar{e}<k>} N_j^{\bar{e}} \, dA$

assemble tangent matrices

FOR $I = 1, \ldots, n_{dim}$

FOR $J = 1, \ldots, n_{dim}$

$\mathbf{KG}\Big(d_1(I), d_2(J)\Big) = \mathbf{KG}\Big(d_1(I), d_2(J)\Big) + \boldsymbol{K}_{\bar{i}\bar{j}}^{\bar{e}<k>}(I, J)$

$\mathbf{KG}\Big(d_1(I), \bar{d}_2(J)\Big) = \mathbf{KG}\Big(d_1(I), \bar{d}_2(J)\Big) + \chi_{\bar{j}} \boldsymbol{H}_{\bar{i}\bar{j}}^{\bar{e}<k>}(I, J)$

$\mathbf{KG}\Big(\bar{d}_1(I), d_2(J)\Big) = \mathbf{KG}\Big(\bar{d}_1(I), d_2(J)\Big) + \chi_{\bar{j}} \boldsymbol{H}_{\bar{i}\bar{j}}^{\bar{e}<k>}(I, J)$

$\mathbf{KG}\Big(\bar{d}_1(I), \bar{d}_2(J)\Big) = \mathbf{KG}\Big(\bar{d}_1(I), \bar{d}_2(J)\Big) + \chi_{\bar{j}} \boldsymbol{\Gamma}_{\bar{i}\bar{j}}^{\bar{e}<k>}(I, J)$

END

END

END

END

Note that, again, the kinematic description given in (205) yields complete elements. From (205), we immediately see that in contrast to formulation given in previous chapter, the strain is not uniform any more over the whole domain, i.e.,

$$\begin{aligned} \boldsymbol{\varepsilon}^{+} &= \frac{1}{2A}\Big[(\boldsymbol{u}_1 + \bar{\boldsymbol{u}}_1) \otimes \bar{\boldsymbol{x}}_{32} + (\boldsymbol{u}_2 + \bar{\boldsymbol{u}}_2) \otimes \bar{\boldsymbol{x}}_{13} + (\boldsymbol{u}_3 + \bar{\boldsymbol{u}}_3) \otimes \bar{\boldsymbol{x}}_{21}\Big]^{s} \\ \boldsymbol{\varepsilon}^{-} &= \frac{1}{2A}\Big[\boldsymbol{u}_1 \otimes \bar{\boldsymbol{x}}_{32} + \boldsymbol{u}_2 \otimes \bar{\boldsymbol{x}}_{13} + \boldsymbol{u}_3 \otimes \bar{\boldsymbol{x}}_{21}\Big]^{s} \end{aligned} \tag{206}$$

which directly highlights that the strain on both side of discontinuity is partially uncoupled. This property, actually, siuts much better to physical phenomena, where we expect some uncoupling in the strain field as the crack opens wide. However, to have this better kinematic description there is a price to pay.

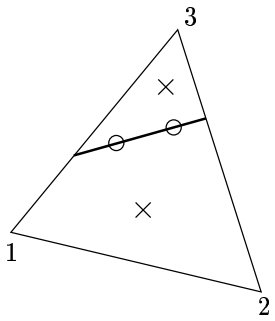

Figure 23: Gauss points necessary for modified quadrature. Crosses denote Gauss points to integrate contributions coming from the bulk, whereas circles are those to integrate contributions coming from the discontinuity.

Since the strain is not uniform over the domain of element, one point integration, which was enough for previous formulations (SOS, KOS, SKON), fails to integrate accurately the strain on both side of the discontinuity. Therefore, for this particular element, one Gauss point must be placed on each side of discontinuity, i.e., the integration scheme has to be modified. To integrate the traction along discontinuity accurately, we also need more than one Gauss point, since the displacement jump is not constant within the element in this formulation (see Figure 23). For higher order elements, more complicated integration schemes might be necessary. For example, in [94] an integration scheme with overall 23 Gauss points, 21 on the bulk and 2 on the discontinuity, for a six-noded quadratic triangle have been used (Figure 24). In the numerical simulations, the performance of both elements will be tested.

- Node Activation
  In the analyses that we perform, the discontinuities are extended through the element domain, although it is possible to embed tip of discontinuity inside the element. When the support of a node is crossed by the discontinuity for the first time, we do not activate the node in order to satisfy zero displacement jump condition at the crack tip. If the discontinuity propagates further and enters into another element, the same node does not lie on the edge where crack tip sits anymore. Therefore this node should be added to active node list and necessary updates should be done at

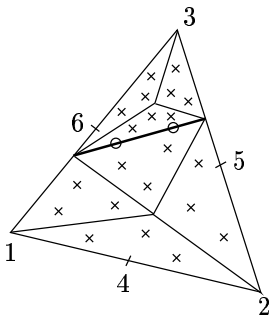

Figure 24: Gauss points necessary for modified quadrature in a six-noded quadratic triangle - One of the possibilities.

the history field of elements having this node in their connectivity. In order to end up with well conditioned system matrices, we perform an area check before activating a node even if its support is crossed in a way described above. The procedure is as follows. Before the node is enhanced, and added to active node list, the total area which belongs to support of that node, and the portion which lies above (on positive side) of the discontinuity is computed (see Figure 25). Then, the ratio $min(A^+, A - A^+)/A$ is compared with a given tolerance. If the ratio is less than the tolerance the node is not activated, i.e., no additional degrees of freedom are assigned to that node. Otherwise, node is activated and added to active node list, and necessary modifications are done in history fields of elements which have that node in their connectivity.

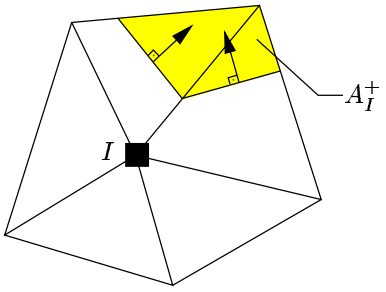

Figure 25: Patch of elements belonging to global node I and the portion which lies above the discontinuity.

5. Numerical Results

In this section, the numerical techniques developed in previous sections based on elemental and nodal enrichments are tested with respect to mesh objectivity. For this purpose, two three-noded linear triangular elements, one enhanced with the kinematics provided by elemental enrichment, namely KOS, SOS and SKON formulations, and the other with nodal enrichment, XFEM, have been developed. In addition, a six-noded quadratic triangular element has also been developed by nodal enrichment strategy to verify a three-point bending test simulation demonstrated in [94].
We present two numerical examples, in which the aim is to simulate the crack propagation in the test specimens in a mesh objective manner. As a constitutive law, a purely linear elastic behavior is assumed in the bulk, whereas a particular form of a damage type traction seperation law derived in Section (2.2) is imposed on the cohesive surface. To keep number of parameters influencing the results at a minimum, the crack path in all simulations is set a priori by the user as appropriate, instead of being calculated from the stress field obtained. This simplification is done in order to make a sound comparison of different numerical approaches.
Before presenting the results obtained, some details about the constitutive equation valid on the cohesive surface is given. As a rule relating displacement jumps to traction components transmitted through the discontinuity, a damage type constitutive equation used in [2; 27; 89; 91; 94; 95] to represent the failure mechanism in quasi-brittle materials is incorporated. In particular to this constitutive equation, the scalar damage variable "d" is related to history dependent parameter "r" with an exponential law given by

$$d = 1 - \exp\Big(- \frac{f_t}{G_f} r \Big) \tag{207}$$

where f_t is the tensile strength and G_f, the fracture energy, is the energy required to create unit area of traction free crack and is assumed to be a material constant [36]. In addition, it is assumed that at the cohesive surface there is a transfer of normal traction component only, i.e., on the crack surface shear component of traction vector does not exist. This consideration, in view of (31), motivates the following form for the normal component transmitted:

$$t_n = (1 - d) T_n \left[\!\left[\boldsymbol{u} \right]\!\right]_n \tag{208}$$

where t_n is the normal component of traction, whereas T_n and $\left[\!\left[\boldsymbol{u} \right]\!\right]_n$ are the elastic stiffness and displacement jump in normal direction, respectively.
The maximum principle tensile stress is checked for the initiation of a crack and to determine its direction. Therefore at the onset of cracking the normal component of the traction is equal to tensile strength f_t of the material, i.e.,

$$\lim_{[\boldsymbol{u}]_n \to 0} t_n = f_t \tag{209}$$

which directly implies that

$$T_n \left[\!\left[\boldsymbol{u} \right]\!\right]_n = f_t \tag{210}$$

By inserting (210) and (207) into (208), we are finally led to (see Figure 26)

$$t_n = f_t \exp\Big(- \frac{f_t}{G_f} r \Big) \tag{211}$$

which is the form also used in [2; 27; 89; 91; 94; 95] (see also [36; 68]). Note that the area under the curve defined by (211) is equal to fracture energy G_f of the material.

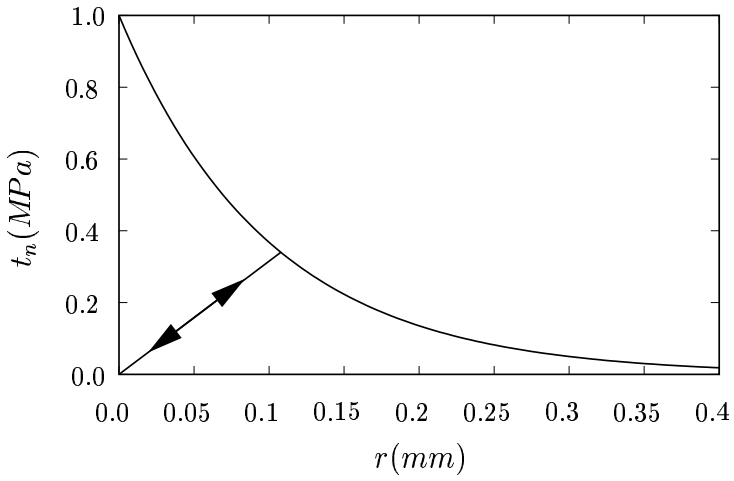

Figure 26: Constitutive relationship for normal component of tarction transmitted through discontinuity.

Moreover, without loss of generality, the criteria to be checked for damage evolution can be replaced by

$$\phi = [\![\boldsymbol{u}]\!]_n - r \leq 0 \tag{212}$$

where "r" is redefined as the maximum normal opening attained at the crack surface in the history of deformation process. The results obtained so far are summarized in Box 6.

Box 6 : A Damage Type Traction Seperation Law – Continuous Formulation

1. Surface Free Energy	$w = (1-d)w_0$, with $w_0 = \frac{1}{2} f_t [\![\boldsymbol{u}]\!]_n$
2. Traction	$t_n = f_t \exp\left(-\frac{f_t}{G_f} r\right)$ $t_s = 0$
3. Elastic Domain	$\phi = [\![\boldsymbol{u}]\!]_n - r \leq 0$
4. Loading/Unloading	$\dot{\mu} \geq 0,\ \phi \leq 0,\ \dot{\mu}\phi = 0$
5. Tangent Moduli	$\dot{\boldsymbol{t}}_n = \boldsymbol{T}_n^{ed} [\![\boldsymbol{v}]\!]_n$, with $\boldsymbol{T}_n^{ed} = -\frac{f_t^2}{G_f} \exp\left(-\frac{f_t}{G_f} [\![\boldsymbol{u}]\!]_n\right)$

Now, based on this continuous form, we give the algorithmic incremental formulation for a deformation driven update in Box 10. In the simulations, the same material properties are used for the bulk and cohesive surface, which are given in Box 7.

Box 7 : Material Properties for the Bulk and Cohesive Surface

E	$= 100MPa$
ν	$= 0.0$
f_t	$= 1.0MPa$
G_f	$= 0.1N/mm$

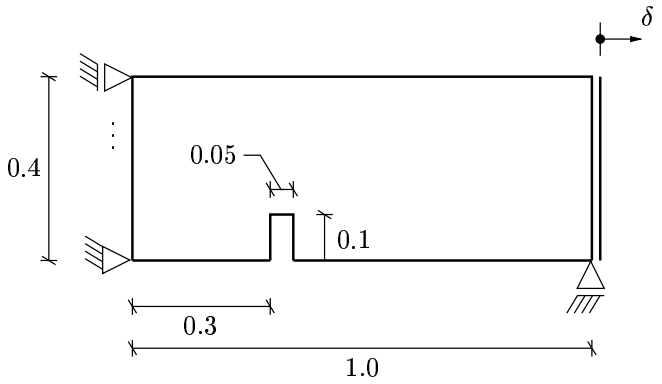

Figure 27: Tension test. Geometry and boundary conditions. (units are in mm)

In the first example a specimen with a notch is pulled under displacement driven process. The geometry and boundary conditions are depicted in Figure (27). In the first simulation an unstructured mesh of three-noded linear triangles is used. The loading history, the number of iterations and size of the incerements, is given in Box 8.

Box 8 : Loading History for Tension Test Simulation

Number of Iteration	Increment
1	0.0037
25	0.0005
80	0.005

As can be seen from Figure $(29)_a$, in elemental enrichment strategy as the crack propagates upwards the coloured elements are activated, i.e., internal degrees of freedom representing the jump in the displacement field are assigned to them, whereas in $(29)_b$, as the crack propagates the circled nodes whose support are cut by the crack are activated, i.e., two additional degrees of freedom are assigned to them in order to be able to interpolate discontinuity in a continuous manner between elements.
In Figure $(30)_a$ the load displacement diagrams obtained by following the enhancement strategies provided by KOS, SOS and SKON formulations are given. As can be figured out, the diagrams by KOS and SKON formulations are top of each other, whereas the one by SOS formulation is not able to follow them. As pointed out in Section (3.1.3), in this unstructured mesh the special conditions to get rid of locking can not be met, therefore locking is unavoidable. Coincidence of the diagrams by KOS and SKON formulation can be explained by the uniformity of the stress field. Under much more complicated stress scneraios, one expects them also differ from each other. In Figure $(30)_b$ the load displacement diagrams obtained by the nodal enrichment, XFEM, strategy

is presented together with the one obtained by SKON formulation based on elemental enrichment. The agreement between these different approaches is particularly noteworthy.

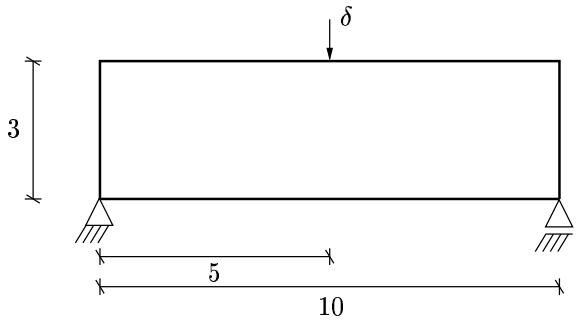

Figure 28: Three-point bending test. Geometry and boundary conditions. (units are in mm)

In the second simulation the performance of the methods is tested by using a structured mesh of three-noded linear triangles. Note that in this case the crack path inside the element domain is set such that it is parallel to one of the edges and has the length equal to half length of the side to which it is parallel. These conditions are those to avoid locking in SOS formulation, which is verified by the load displacement diagrams given in Figure $(32)_a$. The good agreement between different approaches, based on nodal and elemental enrichments, is also obtained for this case (see Figure $(32)_b$).
In the second example, a three-point bending test is simulated using a mesh of six-noded quadratic triangles developed by nodal enrichment strategy. Geometry and boundary conditions are depicted in Figure (28). A similar simulation, with the same geometry and material laws valid for the bulk and cohesive discontinuity is given in [94]. The mesh objectivity is tested by performing the simulation using three different meshes, one structured and two unstructured. The loading history, the number of iterations and size of the incerements, is given in Box 9.

Box 9 : Loading History for Three-Point Bending Test Simulation

	Number of Iteration	Increment
Structured mesh with 1080 elements:	1	0.103
	280	0.005
Unstructured mesh with 986 elements:	1	0.105
	280	0.005
Unstructured mesh with 973 elements:	1	0.11
	280	0.005

Box 10 : A Damage Type Traction Seperation Law – Algorithmic Setting

1. given $\{r^{<k>}, [\boldsymbol{u}]^{<k+1>}\}$
2. compute the normal component of displacement jump
   $[u]_n^{<k+1>} = [\boldsymbol{u}]^{<k+1>} \cdot \boldsymbol{n}$
3. check whether damage grows
   IF $[u]_n^{<k+1>} > r^{<k>}$ THEN
   update history
   $r^{<k+1>} = [u]_n^{<k+1>}$
   compute the components of traction in local basis
   $t_n^{<k+1>} = f_t \; exp(-f_t r^{<k+1>}/G_f)$
   $t_s^{<k+1>} = 0.0$
   compute the algorithmic constant
   $beta = -f_t^2/G_f \; exp(-f_t r^{<k+1>}/G_f)$
   ELSE
   update history
   $r^{<k+1>} = r^{<k>}$
   compute the components of traction in local basis
   $t_n^{<k+1>} = f_t \; exp(-f_t r^{<k+1>}/G_f)/r^{<k+1>}[u]_n^{<k+1>}$
   $t_s^{<k+1>} = 0.0$
   compute the algorithmic constant
   $beta = f_t \; exp(-f_t r^{<k+1>}/G_f)/r^{<k+1>}$
   ENDIF
4. compute the components of traction in global basis
   $t_1^{<k+1>} = \; t_s^{<k+1>} n_2 + t_n^{<k+1>} n_1$
   $t_2^{<k+1>} = -t_s^{<k+1>} n_1 + t_n^{<k+1>} n_2$
5. compute the tangent in global basis $T_{11}^{<k+1>} = beta \cdot n_1^2$
   $T_{12}^{<k+1>} = beta \cdot n_1 n_2$
   $T_{21}^{<k+1>} = T_{12}^{<k+1>}$
   $T_{22}^{<k+1>} = beta \cdot n_2^2$

The crack path and activated nodes together with the deformed shape for each mesh used are given in Figures (33), (34) and (35). The agreement of load displacement diagrams (Figure (36)) in the post-peak regime is found to be quite noteworthy. The peak load attained in our simulations is a little bit lower than that given in [94]. This difference might come from the different modeling considerations for supports and loading. It is also to be noted that undeformed and deformed configurations given in Figures (33), (34) and (35) can not be said identical. Therefore, small strain kinematics does not apply after a certain level of loading is reached, where large rigid body rotation of the parts compansate the response. In our computations, we continued till $\delta = 1.5mm$ just for comparison purposes and to show robustness of the method. As a final remark, we report that the convergence behavior in the analyses based on SKON formulation and XFEM are quadratic almost in each iteration step, especially in tension test simulation. However, in bending test simulation, after the crack reaches to top of the beam quadratic convergence behavior is lost for a certain number of iteration. Later, the convergence behavior is again quadratic. We observed during the simulations that converged solution is reached usually in four iteration step with an tolerance tol=1E-16 defined by energy norm. Furthermore, it is important to note that in the three-point bending test simulation the crack is not allowed to reach top surface of the beam not to have stability problems as already pointed out in [94].

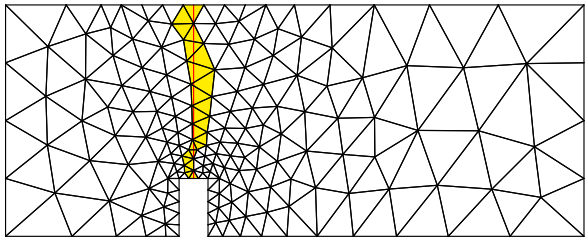

a.

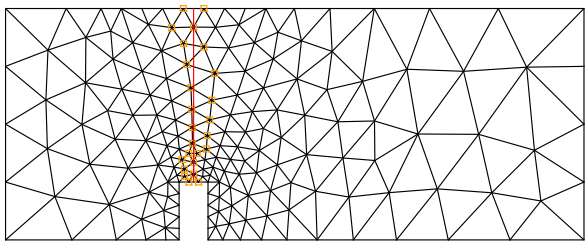

b.

Figure 29: Crack trajectory. a.) Based on elemental enrichment (the coloured elements are cut by the discontinuity) and b.) Based on nodal enrichment (the support of circled nodes are cut by the discontinuity)

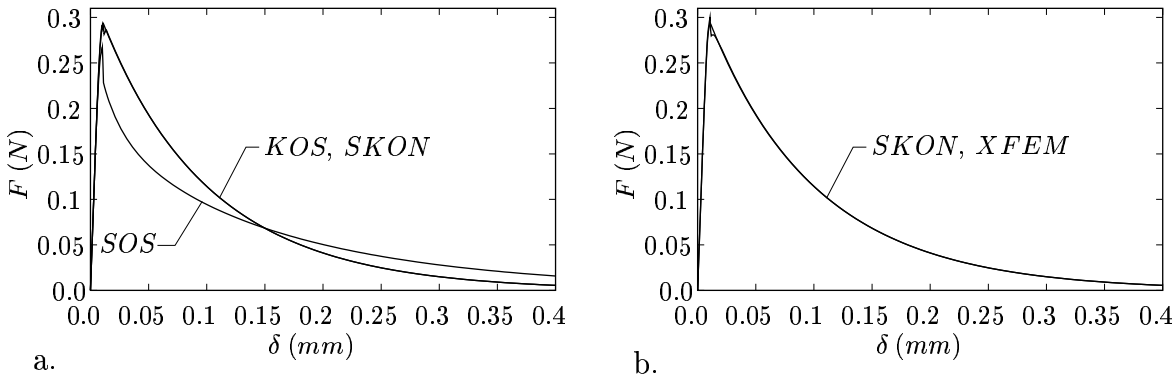

Figure 30: Load–displacement diagrams for the tension test simulation with unstructured mesh of 306 linear triangular elements. a.) Comparison between KOS, SOS and SKON formulations. b.) Comparison between SKON formulation and XFEM

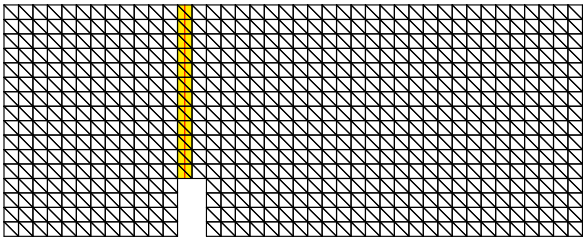

a.

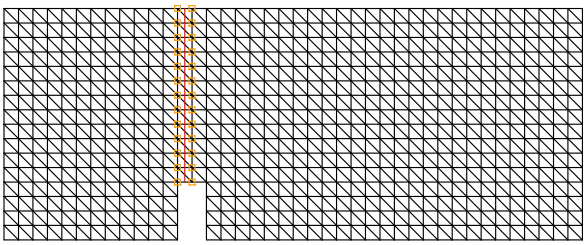

b.

Figure 31: Crack trajectory. a.) Based on elemental enrichment (the coloured elements are cut by the discontinuity) and b.) Based on nodal enrichment (the support of circled nodes are cut by the discontinuity)

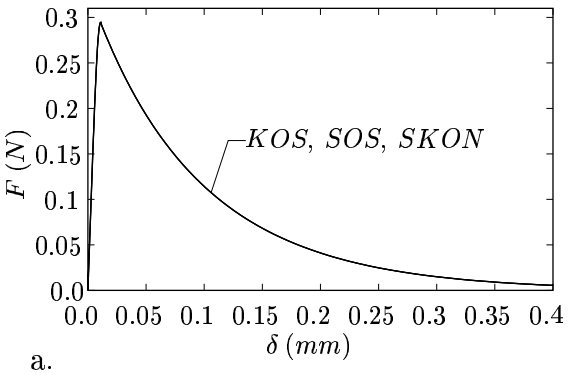

a.

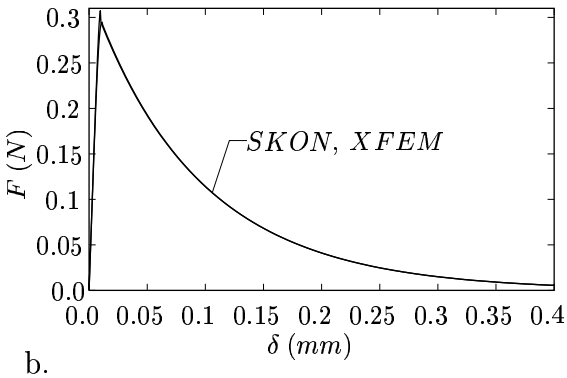

b.

Figure 32: Load–displacement diagrams for the tension test simulation with structured mesh of 1264 linear triangular elements. a.) Comparison between KOS, SOS and SKON formulations. b.) Comparison between SKON formulation and XFEM.

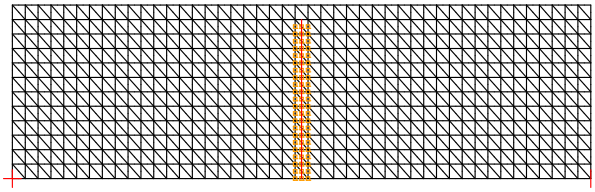

a.

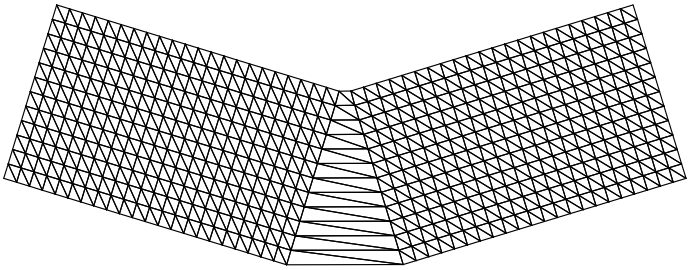

b.

Figure 33: Three-point bending test simulation by structured mesh of 1080 quadratic triangle elements. a.) The crack trajectory (the support of circled nodes are cut by the discontinuity) and b.) Deformed shape (1/1 scale)

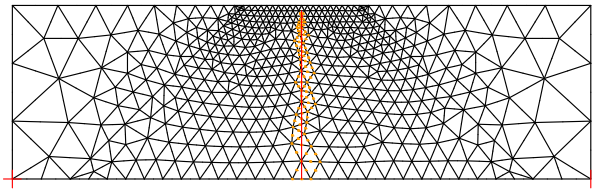

a.

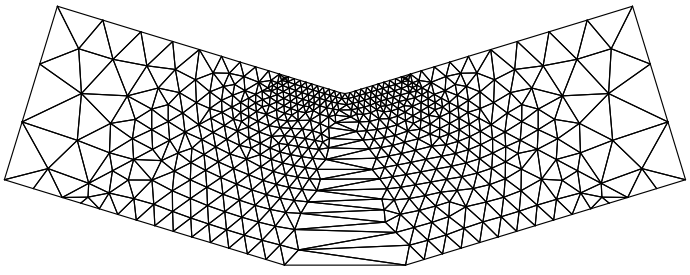

b.

Figure 34: Three-point bending test simulation by unstructured mesh of 973 quadratic triangle elements. a.) The crack trajectory (the support of circled nodes are cut by the discontinuity) and b.) Deformed shape (1/1 scale)

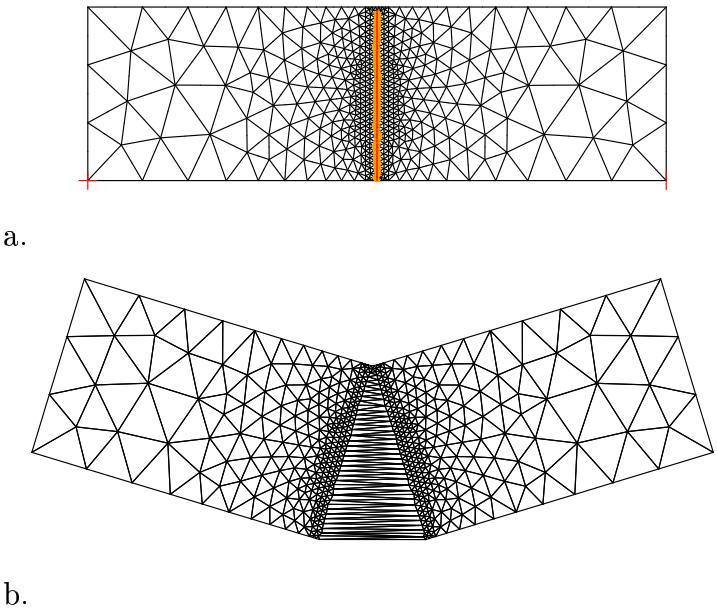

Figure 35: Three-point bending test simulation by unstructured mesh of 986 quadratic triangle elements. a.) The crack trajectory (the support of circled nodes are cut by the discontinuity) and b.) Deformed shape (1/1 scale)

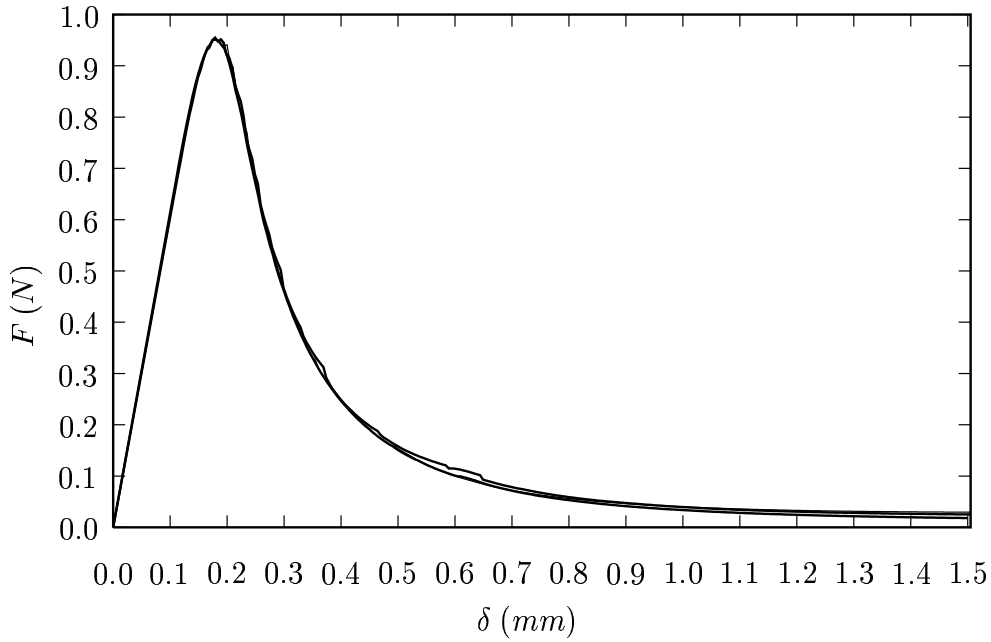

Figure 36: Load–displacement diagrams for three-point bending test simulation obtained by three different, one structured with 1275 elements and two unstructured with 973 and 986 elements, meshes of quadratic triangles.

6. Conclusion

In this study two different approaches, which provides the possibility to embed strong discontinuities (jump in the displacement components) into the finite element domain, have been investigated.
The first approach is based on elemental enrichment, in which the displacement jump is assumed to be interelement discontinuous yielding non-conforming finite element interpolation. An internal node is assigned to the elements which are cut by the discontinuity. The degrees of freedom assigned to those internal nodes reperesent the jump in the displacement field and can be condensed out at element level when the solution procedure is considered. Therefore, there is no need to resize the system matrices in order to account for incerasing number of internal degrees of freedom when an evolving discontinuity problem is considered. There exists three different possible formulations, namely KOS, SOS and SKON formulations. KOS formulation provides better kinematic description but there is a problem in internal equilibrium. Whereas SOS formulation is based on natural traction continuity condition, but it can not reflect the kinematics of a fully opened crack, which leads spurious stresses to develop. In SKON formulation, the positive aspects that KOS and SOS formulations have are combined leading to variationally inconsistent non-symmetric formulation irrespective of the material model used. In addition, if the displacement jump is assumed to be piecewise constant inside element domain, it is not possible to satisfy zero displacement jump condition at the crack tip. Furthermore, in these formulations discontinuities are introduced through the elements, i.e., it is not possible to embed the discontinuity tip within the element domain. Finally, in this approach the strain on both sides of the discontinuity are fully coupled. This brings the advantage that standard quadrature rule can still be used to integrate element contributions. However, for example, in an opened crack one expects at least partially uncoupling between the strain on both sides of the discontinuity.
In the second approach, displacement discontinuities inside the element domains are interpolated with the aid of extra global degrees of freedom assigned to existing nodes of the finite elelment mesh and heaviside step function placed at the discontinuity. Therefore, the resulting formulation is conforming, i.e., the displacement jump is interelement continuous. Because of the globality it is not possible to condense these extra global degrees of freedom at element level. Therefore, for an evolving discontinuity the size of the global matrices has to be readjusted when the discontinuity propagates further. In this formulation it is possible to embed discontinuity tip inside the element domain, and it is easy to maintain zero displacement jump condition at the crack tip. If the material model yields symmetric tangent, the formulation results in symmetric formulation which allows efficient symmetric solvers to be used. Finally, in this approach there is partially uncoupling between the strains on both sides of the discontinuity, i.e., it provides better kinematic description for the region where some of the displacement components are discontinuous. However, in order to have this better kinematic description the standard quadrature rule has to be modified to integrate accurately on both sides of the discontinuity.
In the numerical examples, a tension test and a three-point bending test have been simulated by using constant and quadratic triangular elements, enhanced by the kinematics provided by two different approaches summarized above. In all the analyses a softening damage type traction seperation law have been used. The load displacement diagrams obtained in all the simulations using structured and unstructured meshes were found to be completely mesh independent. In the analyses, quadratic convergence rate were reported

almost at each iteration step. It was observed that the converged solution is reached usually at about four iteration steps.
As the future perspective, the formulations described can be implemented by incorporating the large strain kinematics to, for example, analyse debonding or delamination phenomena. It would be interesting to test the efficiency of the formulations under dynamic loading conditions and extend the formulation to three dimensional continuum. Investigation of branching and intersecting discontinuities might also be a fruitful research direction.

References

[1] Alfaiate J., Sluys L.J. [2002] "Analysis of compression test on concrete using strong embedded discontinuities", *Fifth World Congress on Computational Mechanics, WCCM V*, Mang, H.A., Rammerstorfer, F.G., Eberhardsteiner, J. (eds.), Vienna.

[2] Alfaiate J., Wells J.N. and Sluys L.J. [2002] "On the use of embedded discontinuity elements with crack path continuity for mode-I and mixed mode fracture", *Engineering Fracture Mechanics*, **69**, 661-686.

[3] Armero F. [1997] "Localized anisotropic damage of brittle materials", *Computational Plasticity: Fundamentals and Applications, Proc. COMPLAS V*, Owen D.R.J., Oñate E. (eds.), CIMNE, Barcelona.

[4] Armero F. [1999] "Large-scale modeling of localized dissipative mechanisms in a local continuum: applications to the numerical simulation of strain localization in rate-dependent inelastic solids", *Mechanics of Cohesive Frictional Materials*, **4**, 101-131.

[5] Armero F., Callari L.J. [1999] "An analysis of strong discontinuities in a saturated poro-plastic solid", *International Journal for Numerical Methods in Engineering*, **46**, 1673-1698.

[6] Armero F., Garikipati K. [1995] "Recent advances in the analysis and numerical simulation of strain localization in inelastic solids", *Computational Plasticity: Fundamentals and Applications, Proc. COMPLAS IV*, Owen D.R.J., Oñate E. (eds.), CIMNE, Barcelona.

[7] Armero F., Garikipati K. [1996] "An analysis of strong discontinuities in multiplicative finite strain plasticity and their relation with the numerical simulation of strain localization in solids", *International Journal of Solids and Structures*, **33**, 2863-2885.

[8] Barenblatt G.I. [1962] "The mathematical theory of equilibrium of cracks in brittle fracture", *Advances in Applied Mechanics*, **7**, 55-129.

[9] Belytschko T., Black T. [1999] "Elastic crack growth in finite elements with minimal remeshing", *International Journal for Numerical Methods in Engineering*, **45**, 601-620.

[10] Belytschko T., Fish J. and Engelmann E. [1988] "A finite element with emvedded localization zones", *Computer Methods in Applied Mechanics and Engineering*, **70**, 59-89.

[11] Belytschko T., Moës N., Usui S. and Parimi C. [2001] "Arbitrary discontinuities in finite elements", *International Journal for Numerical Methods in Engineering*, **50**, 993-1013.

[12] Belytschko T., Parimi C., Moës N., Sukumar N. and Usui S. [2003] "Structured extended finite element methods for solids defined by implicit surfaces", *International Journal for Numerical Methods in Engineering*, **56**, 609-635.

[13] Berends A.H., Sluys L.J. and De Borst R. [1997] "Discontinuous modeling of mode-I failure", *Computational Plasticity: Fundamentals and Applications, Proc. COMPLAS V*, Owen D.R.J., Oñate E. (eds.), CIMNE, Barcelona.

[14] Borja R.I. [2000] "A finite element model for strain localization analysis of strongly discontinuous fields based on standard Galerkin approximation", *Computer Methods in Applied Mechanics and Engineering*, **190**, 1529-1549.

[15] Callari C., Armero F. [2002] "Finite element methods for the analysis of strong discontinuities in coupled poro-plastic media", *Computer Methods in Applied Mechanics and Engineering*, **191**, 4371-4400.

[16] Camacho G.T., Ortiz M. [1996] "Computational modeling of impact damage in brittle materials", *International Journal of Solids and Structures*, **33**, 2899-2938.

[17] Chessa J., Belytschko T. [2003] "An extended finite element method for two-phase fluids", *ASME Journal of Applied Mechanics*, **70**, 10-17.

[18] Chopp D.L., Sukumar N. [2003] "Fatique crack propagation of multiple coplanar cracks with the coupled extended finite element/fast marching method", *International Journal of Engineering Science*, **41**, 845-869.

[19] Daux C., Moës N., Dolbow J., Sukumar N. and Belytschko T. [2000] "Arbitrary branched and intersecting cracks with the extended finite element method", *International Journal for Numerical Methods in Engineering*, **48**, 1741-1760.

[20] De Borst R. [2001] "Some recent issues in computational failure mechanics", *International Journal for Numerical Methods in Engineering*, **52**, 63-95.

[21] Dolbow J. [1999] "An extended finite element method with discontinuous enrichment for applied mechanics", PhD thesis, Northwestern University.

[22] Dolbow J., Gosz M. [2002] "On the computation of mixed-mode stress intensity factors in functionally graded materials", *International Journal of Solids and Structures*, **39**, 2557-2574.

[23] Dolbow J., Moës N. and Belytschko T. [2000] "Discontinuous enrichment in finite elements with a partition of unity method", *Finite Elements in Analysis and Design*, **36**, 235-260.

[24] Dolbow J., Moës N. and Belytschko T. [2000] "Modeling fracture in Mindlin-Reissner plates with the extended finite element method", *International Journal of Solids and Structures*, **33**, 7161-7183.

[25] Dolbow J., Moës N. and Belytschko T. [2001] "An extended finite element method for modeling crack growth with frictional contact", *Computer Methods in Applied Mechanics and Engineering*, **19**, 6825-6846.

[26] Dugdale D.S. [1960] "Yielding of steel sheets containing slits", *Journal of Mechanics and Physics of Solids*, **8**, 100-108.

[27] Dumstorff P., Mosler J. and Meschke G. [2003] "Advanced discretization methods for cracked structures: strong discontinuity approach vs. the extended finite element method", *Computational Plasticity: Fundamentals and Applications, Proc. COMPLAS 2003*, Owen D.R.J., Oñate E. (eds.), CIMNE, Barcelona.

[28] Dvorkin E.N., Cuitiño A.M. and Gioia G. [1990] "Finite elements with displacement interpolated embedded localization lines insensitive to mesh size and distortions", *International Journal for Numerical Methods in Engineering*, **30**, 541-564.

[29] Garikipati K.R. [1996] "On strong discontinuities in inelastic solids and their numerical simulation", PhD thesis, Stanford University.

[30] Ehlers W. [2002] "C1-Continuum Mechanics", Lecture Notes, COMMAS, Stuttgart.

[31] Ehlers W. [2002] "E1-Foundations of Single- and Multiphasic Materials", Lecture Notes, COMMAS, Stuttgart.

[32] Hillerborg A., Modéer M. and Peterson P.E. [1976] "Analysis of crack propagation and crack growth in concrete by means of fracture mechanics and finite elements", *Cement and Concrete Research*, **6**, 773-782.

[33] Ji H., Chopp D. and Dolbow J. [2002] "A hybrid extended finite/level set method for modeling phase transformations", *International Journal for Numerical Methods in Engineering*, **54**, 1209-1233.

[34] Jirásek M. [2000] "Conditions of uniqueness for finite elements with embedded cracks", *Proceedings of the Sixth International Conference on Computational Plasticity*, pages CD-ROM, Barcelona.

[35] Jirásek M. [2000] "Comparative study on finite elements with embedded cracks", *Computer Methods in Applied Mechanics and Engineering*, **188**, 307-330.

[36] Jirásek M. [2001] "Modeling of damage and fracture in quasi-brittle materials", Lecture Notes, COMMAS Summer School, Stuttgart.

[37] Jirásek M. Belytschko T. [2002] "Computational resolution of strong discontinuities", *Fifth World Congress on Computational Mechanics, WCCM V*, Mang, H.A., Rammerstorfer, F.G., Eberhardsteiner, J. (eds.), Vienna.

[38] Jirásek M., Zimmermann T. [2001] "Embedded crack model: I. basic formulation", *International Journal for Numerical Methods in Engineering*, **50**, 1269-1290.

[39] Jirásek M., Zimmermann T. [2001] "Embedded crack model. part II: combination with smeared cracks", *International Journal for Numerical Methods in Engineering*, **50**, 1291-1305.

[40] Klisinski M., Runesson K. and Sture S. [1991] "Finite element with inner softening band", *ASCE Journal of Engineering Mechanics*, **117**, 575-587.

[41] Larsson R., Runesson K. and Sture S. [1996] "Embedded localization band in undrained soil based on regularized strong discontinuity–theory and fe-analysis", *International Journal of Solids and Structures*, **33**, 3081-3101.

[42] Larsson R., Steinmann P. and Runesson K. [1998] "Finite element embedded localization band for finite strain plasticity based on a regularized strong discontinuity", *Mechanics of Cohesive Frictional Materials*, **4**, 171-194.

[43] Lofti H.R., Shing P.B. [1994] "Analysis of concrete fracture with an embedded crack approach", *Computational Modeling of Concrete Structures, Proc. EURO-C 1994*, Mang H., Bićanić N., De Borst R. (eds.), Pineridge, Swansea.

[44] Malvern L.E. [1969] "Introduction to Mechanics of a Continuous Media", Englewood Cliffs, N.J., Prentice Hall.

[45] Melenk J.M., Babuška I. [1996] "The partition of unity finite element method: basic theory and applications", *Computer Methods in Applied Mechanics and Engineering*, **139**, 289-314.

[46] Merle R., Dolbow J. [2002] "Solving thermal and phase change problems with the extended finite element method", *Computational Mechanics*, **28**, 339-350.

[47] Miehe C., Schröder J. [1994] "Post-critical discontinuous localization analysis of small-strain softening elastoplastic solids", *Archive of Applied Mechanics*, **64**, 267-285.

[48] Miehe C. [1995] "Discontinuous and continuous damage evolution in Ogden-type large-strain elastic materials", *European Journal of Mechanics A/Solids*, **14**, 697-720.

[49] Miehe C. [2002] "C5-Computational Mechanics of Materials", Lecture Notes, COMMAS, Stuttgart.

[50] Miehe C. [2002] "E5-Micromechanics of Materials and Homogenization Methods", Lecture Notes, COMMAS, Stuttgart.

[51] Moës N., Belytschko T. [2002] "Extended finite element method for cohesive crack growth", *Engineering Fracture Mechanics*, **69**, 813-833.

[52] Moës N., Dolbow J. and Belytschko T. [1999] "A finite element method for crack growth without remeshing", *International Journal for Numerical Methods in Engineering*, **46**, 131-150.

[53] Moës N., Gravouil A. and Belytschko T. [2001] "The extended finite element and level set methods for non-planar 3D crack growth", *Symposium on Computational Mechanics of Solid Materials at Large Strains, IUTAM 2001*, Miehe C. (ed.), Stuttgart.

[54] Needleman A. [1987] "A continuum model for void nucleation by inclusion debonding", *ASME Journal of Applied Mechanics*, **54**, 525-531.

[55] Needleman A. [1988] "Material rate dependence and mesh sensitivity in localization problems", *Computer Methods in Applied Mechanics and Engineering*, **67**, 69-85.

[56] Oliver J. [1989] "A consistent characteristic length for smeared cracking models", *International Journal for Numerical Methods in Engineering*, **28**, 461-474.

[57] Oliver J. [1996] "Modeling strong discontinuities in solid mechanics via strain softening constitutive equations. part 1: fundamentals", *International Journal for Numerical Methods in Engineering*, **39**, 3575-3600.

[58] Oliver J. [1996] "Modeling strong discontinuities in solid mechanics via strain softening constitutive equations. part 2: numerical simulation", *International Journal for Numerical Methods in Engineering*, **39**, 3601-3623.

[59] Oliver J. [2000] "On the discrete constitutive models induced by strong discontinuity kinematics and continuum constitutive equations", *International Journal of Solids and Structures*, **37**, 7207-7229.

[60] Oliver J. [2002] "The strong discontinuity approach to fracture mechanics", Lecture Notes, COMMAS Summer School, Stuttgart.

[61] Oliver J., Cervera M. and Manzoli O. [1997] "On the use of J2 plasticity models for the simulation of 2D strong discontinuities in solids", *Computational Plasticity: Fundamentals and Applications, Proc. COMPLAS V*, Owen D.R.J., Oñate E. (eds.), CIMNE, Barcelona.

[62] Oliver J., Huespe A.E., Pulido M.D.G. and Chaves E. [2002] "From continuum mechanics to fracture mechanics: the strong discontinuity approach", *Engineering Fracture Mechanics*, **69**, 113-136.

[63] Oliver J., Simo J.C. [1994] "Modeling strong discontinuities by means of strain softening constitutive equations", *Computational Modeling of Concrete Structures, Proc. EURO-C 1994*, Mang H., Bićanić N., De Borst R. (eds.), Pineridge, Swansea.

[64] Olofsson T., Klisinski M. and Nedar P. [1994] "Inner softening bands: a new approach to localization in finite elements", *Computational Modeling of Concrete Structures, Proc. EURO-C 1994*, Mang H., Bićanić N., De Borst R. (eds.), Pineridge, Swansea.

[65] Ortiz M., Leroy Y. and Needleman A. [1987] "A finite element method for localized failure analysis", *Computer Methods in Applied Mechanics and Engineering*, **61**, 189-214.

[66] Ortiz M. [1988] "Microcrack coalescence and macroscopic crack growth initiation in brittle solids", *International Journal of Solids and Structures*, **24**, 231-250.

[67] Ortiz M., Pandolfi A. [1999] "Finite-deformation irreversible cohesive elements for three-dimensional crack-propagation analysis", *International Journal for Numerical Methods in Engineering*, **44**, 1267-1282.

[68] Ozbolt J. [2002] "E2-2 Engineering Materials: Concrete", Lecture Notes, COMMAS, Stuttgart.

[69] Pandolfi A., Krysl P. and Ortiz M. [1999] "Finite element simulation of ring expansion and fragmentation", *International Journal of Fracture*, **95**, 279-297.

[70] Patzák B., Jirásek M. [2003] "Process zone resolution by extended finite elements", *Engineering Fracture Mechanics*, **70**, 957-977.

[71] Ramm E., Wall W.A. [2002] "C7-Computational Mechanics of Structures", Lecture Notes, COMMAS, Stuttgart.

[72] Ramm E., Wall W.A. [2002] "E7-Advanced Computational Structural Mechanics", Lecture Notes, COMMAS, Stuttgart.

[73] Regueiro R.A., Borja R.I. [1999] "A finite element model of localized deformation in frictional materials taking a strong discontinuity approach", *Finite Elements in Analysis and Design*, **190**, 283-315.

[74] Simo J.C., Ju J.W. [1987] "Strain- and stress-based continuum damage models–I. formulation", *International Journal of Solids and Structures*, **23**, 821-840.

[75] Simo J.C., Rifai S. [1990] "A class of mixed assumed strain methods and the method of incompatible modes", *International Journal for Numerical Methods in Engineering*, **29**, 1595-1638.

[76] Simo J.C., Oliver J. and Armero F. [1993] "An analysis of strong discontinuities induced by strain-softening in rate-independent inelastic solids", *Computational Mechanics*, **12**, 277-296.

[77] Simo J.C., Oliver J. [1994] "A new approach to the analysis and simulation of strain softening in solids", *Fracture and Damage in Quasibrittle Structures*, Bazant Z.P., Bittnar Z., Jirásek M. and Mazars J. (eds.), Praque.

[78] Sluys L.J. [1997] "Discontinuous modeling of shear banding", *Computational Plasticity: Fundamentals and Applications, Proc. COMPLAS V*, Owen D.R.J., Oñate E. (eds.), CIMNE, Barcelona.

[79] Steinmann P. [1999] "A finite element formulation for strong discontinuities in fluid-saturated porous media", *Mechanics of Cohesive Frictional Materials*, **4**, 133-152.

[80] Steinmann P., Larsson R. and Runesson K. [1997] "On the localization properties of multiplicative hyperelasto-plastic continua with strong discontinuities", *International Journal of Solids and Structures*, **34**, 969-990.

[81] Stolarska M., Chopp D.L., Moës N. and Belytschko T. [2001] "Modeling crack growth by level sets in the extended finite element method", *International Journal for Numerical Methods in Engineering*, **51**, 943-960.

[82] Sukumar N., Chopp D.L., Moës N. and Belytschko T. [2001] "Modeling holes and inclusions by level sets in the extended finite element method", *Computer Methods in Applied Mechanics and Engineering*, **190**, 6183-6200.

[83] Sukumar N., Chopp D.L. and Moran B. [2003] "Extended finite element method and fast marching method for three dimensional crack propagation", *Engineering Fracture Mechanics*, **70**, 29-48.

[84] Sukumar N., Moës N., Moran B. and Belytschko T. [2000] "Extended finite element method for three-dimensional crack modeling", *International Journal for Numerical Methods in Engineering*, **48**, 1549-1570.

[85] Sukumar N., Srolovitz D.J., Baker T.J. and Prévost J.H. [2001] "Brittle fracture in polycrystalline microstructures with the extended finite element method", *International Journal for Numerical Methods in Engineering*, **00**, 1-22.

[86] Tvergaard V., Hutchinson J.W. [1992] "The relation between crack growth resistance and fracture process parameters in elastic-plastic solids", *Journal of Mechanics and Physics of Solids*, **40**, 1377-1397.

[87] Tvergaard V., Hutchinson J.W. [1993] "The influence of plasticity on mixed mode interface toughness", *Journal of Mechanics and Physics of Solids*, **41**, 1119-1135.

[88] Wagner G.J., Moës N., Liu W.K. and Belytschko T. [2001] "The extended finite element method for rigid particles in Stokes flow", *International Journal for Numerical Methods in Engineering*, **51**, 293-313.

[89] Wells G.N. [2001] "Discontinuous modeling of strain localisation and failure", PhD thesis, Delft University.

[90] Wells G.N., Remmers J.J.C., De Borst R. and Sluys L.J. [2001] "A large strain discontinuous finite element approach to laminated composites", *Symposium on Computational Mechanics of Solid Materials at Large Strains, IUTAM 2001*, Miehe C. (ed.), Stuttgart.

[91] Wells G.N., Sluys L.J. [2000] "Application of embedded discontinuities for softening solids", *Engineering Fracture Mechanics*, **65**, 263-281.

[92] Wells G.N., Sluys L.J. [2000] "Discontinuous analysis of softening solids under impact loading", *International Journal for Numerical Methods in Engineering*, **25**, 691-709.

[93] Wells G.N., Sluys L.J. [2001] "Analysis of slip planes in three-dimensional solids", *Computer Methods in Applied Mechanics and Engineering*, **190**, 3591-3606.

[94] Wells G.N., Sluys L.J. [2001] "A new method for modeling cohesive cracks using extended finite elements", *International Journal for Numerical Methods in Engineering*, **50**, 2667-2682.

[95] Wells G.N., Sluys L.J. [2001] "Three-dimensional embedded discontinuity model for brittle fracture", *International Journal of Solids and Structures*, **38**, 897-913.

[96] Wells G.N., Sluys L.J. and De Borst R. [2002] "Simulating the propagation of displacement discontinuities in a regularized strain softening medium", *International Journal for Numerical Methods in Engineering*, **53**, 1235-1256.